**University of Calgary**

**PRISM Repository** **https://prism.ucalgary.ca**

The Vault Open Theses and Dissertations

2018-05-10

# Fundamental Mechanisms of Astrocyte and Cerebrovascular Regulation by Potassium in the Neocortex

Shin, Steven Seungjae

Shin, S. S. (2018). Fundamental Mechanisms of Astrocyte and Cerebrovascular Regulation by Potassium in the Neocortex (Master's thesis, University of Calgary, Calgary, Canada). Retrieved from https://prism.ucalgary.ca. doi:10.11575/PRISM/31919

http://hdl.handle.net/1880/106638

*Downloaded from PRISM Repository, University of Calgary*

UNIVERSITY OF CALGARY

# Fundamental Mechanisms of Astrocyte and Cerebrovascular Regulation by Potassium in the Neocortex

by

Steven Seungjae Shin

A THESIS

SUBMITTED TO THE FACULTY OF GRADUATE STUDIES

IN PARTIAL FULFILMENT OF THE REQUIREMENTS FOR THE

DEGREE OF MASTER OF SCIENCE

GRADUATE PROGRAM IN NEUROSCIENCE

CALGARY, ALBERTA

MAY, 2018

© Steven Seungjae Shin 2018

## Abstract

Astrocytes can control local cerebral arteriole tone through $Ca^{2+}$ dependent mechanisms. Modest elevations of the external $K^+$ concentration in the brain are thought to have little effect on astrocyte free $Ca^{2+}$, yet $K^+$ dilates parenchymal arterioles. It remains unclear whether fluctuations in external $K^+$, within the low to moderate range, controls arteriole diameter through an astrocyte $Ca^{2+}$ dependent mechanism. Using relative and quantitative two-photon fluorescence $Ca^{2+}$ imaging in acute brain slices of the somatosensory cortex from Sprague Dawley rats, we found that elevations in external $K^+$ from 2.5 mM to 3.5 or 5.0 mM decreased astrocyte free $Ca^{2+}$ and caused arteriole dilation. The phenomenon relied on external $Ca^{2+}$, $Cl^-$, and bicarbonate, as well as, unexpectedly, the potassium chloride cotransporter (KCC). These data highlight novel aspects of $K^+$-astrocyte dynamics that involve the subtle regulation of free astrocyte $Ca^{2+}$ via $Cl^-$ and bicarbonate fluxes with corresponding changes to arteriole tone.

**Acknowledgements**

I would like to acknowledge and thank everyone who, in one way or another, made this project possible. First and foremost, a huge thank you to my awesome supervisor, Dr. Grant Gordon, for his guidance, patience, words of encouragement, and for believing in me, as well as the significant amount of time and effort he has invested into teaching me. For that I will always be very grateful. I would like to thank my supervisory committee, Dr. Jaideep Bains and Dr. Tuan Trang for providing meaningful feedback, as well as Dr. Roger Thompson and Dr. Richard Hawkes for serving on my thesis exam committee. I would like to acknowledge and thank Dr. Nicholas Weilinger and Dr. Brian MacVicar for generously performing and sharing the results of FLIM experiments, which are crucial pieces of evidence and are included in this thesis. A big thank you goes out to all members of the Gordon lab (who I have had the pleasure of working with) for their assistance, advice, and cooperation. The combination of their support, along with the occasional puns and conversations regarding world events and life in general, have been essential in creating an exceptional lab environment to work in. These individuals include: Dr. Zhonghang Zhao, Dr. David Rosenegger, Dr. Cam Ha Tran, Dr. Adam Institoris, Dr. Ciaran Murphy-Royal, Eslam (Essie) Mehina, Jordan Haidey, Govind Peringod, and Aaron Lanz. Finally, I would like to thank my wonderful family and friends for their unwavering support.

## Dedication

Dedicated to my parents and my sister, who have always been there through thick and thin.

## Table of Contents

Abstract ..... ii
Acknowledgements ..... iii
Dedication ..... iv
Table of Contents ..... v
List of Figures and Illustrations ..... vii
List of Symbols, Abbreviations and Nomenclature ..... viii

CHAPTER 1: INTRODUCTION ..... 1
1.1 General Introduction ..... 1
1.2 Astrocyte $Ca^{2+}$ Signals and Resting $Ca^{2+}$ Levels ..... 2
1.3 Gliotransmitters and Synaptic Modulation ..... 6
1.4 Neurovascular Coupling ..... 8
1.4.1 Neurovascular Coupling and Extracellular $K^+$ ..... 10
1.4.2 The Cerebrovasculature ..... 11
1.5 Extracellular $K^+$ Homeostasis ..... 14
1.6 Astrocyte Handling of $Cl^-$ Ions ..... 17
1.6.1 $K^+$-$Cl^-$ Cotransporters (KCCs) ..... 19
1.6.2 Astrocyte Swelling Independent of $Cl^-$ or KCCs ..... 23
1.6.3 KCCs and the vasculature ..... 23
1.7 Hypothesis ..... 24

CHAPTER TWO: MATERIALS AND METHODS ..... 26
2.1 Acute Brain Slice Preparation ..... 26
2.2 Contents of Various ACSF Solutions ..... 26
2.3 Loading Dyes in Astrocytes, Neurons, and Arterioles ..... 28
2.4 Two-Photon Fluorescence Microscopy ..... 29
2.5 Fluorescence Lifetime Imaging Microscopy (FLIM) ..... 29
2.6 Enriched Environment ..... 31
2.7 Astrocyte Patch-Clamp ..... 31
2.8 Data Collection ..... 32

CHAPTER THREE: RESULTS ..... 33
3.1 Modest changes in external $[K^+]_o$ bidirectionally control astrocyte resting free $Ca^{2+}$ and soma volume ..... 33
3.2 FLIM reveals a quantitative decrease in astrocyte free $Ca^{2+}$ in response to a modest elevation in external $K^+$ ..... 37
3.3 $K^+$-mediated astrocyte $Ca^{2+}$ decrease does not depend on neuronal firing or display plastic changes ..... 41
3.4 $K^+$-mediated astrocyte $Ca^{2+}$ decrease depends on external $Ca^{2+}$ and not ER stored $Ca^{2+}$ ..... 45
3.5 $K^+$-mediated astrocyte $Ca^{2+}$ decrease relies on bicarbonate but not carbonic anhydrase-mediated pH changes ..... 48
3.6 $K^+$-mediated astrocyte $Ca^{2+}$ decrease is independent of inward rectifiers, the SLC4A4-sAC pathway, or $Na^+$ ions ..... 51

3.7 Anion channels separately control $K^+$-mediated astrocyte $Ca^{2+}$ decrease and swelling .....54
3.8 $K^+$-mediated vasodilation is sensitive to KCC blockade and astrocyte patching ....58

CHAPTER FOUR: DISCUSSION .....62
4.1 Conclusion .....72

REFERENCES .....74

## List of Figures and Illustrations

Figure 1: Modest changes in external [$K^+$] bidirectionally control astrocyte resting free $Ca^{2+}$ and soma volume ..... 36

Figure 2: Fluorescence Lifetime Imaging Microscopy (FLIM) reveals a quantitative decrease in astrocyte free $Ca^{2+}$ in response to a modest elevation in external $K^+$ ..... 40

Figure 3: The $K^+$ mediated decrease in astrocyte $Ca^{2+}$ does not exhibit a reliance on neural firing or display plastic changes ..... 44

Figure 4: The $K^+$ effect does not depend on ER stored $Ca^{2+}$ but on external $Ca^{2+}$ ..... 47

Figure 5: The $K^+$ effect depends on bicarbonate but not carbonic anhydrase-mediated pH changes ..... 50

Figure 6: The $K^+$ mediated $Ca^{2+}$ decrease does not depend on inward rectifiers, $Na^+$ ions or the SLC4A4-sAC pathway ..... 53

Figure 7: Anion channels and the potassium chloride co-transporter separately control cell swelling and the $Ca^{2+}$ decrease in response to high $[K^+]_o$ ..... 57

Figure 8: $K^+$-mediated vasodilation is sensitive to KCC blockade and astrocyte patching ..... 61

## List of Symbols, Abbreviations and Nomenclature

| Symbol | Definition |
|---|---|
| ATP | Adenosine Triphosphate |
| mGluR | Metabotropic Glutamate Receptor |
| GPCR | G-Protein Coupled Receptor |
| PLC | Phospholipase C |
| $PIP_2$ | Phosphatidylinositol 4,5-bisphosphate |
| DAG | Diacylglycerol |
| $IP_3$ | Inositol Triphosphate |
| ER | Endoplasmic Reticulum |
| GECI | Genetically Encoded $Ca^{2+}$ Indicators |
| TRPA1 | Transient Receptor Potential Ankyrin 1 |
| FLIM | Fluorescence Lifetime Imaging Microscopy |
| PLA2 | Phospholipase $A_2$ |
| NMDA | N-Methyl-D-Aspartate |
| LTP | Long-Term Potentiation |
| BAPTA | 1,2-bis(o-aminophenoxy)ethane-N,N,N′,N′-tetraacetic acid |
| COX | Cyclooxygenase |
| EET | Epoxyeicosatrienoic Acid |
| CYP450 | Cytochrome P450 |
| PGE2 | Prostaglandin E2 |
| $K_{Ca}$ | Calcium Activated Potassium Channel |
| 20-HETE | 20-Hydroxyeicosatetraenoic Acid |
| NO | Nitric Oxide |
| $K_{ir}$ | Inward Rectifying Potassium Channel |
| $E_K$ | Reversal Potential of Potassium |
| MCA | Middle Cerebral Artery |
| VSMC | Vascular Smooth Muscle Cell |
| EAAT | Excitatory Amino Acid Transporter |
| NBC | Sodium Bicarbonate Cotransporter |
| sAC | Soluble Adenylyl Cyclase |
| cAMP | Cyclic Adenosine Monophosphate |
| GABA | γ-aminobutyric acid |
| VRAC | Volume Regulated Anion Channel |
| CaCC | $Ca^{2+}$-activated $Cl^-$ channel |
| NPPB | 5-nitro-2-(3-phenylpropylamino)benzoic acid |
| NKCC | $Na^+$-$K^+$-$Cl^-$ Cotransporter |
| KCC | $K^+$-$Cl^-$ Cotransporter |
| CNS | Central Nervous System |
| RVD | Regulatory Volume Decrease |
| RVI | Regulatory Volume Increase |
| WNK | Lysine Deficient Protein Kinase |
| SPAK | SPS1-related proline/alanine-rich kinase |

| | |
|---|---|
| OSR1 | Oxidative Stress-Response Kinase 1 |
| AQP4 | Aquaporin 4 |
| ACSF | Artificial Cerebrospinal Fluid |
| HEPES | 4-(2-hydroxyethyl)-1-piperazineethanesulfonic acid |
| Rhod-2 | Rhodamine-2 |
| AM | Acetoxymethyl Ester |
| FITC | Fluorescein Isothiocyanate |
| SR101 | Sulforhodamine 101 |
| OGB-1 | Oregon Green 488 BAPTA-1 |
| TTX | Tetrodotoxin |
| SERCA | Sarco/Endoplasmic Reticulum $Ca^{2+}$-ATPase |
| S0859 | 2-chloro-N-[[2′-[(cyanoamino)sulfonyl][1,1′-biphenyl]-4-yl]methyl]-N-[(4-methylphenyl)methyl]-benzamide |
| KH7 | (E)-2-(1H-Benzo[d]imidazol-2-ylthio)-N′-(5-bromo-2-hydroxybenzylidene)propanehydrazide |
| DIDS | 4,4′-diisothiocyanatostilbene-2,2′-disulfonate |

# CHAPTER 1: INTRODUCTION

## 1.1 General Introduction

Neurons are the electrically excitable cells of the nervous system, communicating from cell-to-cell through the use of fast propagating action potentials and special chemical junctions called synapses (Waites et al., 2005). Of the approximately 100 billion cells estimated to make up the human brain, only ~10% is attributed to neurons, while the remaining ~90% are thought to be non-excitable glial cells (Kuffler, 1967; Oberheim et al., 2006; Mishima and Hirase, 2010). Astrocytes, also known as astroglia, are one of the major types of glial cells (Kettenmann and Ransom, 2004). While the brains of smaller mammals consist of fewer absolute numbers of cells, the ratio of astrocytes to neurons tends to decline with brain size (Nedergaard et al., 2003). The ratio also varies between brain regions: nearly 80% of cells of the human cerebral cortex are composed of glia, while accounting for only ~20% of cells in the cerebellum (Azevedo et al., 2009).

Astrocytes occupy space in a manner such that each astrocyte's "territory", or domain, does not overlap with those of neighboring astrocytes (Bushong et al., 2002). During development, rodent astrocyte processes are interweaved with the processes of neighboring astrocytes, and then gradually segregate into separate domains during the second postnatal week in a process called astrocyte tiling (Distler et al., 1991). Astrocytes often lose the non-overlapping tiling of their processes in certain pathological conditions, such as epilepsy (Oberheim et al., 2008) or following an injury (Oberheim et al., 2009), suggesting that the establishment of separate domains may be required for the nervous system to function properly. The pre- and post-synaptic neuronal terminals are surrounded by astrocyte processes, forming the "tripartite synapse" (Araque et al., 1999). Astrocyte processes act as physical barriers,

hindering neurotransmitter diffusion away from the synapse (Piet et al., 2004). Intricate positioning amongst neurons and the extension of multiple fine processes from each astrocyte allows a given astrocyte to envelope and make contact with thousands of neuronal synapses; one astrocyte can contact up to ~140,000 neuronal synapses in the adult rodent hippocampus (Bushong et al., 2002), and ~100,000 synapses in the cortex (Halassa et al., 2007). This close positioning of astrocytes amongst neurons and the lack of electrical excitability means that astrocyte activation is achieved via receptors for various neurotransmitters, often resulting in downstream astrocyte calcium signaling (Porter and McCarthy, 1996; Agulhon et al., 2008; Attwell et al., 2010). Sensitivity to neurotransmitters and other signals from neurons provides mechanisms through which astrocytes pay attention to synaptic transmission and respond if necessary. Beyond fine processes, astrocytes also possess a specialized appendage that extends towards and directly apposes nearby microvasculature, known as an "endfoot" (Simard et al., 2003; Mathiisen et al., 2010). Collectively, astrocyte endfeet completely envelope the vasculature within the brain (Mathiisen et al., 2010), thus ensuring their involvement at the brain-blood interface.

### 1.2 Astrocyte $Ca^{2+}$ Signals and Resting $Ca^{2+}$ Levels

Since astrocytes are electrically non-excitable (Kuffler, 1967; Mishima and Hirase, 2010), astrocytes were at first believed to detect and respond to neuronal activity through long range $Ca^{2+}$ signaling (Cornell-Bell et al., 1990; Porter and McCarthy, 1996; Agulhon et al., 2008; Attwell et al., 2010). Astrocytes were found to respond to the release of the neurotransmitter glutamate with increased intracellular $Ca^{2+}$, which can propagate as a "$Ca^{2+}$ wave" to neighboring astrocytes via gap junctions (Cornell-Bell et al., 1990; Rouach et al., 2000; 2008),

and via secreted ATP acting in a paracrine manner (Hassinger et al., 1996; Arcuino et al., 2002; Anderson et al., 2004). However, the extent to which $Ca^{2+}$ waves are utilized *in vivo* is still a matter of debate (Rusakov, 2015). Nevertheless, the metabotropic glutamate receptor 5 (mGluR5) is highly expressed on the astrocyte soma in young rodents (<P14) (Sun et al., 2013), and the binding of glutamate with mGluR5 leads to the release of $Ca^{2+}$ from intracellular stores, thereby generating $Ca^{2+}$ signals (Sun et al., 2013). Glutamate binding with mGluR5, a $G_q$-coupled G-protein coupled receptor (GPCR), activates the enzyme phospholipase C (PLC), which cleaves phosphatidylinositol 4,5-bisphosphate ($PIP_2$) into the secondary messengers diacyl glycerol (DAG) and inositol triphosphate ($IP_3$) (Petravicz et al., 2008). The $IP_3$ receptors ($IP_3R$) are intracellular $Ca^{2+}$ permeable channels that are mostly localized to the endoplasmic reticulum (ER), and they mediate $Ca^{2+}$ release from the ER via $IP_3$ binding (Petravicz et al., 2008). Indeed, hippocampal astrocytes without $IP_3R_2$s lack GPCR-mediated $Ca^{2+}$ signals in the soma (Petravicz et al., 2008; Agulhon et al., 2010). More recent findings have found only partially reduced spontaneous $Ca^{2+}$ signaling in astrocyte processes of $IP_3R_2^{-/-}$ mice, while somatic $Ca^{2+}$ signaling was eliminated (Kanemaru et al., 2014; Srinivasan et al., 2015). Other $IP_3R$ isoforms, $IP_3R_1$ and $IP_3R_3$, are also functional in astrocytes, and are suspected to be responsible for some astrocyte functions that cannot be attributed to $IP_3R_2$ (Sherwood et al., 2017). Finally, recent evidence suggests astrocytes replace mGluR5 with mGluR3 when moving into adulthood (Sun et al., 2013). Though mGluR3 is not $G_q$-coupled, its activation also results in a $Ca^{2+}$ transient in astrocytes, but through an unknown mechanism (Haustein et al., 2014), which could also account for $Ca^{2+}$ signals that occur independent of $IP_3R_2$.

Genetically encoded calcium indicators (GECIs) have more clearly demonstrated the large degree of transient $Ca^{2+}$ signals that occur in astrocyte fine processes, or microdomains

(Shigetomi et al., 2013a), occurring much more frequently than in the soma (Grosche et al., 1999; Kanemaru et al., 2014). Individual astrocyte processes generate $Ca^{2+}$ transients at different times (Nett et al., 2002). The $Ca^{2+}$ transients that occur deeper within the cytoplasm also differs from $Ca^{2+}$ transients that occur just beneath the cell membrane (Shigetomi et al., 2010). Underlying $Ca^{2+}$ transients that mainly occur near the membrane are transient receptor potential ankyrin type 1 (TRPA1) channels in the astrocyte membrane that open spontaneously (Shigetomi et al., 2012). However, recent evidence argues against a significant role of TRPA1-mediated $Ca^{2+}$ in adult astrocytes (Rungta et al., 2016). Nevertheless, the frequency of $Ca^{2+}$ transients in astrocyte processes are greater than in the soma by approximately eight fold (Kanemaru et al., 2014; Srinivasan et al., 2015), with no known physiological function. These examples highlight the complexity of astrocyte $Ca^{2+}$ dynamics and some of the key differences between $Ca^{2+}$ signaling in the soma versus signaling in the fine processes of astrocytes.

Frequent changes in intracellular $Ca^{2+}$ levels involved in astrocyte $Ca^{2+}$ signaling suggest that basal levels of $Ca^{2+}$, or resting $Ca^{2+}$ levels, may also be physiologically meaningful. Recent quantitative measurements of resting $Ca^{2+}$ levels have been performed using Fluorescence Lifetime Imaging Microscopy (FLIM), a technique that measures the average amount of time a fluorophore spends excited before returning to the ground state (Lackowicz, 2006). The time spent in the excited state is correlated with the concentration of $Ca^{2+}$ (Wilms et al., 2006; Wilms and Eilers, 2007) and can be calibrated for quantitative measurements that are insensitive to dye concentration. The $Ca^{2+}$ concentration in hippocampal astrocyte somata was measured to be ~100 nM, with a measurement of ~125 nM in astrocyte processes (Zheng et al., 2015). Of note, further investigation suggests that resting $Ca^{2+}$ levels of the soma are not uniform amongst astrocytes, and each astrocyte falls into one of two groups – one group with a mean resting $Ca^{2+}$

concentration of ~70-75 nM, versus the other group with mean concentrations of ~120-130 nM (Zheng et al., 2015). Notably, even small deviations from resting $Ca^{2+}$ levels (up or down) may have physiological consequences for functions such as gliotransmission (Parpura and Haydon, 2000; Shigetomi et al., 2013b), synaptic modulation (Panatier et al., 2011), and tonic brain blood flow control (Rosenegger et al., 2015).

The primary focus of many studies have been on understanding large transient increases in astrocyte $Ca^{2+}$ occurring due to neuronal activity, and how these $Ca^{2+}$ increases lead to changes in synaptic strength and vascular diameter. As a result, much less is known about the physiological role(s) of free cytosolic $Ca^{2+}$ in astrocytes at rest. A recent example of functional relevance suggests that changes in astrocyte resting $Ca^{2+}$ is associated with their tonic manner of action (Rosenegger et al., 2015), which likely occurs on slower time scales compared to large $Ca^{2+}$ increases (Rosenegger and Gordon, 2015). Moreover, many intracellular proteins have an affinity for $Ca^{2+}$ near the resting concentration of $Ca^{2+}$ in the cytoplasm, such as the sarco/endoplasmic reticulum $Ca^{2+}$-ATPases (SERCA pumps) (Verboomen et al., 1992) and c-phospholipase $A_2$ (PLA2) (Pettus et al., 2004). While $IP_3Rs$ (mentioned above) mediate $Ca^{2+}$ release from the ER via $IP_3$ binding, SERCA pumps sequester free cytosolic $Ca^{2+}$ back into the ER (Verboomen et al., 1992; Simpson and Russell, 1997; Beck et al., 2004), thereby restoring baseline $Ca^{2+}$ levels after transient increases. Therefore, it is plausible that modulation of these proteins has consequences for astrocyte functions via changes in resting $Ca^{2+}$. However, it is still unclear what determines and regulates the cytosolic $Ca^{2+}$ concentrations of astrocytes at rest, and how this may affect neighbouring cells.

### 1.3 Gliotransmitters and Synaptic Modulation

In response to molecular signals resulting from the activity of nearby neurons, astrocyte intracellular $Ca^{2+}$ increases, resulting in astrocyte release of transmitter molecules known as "gliotransmitters" (Porter and McCarthy, 1996; Panatier et al., 2006). Gliotransmitters activate their appropriate receptors on nearby neurons, thereby allowing astrocytes to modulate neuronal synaptic transmission (Panatier et al., 2006).

Similar to neurotransmitters, a given gliotransmitter may interact with multiple targets. Glutamate is a gliotransmitter released from astrocytes that potentiates excitatory transmission in the hippocampus by binding with presynaptic NMDA receptors (NMDARs) in the dentate gyrus (Jourdain et al., 2007). Astrocyte released glutamate binds with presynaptic mGluRs of CA3-CA1 synapses of the hippocampus, also potentiating synaptic transmission (Navarrete and Araque, 2010). In the CA1 region of the hippocampus, astrocyte released glutamate activate presynaptic kainate receptors to potentiate inhibitory transmission (Liu et al., 2004). These examples demonstrate that a given gliotransmitter can produce different physiological outcomes depending on its targeted receptors and neurons.

Astrocytes release other gliotransmitters as well, such as D-serine (Panatier et al., 2006; Henneberger et al., 2010; Zhuang et al., 2010). The amino acid D-serine is a co-ligand of NMDARs, and the presence of D-serine is required for NMDAR activation, which contributes to long-term potentiation (LTP) (Mothet et al., 2000; Yang et al., 2003; Panatier et al., 2006). The requirement of D-serine for NMDAR mediated LTP is supported by findings that show a high degree of co-localization of D-serine with NMDARs (Schell et al., 1995; 1997). The reduction of NMDAR mediated $Ca^{2+}$ entry following selective enzymatic degradation of D-serine (Mothet et al., 2000; Yang et al., 2003) also provides support to this model.

ATP is another gliotransmitter released in the CA1 region (Zhang et al., 2003). After release, ATP is converted into adenosine, which binds with presynaptic $A_1$ receptors to dampen excitatory neurotransmitter release (Pascual et al., 2005; Serrano et al., 2006), or with presynaptic $A_{2A}$ receptors to enhance excitatory neurotransmitter release (Panatier et al., 2011). This modulation of presynaptic neurotransmitter release via adenosine may set the base level of presynaptic excitability (Panatier et al., 2011). In the hypothalamus and spinal cord, astrocyte-derived ATP contributes to a form of long-term postsynaptic strengthening referred to as 'scaling' (Gordon et al., 2005; 2009) or gliogenic LTP (Kronschläger et al., 2016) via P2X7 receptors. By releasing D-serine and ATP in addition to glutamate, the combination of gliotransmitters and multiple downstream targets adds complexity and versatility to astrocyte-neuron interactions.

In addition to phasic gliotransmitter release that coincides with neuronal activity, constant release of gliotransmitters may allow astrocytes to act in a continual manner. Many studies that have demonstrated gliotransmission with a subsequent change to neuronal function in brain slices have relied on $Ca^{2+}$ or $IP_3$ uncaging techniques to selectively increase free $Ca^{2+}$ in astrocytes (Mulligan and MacVicar, 2004; Straub et al., 2006; Gordon et al., 2008). Some of these increases can be blocked with intracellular application of the high affinity $Ca^{2+}$ buffer BAPTA into astrocytes. For example, applying BAPTA via patch clamp to decrease intracellular free $Ca^{2+}$ in astrocytes has the effect of decreasing basal excitatory synaptic strength in the hippocampus (Panatier et al., 2011). This mechanism involves ATP and its conversion to adenosine, which then interacts with neurons (Panatier et al., 2011). Therefore, astrocytes may be constantly releasing ATP in a manner that is dependent on cytosolic $Ca^{2+}$ levels in order to tonically regulate synaptic strength. This highlights a possible example of astrocyte resting $Ca^{2+}$ levels playing a functional role, which may justify further investigation.

### 1.4 Neurovascular Coupling

The brain possesses the ability to regulate blood flow to localized regions in response to changes in brain activity. This allows the delivery of additional oxygen and glucose in order to meet the tissue's metabolic needs while sustaining neuronal function – this response is known as functional hyperemia (Attwell et al., 2010). Understanding the mechanisms underlying functional hyperemia is required in order to combat defective blood flow control as seen in disorders such as stroke (Kunz et al., 2007), hypertension (Girouard and Iadecola, 2006), and Alzheimer's disease (Iadecola, 2004; Girouard and Iadecola, 2006).

The special positioning of astrocytes between neurons and vasculature make astrocytes ideal for involvement in neurovascular coupling. Astrocytes possess fine processes that envelop neuronal synapses (Bushong et al., 2002), and have specialized appendages that extends towards and directly opposes nearby microvasculature, known as "endfeet" (Simard et al., 2003; Mathiisen et al., 2010). Collectively, astrocyte endfeet completely envelope the vasculature within the brain (Mathiisen et al., 2010).

Multiple molecular signals derived from arachidonic acid metabolism in astrocytes modulate blood vessel diameter in response to neuronal activity (Zonta et al., 2003; Mulligan and MacVicar, 2004). Synaptic glutamate release, which diffuses beyond the synaptic cleft and activates astrocyte mGluRs, results in elevated intracellular $Ca^{2+}$ in the astrocyte soma (Porter and McCarthy, 1996; Attwell et al., 2010). The $Ca^{2+}$ rise activates c-phospholipase $A_2$ (PLA2), which produces arachidonic acid (Zonta et al., 2003). Accumulated arachidonic acid is metabolized into prostaglandins via cyclooxygenases (COX), and into epoxyeicosatrienoic acids (EETs) via cytochrome P450 (CYP) epoxygenases (Zonta et al., 2003; Peng et al., 2004; Metea

and Newman, 2006; Gordon et al., 2008). Both prostaglandins and EETs are generated in astrocyte endfeet, where their appropriate enzymes are expressed (Amruthesh et al., 1993; Takano et al., 2006). Specifically, prostaglandin E2 (PGE2) (Zonta et al., 2003), 11,12-EET, and 14,15-EET (Amruthesh et al., 1993; Alkayed et al., 1996b; Harder et al., 1998) are major vasodilators of nearby arterioles. PGE2 produces vasodilation by relaxing vascular smooth muscle cells (Davis et al., 2004), while EETs promote dilation by directly enhancing $Ca^{2+}$ activated potassium channels ($K_{Ca}$) in smooth muscle cells (Campbell and Fleming, 2010). Additionally, arachidonic acid can be converted in smooth muscle cells to 20-hydroxy-eicosatetraenoic acid (20-HETE), a vasoconstrictor, via the enzyme CYP4A (Metea and Newman, 2006). The $Ca^{2+}$ rise in the astrocyte soma, which precedes arachidonic acid build up, can therefore result in either dilation or constriction.

The oxygen content of the extracellular space helps to select between dilation versus constriction following arachidonic acid metabolism (Gordon et al., 2008). Intracellular $Ca^{2+}$ rises in astrocyte somata result in arteriole constriction when brain slices are superfused with solution containing higher $O_2$ content (95%) than physiological values (Gordon et al., 2008). With high $O_2$, arachidonic acid metabolism favours the formation of 20-HETE (Gordon et al., 2008), and thus vasoconstriction (Metea and Newman, 2006). Conversely, a more physiological $O_2$ content (20%) leads to arteriole dilation in response to intracellular $Ca^{2+}$ rises. Enzymes that generate 20-HETE (vasoconstrictor) and EETs (vasodilator) are inhibited by nitric oxide (NO) (Roman, 2002). Lower $O_2$ results in less neuron derived NO, thus reducing the inhibition of EET production, while separately suppressing the production of 20-HETE. Hence, vasodilation is favoured. Low $O_2$ also reduces the rate of ATP synthesis, causing a rise in extracellular adenosine, which binds with adenosine $A_{2A}$ receptors on vascular smooth muscle cells to block

$Ca^{2+}$ channels that normally constrict smooth muscle (Murphy et al., 2003). Additionally, low $O_2$ reduces the rate of oxidative phosphorylation, while glycolysis is enhanced; the result is lactate accumulation in the extracellular space via glycolysis (Gordon et al., 2008). Lactate decreases PGE2 uptake via prostaglandin transporters of neurons and astrocytes, increasing extracellular PGE2, which leads to greater arteriole dilations (Gordon et al., 2008). Depending on the metabolic state of brain tissue, astrocytes favour one arachidonic acid metabolite over another in order to modulate cerebral blood flow.

### *1.4.1 Neurovascular Coupling and Extracellular $K^+$*

Extracellular $[K^+]$ may be another method through which astrocytes engage in neurovascular coupling (Attwell et al., 2010). Moderate elevations in extracellular $[K^+]$ (up to approximately 15 mM or less) result in arteriole dilation (Knot et al., 1996; Girouard et al., 2010). However, the underlying mechanisms are not yet clear.

One theory suggests that neurovascular coupling is mediated via astrocytes siphoning $K^+$ (Paulson and Newman, 1987; Knot et al., 1996; Kofuji and Newman, 2004). In this siphoning model, neuronal activity increases extracellular $K^+$, which causes $K^+$ influx into astrocytes, followed by astrocyte endfeet releasing $K^+$ directly onto arterioles (Paulson and Newman, 1987; Kofuji and Newman, 2004). Elevated $K^+$ activates inward rectifier $K^+$ channels ($K_{ir}$) on smooth muscle cells, which become hyperpolarized and closes voltage gated $Ca^{2+}$ channels, thus dilating arterioles (Knot et al., 1996). However, directly depolarizing glial cells, thereby facilitating the efflux of $K^+$ onto nearby arterioles, does not elicit vasodilation (Metea et al., 2007), which does not support the $K^+$ siphoning model.

Another $K^+$ mediated mechanism for neurovascular coupling has also been suggested. Intracellular $Ca^{2+}$ increases in astrocyte somata evoked by neuronal glutamate opens large conductance $Ca^{2+}$-activated $K^+$ (BK) channels on astrocyte endfeet, which releases $K^+$ directly onto arterioles (Filosa et al., 2006). Obstructing BK channels with genetic and pharmacological methods does seem to reduce blood flow increases in response to whisker stimulation (Filosa et al., 2006; Girouard et al., 2010). However, the location of the BK channels is not clear. Astrocytes show no transcriptome evidence of BK channels (Zhang et al., 2014), even though this channel may be a key protein involved in terminating vasoconstriction in vascular smooth muscle cells (Sachse et al., 2014). Furthermore, there is little driving force for significant $K^+$ efflux from astrocytes as these cells rest close to $E_K$ (reversal potential of $K^+$). Although investigations have yet to produce findings that contradict this theory, there are likely further gains to be made in elucidating a $K^+$ mediated mechanism for neurovascular coupling.

### *1.4.2 The Cerebrovasculature*

The vasculature populates the cortex with high density, having approximately one meter of vascular length within one microliter of cortical volume (Blinder et al., 2013). In order to supply the cortex and neighbouring areas, the vasculature within the cortex has three distinct physical features, or tiers through which blood passes through (Shih et al., 2015; Filosa et al., 2016). These are: arterioles and venules on the pial surface, the microvascular network below the pial surface, and the penetrating arterioles and venules that connect the two (Shih et al., 2015).

The pial surface of the cortex has a vast network of surface arteries and arterioles (Shih et al., 2015). The middle cerebral artery (MCA) feeds a significant portion of these vessels (Shih et al., 2015). The MCA, which emerges from the circle of Willis located near the base of the brain,

consists of a network of two-dimensional loops of branches that frequently reconnect, known as anastomoses (Blinder et al., 2010).

Branching off of surface arteries and diving into the cortex in a perpendicular direction are penetrating arterioles (Nishimura et al., 2007), which are also known as parenchymal arterioles (Filosa et al., 2016). More than 80% of penetrating arterioles are estimated to be single branches, which dive into the cortex without any further branching (Blinder et al., 2010). Penetrating arterioles have a layer of vascular smooth muscle cells (VSMCs), which are encircled by astrocyte and neuronal processes, as well as pericytes (Filosa et al., 2016). After entering the cortex, penetrating arterioles gradually branch out into pre-capillary arterioles, before forming a dense mesh of interconnected capillaries, which collectively form the microvascular network below the pial surface (Blinder et al., 2010).

Unlike the two dimensional network of surface arterioles, the microvascular network (that penetrating arterioles feed into) occupy a three dimensional space. Capillaries are located within this network, and are distributed somewhat evenly throughout (Tsai et al., 2009). However, VSMCs possessed by surface arteries and penetrating arterioles are absent in capillaries; therefore, astrocytes, neurons, and pericytes form the neurovascular unit around capillary endothelial cells (Filosa et al., 2016). Cerebral blood flow must pass through this network in order to resupply brain cells and subsequently exit the brain. Post-capillary venules of the microvascular network join to form penetrating venules that run perpendicular to the pial surface, through which blood ascends to the pial surface (Nguyen et al., 2011).

Vascular responses mediated by neurovascular coupling occur in both the penetrating arterioles and the microvascular network (Filosa et al., 2016). However, the responses may occur in the capillaries before taking place in the penetrating arterioles that feed them (Filosa et al.,

2016; Mishra et al., 2016). This could be due to separate mechanisms of neurovascular coupling at the capillaries versus penetrating arterioles (Mishra et al., 2016). The ATP receptor P2X1 mediated $Ca^{2+}$ entry raises intracellular $Ca^{2+}$ in astrocytes, generating prostaglandin E2, which binds to $EP_4$ receptors of pericytes to ultimately dilate capillaries (Mishra et al., 2016). This initial dilation, may then propagate to upstream vasculature (penetrating arteriole, then pial arteriole) via endothelial-mediated conduction (Chen et al., 2011). Another mechanism initiating conduction at the capillary level involves the effect of $K^+$ directly onto capillaries which then act as 'electrical wires' to conduct a hyperpolarizing signal up the vasculature tree (Longden et al., 2017). However, the initiating $K^+$ stimulus in this work (8-10 mM) was beyond the physiological range. Nevertheless, this may account for recent observations suggesting that neurovascular coupling via astrocyte $Ca^{2+}$ increase does not require the 'traditional' receptors mGluR5 and $IP_3R_2$, at least in adult mice (Sun et al., 2013; Bonder and McCarthy, 2014; Srinivasan et al., 2015). In contrast, arteriole dilation may require NMDAR mediated $Ca^{2+}$ entry in interneurons, facilitating NO release onto arterioles, possibly bypassing astrocytes altogether (Mishra et al., 2016). However, local astrocyte-specific effects on adjacent arterioles, independent of conduction, are also likely involved, as many studies have observed vasodilation and vasoconstriction evoked by stimulating adjacent astrocytes (Mulligan and MacVicar, 2004; Straub et al., 2006; Takano et al., 2006; Gordon et al., 2008). Taken together, it can be concluded that separate signalling mechanisms control cerebral blood flow through penetrating arterioles versus capillaries of the microvasculature, but how these separate cell pathways and separate locus of action within the vascular tree operate in a coordinated fashion is at present unclear.

### 1.5 Extracellular $K^+$ Homeostasis

During neuronal action potentials, $K^+$ ions leave depolarized neurons in order to hyperpolarize the membrane potential (Carter and Bean, 2009). Additionally, neurons have leak $K^+$ conductance that play an important role in determining resting membrane potential. Even small fluctuations in extracellular $K^+$ concentration ($[K^+]$) will shift $E_K$ (the reversal potential of $K^+$) and lead to changes in the neuronal resting membrane potential (Wang et al., 2012). Therefore, the absolute difference between the neuronal resting membrane potential and the textbook threshold of -55 mV at which action potentials are triggered (Carter and Bean, 2009) will be altered, ultimately enhancing or diminishing neuronal excitability (Wang et al., 2012). Controlling extracellular $K^+$ is not only important for modest changes in excitability; it is also critical for limiting pathological situations. In sufficiently large amounts, local application of $K^+$ in the cortex of awake, wild-type mice triggers myoclonic seizures within minutes (Rangroo Thrane et al., 2013), or can trigger waves of cortical spreading depression (Ayata and Lauritzen, 2015).

Although neuronal $Na^+/K^+$-ATPases work to restore the intracellular and extracellular ionic compositions after action potential firing (Carter and Bean, 2009), astrocytes provide an additional solution for extracellular $K^+$ homeostasis. Leak channels that are highly selective for and permeable to $K^+$ give mature astrocytes passive electrical properties (Zhou et al., 2009; Kimelberg, 2010). As a result, astrocytes have a very low membrane input resistance with a resting membrane potential close to $E_K$ (Zhou et al., 2009; Kimelberg, 2010). $K_{ir}4.1$ contributes to establishing the resting membrane potential of astrocytes, and play a significant role in buffering local $K^+$ increases (Chever et al., 2010). The sodium potassium chloride cotransporter (NKCC) is another potential means through which external $K^+$ could be managed. However,

levels of NKCC expression by astrocytes in the adult rodent brain are low (Larsen et al., 2014); therefore, NKCC is likely not involved in buffering $K^+$ increases. Increases in extracellular $K^+$ are also offset by astrocyte uptake of $K^+$ via $Na^+/K^+$-ATPase activity (Wallraff et al., 2006; Larsen et al., 2014), which could be linked to intracellular $Na^+$ increasing from glutamate uptake via EAAT1 and the need to expel excess $Na^+$ (Bergles and Jahr, 1998; Marcaggi and Attwell, 2004). These mechanisms make astrocytes able to perform extracellular $K^+$ homeostasis, and as a result, stabilize neuronal membrane potentials (Larsen et al., 2014).

Since preventing build-ups of extracellular $K^+$ is essential in order to avoid pathology, astrocytes typically help maintain a baseline extracellular $[K^+]$ of ~3 mM (Vyskocil et al., 1972; Prince et al., 1973; Katzman, 1976; Walz, 2000). Measurements using $K^+$-selective microelectrodes have revealed that in healthy brain tissue, neuronal action potentials lead to increases in extracellular $[K^+]$ ranging 1-3 mM from baseline from electrical stimulation (Somjen, 1979). Spontaneous neuronal bursts in the reticular formation increases extracellular $[K^+]$ by only 0.2 mM or less (Syková et al., 1974), and optical stimuli in the cat visual cortex *in vivo* transiently increase $[K^+]$ by 0.5 mM or less (Singer and Lux, 1975; Connors et al., 1979; Somjen, 2002). Extracellular $[K^+]$ in the central nervous system of healthy mammals is thought to have a physiological ceiling of ~5 mM (Somjen, 1979). Below this ceiling, the impact of extracellular $[K^+]$ on synaptic transmission is considered negligible (Somjen, 1979). Intense neuronal activity, especially seizures, overwhelm extracellular $K^+$ clearance mechanisms and increases $[K^+]$ up to ~12 mM (Lothman et al., 1975; Heinemann and Lux, 1977; Hansen and Zeuthen, 1981). If a stimulus is strong enough and simultaneously depolarizes a minimum volume of brain tissue (~1 $mm^3$ in rodent cortex *in vivo* (Matsuura and Bures, 1971) and even less in cortical slices (Tang et al., 2014)), multiple nonselective large-conductance cation

channels open through a process that is still not well understood (Ayata and Lauritzen, 2015). This results in an enormous $K^+$ efflux that rapidly increases extracellular [$K^+$] from a baseline of ~3 mM to a range of ~30-50 mM in an all-or-none manner (Vyskocil et al., 1972; Lothman et al., 1975; Hansen and Zeuthen, 1981), a phenomenon known as spreading depression (Matsuura and Bures, 1971; Tang et al., 2014). The massive $K^+$ efflux leads to large $Na^+$ and $Cl^-$ influx that also pulls in water, which results in widespread cell swelling (Hansen and Zeuthen, 1981), and produces an intense depolarization that prevents new action potentials. Conditions become progressively worse as extracellular [$K^+$] increases beyond physiological levels; therefore, astrocytes use $K^+$ clearance mechanisms to tightly regulate [$K^+$].

Switching between sleep-awake states can lead to fluctuations in extracellular [$K^+$] (Ding et al., 2016). Inducing sleep in mice via isoflurane anesthesia consistently leads to a sharp decrease in extracellular [$K^+$] from ~4.3 mM to ~3.7 mM (Ding et al., 2016). The lowered [$K^+$] only returns to baseline levels seen in the awake-state when anesthesia is discontinued. Sleep/awake state-dependent changes in [$K^+$] occur regardless of whether sleep occurs naturally or is induced by anesthesia, and both sleep states exhibit similar magnitudes of [$K^+$] changes versus the awake-state (Ding et al., 2016). These findings suggest that the state of being asleep or awake influences neuronal activity via modulating extracellular [$K^+$].

Astrocytes are sensitive to changes in extracellular [$K^+$] beyond simply buffering against [$K^+$] increases; changes in [$K^+$] is coupled to intracellular signaling in astrocytes (Choi et al., 2012). Small increases in extracellular $K^+$ resulting from neuronal action potentials leads to an electrogenic transport of bicarbonate ($HCO_3^-$) facilitated by the sodium-bicarbonate co-transporter (NBC) (Ransom, 1992; Schmitt et al., 2000). Bicarbonate mediates the activation of soluble adenylyl cyclase (sAC) (Zippin et al., 2001), which results in the production of the

second messenger cAMP (Chen et al., 2000). Elevated cAMP in astrocytes leads to glycogenolysis (Sorg and Magistretti, 1992) followed by the generation of lactate, which can be delivered to neurons for use as an alternate energy source, rather than glucose (Choi et al., 2012). Of note, bicarbonate is also utilized by astrocytes in order to maintain intracellular pH (Larsen and MacAulay, 2017), and the NBC is the main net acid extruder of astrocytes (Ransom, 2000; Larsen and MacAulay, 2017). Increased extracellular [$K^+$] evokes bicarbonate influx into astrocytes via NBCs, followed by alkalization (increased pH) of astrocyte cytosol (Ransom, 2000), which is equivalent to acid extrusion. Extracellular [$K^+$] increase from 3 mM to 6 mM leads to an alkaline shift of approximately 0.1 pH units (Ransom, 2000). Furthermore, bicarbonate influx also results in astrocyte swelling (Florence et al., 2012). A 3 mM increase in extracellular [$K^+$] swells astrocytes by ~9% after 10 minutes (Florence et al., 2012). Conversely, bicarbonate efflux via $GABA_A$ channels shrinks astrocytes (Florence et al., 2012). Therefore, bicarbonate influences crucial astrocyte intracellular signals by coupling to changes in extracellular [$K^+$], and is involved in neuronal metabolism (Choi et al., 2012), astrocyte intracellular pH regulation (Ransom, 2000; Larsen and MacAulay, 2017), and astrocyte volume changes (Florence et al., 2012). These examples demonstrate how astrocyte sensitivity to changes in extracellular [$K^+$] can influence crucial functions of both neurons and astrocytes.

### 1.6 Astrocyte Handling of $Cl^-$ Ions

In astrocytes, anion channels are inactive at rest, until triggered into action by a stimulus (Kimelberg et al., 2006). Due to their abundance, $Cl^-$ ions serve as the main anion and are involved in the regulation of cellular volume in numerous types of cells, including astrocytes (Kimelberg et al., 2006). Astrocytes are known to have a higher concentration of intracellular $Cl^-$

than neurons, with approximately 30 mM in astrocytes versus 5 mM in neurons (Verkhratsky and Nedergaard, 2018).

The volume regulated anion channels (VRAC) are one type of anion channel possessed by astrocytes (Kimelberg et al., 2006). Activation of $Cl^-$ conductance requires a change in astrocyte morphology, such as cell swelling (Lascola and Kraig, 1996; Kimelberg et al., 2006). This relationship to astrocyte morphology is thought to be due to the direct control of astrocyte $Cl^-$ channels by cytoskeletal actin (Lascola et al., 1998). When the extracellular space becomes hypotonic, cells of various types swell due to osmotic stress; in astrocytes, this swelling is then followed by regulatory volume decreases facilitated by VRACs (Kimelberg et al., 2006). Increased concentrations of $Na^+$ ions in the cytosol may control VRACs by inhibiting their activity (Minieri et al., 2015). Of note, VRAC activity is thought to mediate a release of glutamate that is induced by swelling (Basarsky et al., 1999; Takano et al., 2005).

One type of $Cl^-$ channel, known as $Ca^{2+}$-activated $Cl^-$ channels (CaCC), requires an increase in intracellular $Ca^{2+}$ in order to trigger channel activity (Kimelberg et al., 2006; Park et al., 2009). This has implications for electrically excitable cells, such as neurons, and indeed, CaCCs have been found to modulate the action potentials of certain hippocampal neurons (Huang et al., 2012). In astrocytes, the *Best1* gene is responsible for encoding the CaCC (Hartzell et al., 2008). Mutations of the *Best1* gene is attributed to being the primary cause of Best vitelliform macular dystrophy, a form of macular degeneration that is inherited in an autosomal dominant manner (Hartzell et al., 2008). Astrocytes are thought to make up most of the *Best1* expression in the brain (Park et al., 2009), mostly clustered in perisynaptic regions (Park et al., 2013). These *Best1* encoded CaCCs mediate $Cl^-$ currents that are blocked by the broad-spectrum $Cl^-$ channel antagonists NPPB and niflumic acid (Park et al., 2009). Of note, there are

suggestions that astrocytes may tonically release GABA through *Best1* encoded CaCCs (Lee et al., 2010); however, not everyone agrees (Diaz et al., 2011).

As previously mentioned, astrocytes utilize the movement of bicarbonate across the cell membrane in order to regulate intracellular pH; to combat intracellular acidity, astrocytes rely upon the NBC for a combined influx of $Na^+$ and bicarbonate in a 1:3 ratio, which results in increased alkalinity (Ransom, 2000). Conversely, in order to avoid excessive alkalinity in the cell, astrocytes rely on the $Cl^-$/bicarbonate exchanger, which mediates an electroneutral exchange of $Cl^-$ and bicarbonate in a 1:1 ratio, where bicarbonate gets extruded from the cell (Ransom, 2000). This is supported by observations involving the removal of extracellular $Cl^-$, which was subsequently followed by alkalization of the cytosol, in astrocytes located in both the cerebellum (Brune et al., 1994) and the cortex (Mellergård et al., 1993; Shrode and Putnam, 1994). These observations held true in the absence of external $Na^+$, and only when pH was elevated beyond baseline (Shrode and Putnam, 1994). Of note, the astrocytic $Cl^-$/bicarbonate exchanger is likely not the same $Cl^-$/bicarbonate exchanger found in neurons. Neurons express anion exchanger 3 (Ruffin et al., 2014), whereas astrocytes do not express this subtype (Salameh et al., 2017).

### *1.6.1 $K^+$-$Cl^-$ Cotransporters (KCCs)*

$K^+$-$Cl^-$ cotransporters (KCC) are one of two groups categorized as electroneutral cation-chloride cotransporters (CCCs), the other being the $Na^+$-$K^+$-$Cl^-$ cotransporter (NKCC) (Arroyo et al., 2013). Both KCCs and NKCCs function as ion transporters on the plasma membrane (Arroyo et al., 2013). While NKCCs rely on $Na^+$ gradients across the cell membrane to import $Cl^-$ into cells, KCCs rely on $K^+$ gradients to drive the export of $Cl^-$ out of cells (Gamba, 2005; Arroyo et al., 2013). Seeing that $[Cl^-]_i$ plays an important role in volume regulation, the balance of $Cl^-$ entry

and extrusion from a given cell through both of these transporters may help set a "baseline" for cellular volume (Ringel and Plesnila, 2008; Kahle et al., 2009). KCCs are known to exist in four isoforms, which are numbered from KCC1 to KCC4 (Mount et al., 1999; Race et al., 1999; Song et al., 2002; Gagnon et al., 2007). KCC1 is widely expressed across various types of tissues, and a physiological role that is specific to KCC1 has yet to be identified. However, a double knockout with KCC3 may have physiological significance for red blood cell volume regulation (Rust et al., 2007). KCC2 expression is specific to neurons (Rivera et al., 1999; Song et al., 2002), while KCC3 is widely expressed throughout the CNS, the heart/vasculature, and the kidneys (Mount et al., 1999; Rust et al., 2006). KCC4 expression is predominantly in tissues of the kidney, heart, lung, and liver (Mount et al., 1999).

In mature neurons, a key determinant of low $[Cl^-]_i$ is the upregulation of the $K^+$-$Cl^-$ cotransporter 2 (KCC2) during maturation, which is maintained in mature neurons and is a $Cl^-$ extruder specific to neurons (Rivera et al., 1999; Song et al., 2002). Deficiencies or an absence of KCC2 results in higher $[Cl^-]_i$, which reduces the inhibitory influence of GABA acting on ionotropic $GABA_A$Rs, which rely on a large $Cl^-$ gradient (Rivera et al., 1999; Hübner et al., 2001; Song et al., 2002). Moreover, increases in $[Cl^-]_i$ due to deficient KCC2 have been implicated in various neurological disorders, such as epilepsy (Palma et al., 2006), neuropathic pain (Coull et al., 2003), and spasms due following spinal cord injury (Boulenguez et al., 2010). These findings suggest that the role of KCC2 in regulating the $[Cl^-]_i$ of neurons is crucial in order for neurons to function properly.

In astrocytes, KCCs regulate intracellular $[Cl^-]$ and are involved in the regulation of cell volume (Adragna et al., 2004; Benesova et al., 2012). Astrocytes, like many other cell types, defensively respond to increases in cellular volume (which can be harmful if left unchecked) by

undergoing a phenomenon known as regulatory volume decrease (RVD) (Pedersen et al., 2011). Conversely, cellular shrinkage is followed by regulatory volume increase (RVI) (Pedersen et al., 2011). KCCs, which facilitate the electrogenic neutral extrusion of $K^+$ and $Cl^-$ in a 1:1 ratio (Lauf and Adragna, 2000), contribute to regulatory volume decreases due to water molecules subsequently following the ions exiting the cell (Lauf and Adragna, 2000; Ringel and Plesnila, 2008). In contrast, the NKCCs work towards cell swelling through the influx of $Na^+$, $K^+$, and $Cl^-$ ions in a 1:1:2 ratio (Kahle et al., 2009) in order to achieve RVI. The combination of functional KCCs and NKCCs, when in balance, are thus believed to exert control over the opposing phenomena of swelling and shrinking in astrocytes (Ringel and Plesnila, 2008; Kahle et al., 2009). However, unlike cultured astrocytes, NKCC1 is not highly expressed by astrocytes in rat brain tissue (Larsen et al., 2014). Interestingly, very high extracellular [$K^+$] (25 mM and higher) may result in KCCs of retinal Müller cells operating in reverse, resulting in cell swelling (Ochoa-de la Paz et al., 2005). While this particular investigation was performed beyond physiological levels of extracellular [$K^+$] with a different type of cell (Ochoa-de la Paz et al., 2005), these findings are consistent with the role of KCCs in cell volume regulation and are noteworthy for the work presented here because they additionally suggest that smaller elevations in external $K^+$ slow $K^+$ extrusion through KCCs.

One of the first ideas regarding mechanisms regulating the sensitivity of KCCs to cellular swelling suggested that KCCs were activated by dephosphorylation, whereas phosphorylation inhibited KCCs (Jennings and Schulz, 1991). A combination of cellular swelling, accumulation of intracellular $Cl^-$, and activity of protein phosphatases, which results in the dephosphorylation of two threonine sites within the C terminus of KCCs (referred to as site 1 and site 2), leads to the activation of the cotransporter itself (Piechotta et al., 2002; de Los Heros et al., 2014). In

contrast, cellular shrinking, depletion of intracellular $Cl^-$, and inhibition of protein phosphatases leads to the phosphorylation of the two threonine sites within the C terminus, and ultimately results in the inhibition of KCC activity (Piechotta et al., 2002). Of note, the same set of conditions that activate KCCs by dephosphorylation of the two threonine sites within the C terminus of KCCs, also inhibits NKCCs via threonine sites within the N terminus (Piechotta et al., 2002). Mutation of both threonine residues in KCCs to alanine, which prevents phosphorylation at those sites, results in KCCs that stay active with a ~25-fold increase in activity versus wildtype KCCs (de Los Heros et al., 2014). The two threonine residues in the C terminus, while having slight variations in the exact position amongst all four KCC isoforms, thus serve as the primary regulatory points for KCC sensitivity to cellular volume (de Los Heros et al., 2014).

Isoforms of lysine deficient protein kinases (WNK), which are serine/threonine kinases, have been identified as a regulator of KCC activity (de Los Heros et al., 2014). Inhibition of WNK1 via small interfering RNA (siRNA) knockdown results a partial prevention of phosphorylation at regulatory threonine sites (site 1 and site 2) in the C terminus of KCC3 (Rinehart et al., 2009). While overexpression of WNK2 and WNK3 isoforms suppresses KCC activity, overexpression of dominant-negative WNK3 drastically increases KCC activity by at least 100-fold (de Los Heros et al., 2006). The substrates of WNK kinases are SPS1-related proline/alanine-rich kinase (SPAK) and oxidative stress-responsive kinase 1 (OSR1) (de Los Heros et al., 2014). When activated by WNK, SPAK/OSR1 activity (along with a regulatory subunit MO25) results in the inhibition of all four isoforms of KCC via phosphorylation of site 2 (de Los Heros et al., 2014). In *Drosophila*, KCC knockdown in glia contributed to reduced seizure thresholds via impaired regulation of cellular volume and regulation of ion contents in

the extracellular space (Rusan et al., 2014). These findings suggest that impairments in cellular volume regulation via KCCs have negative physiological consequences.

### *1.6.2 Astrocyte Swelling Independent of Cl⁻ or KCCs*

Astrocytes contribute to the regulation of extracellular space volume by passing water through aquaporin channels (Nagelhus and Ottersen, 2013). The vast majority of aquaporin channels in astrocytes consist of aquaporin 4 (AQP4) (Nagelhus and Ottersen, 2013), with robust expression found in astrocytes of the cerebellum, hippocampus, and cortex (Hubbard et al., 2015). Expression is concentrated at perivascular endfeet; despite their colocalization with $K_{ir}4.1$ channels in endfeet (Amiry-Moghaddam and Ottersen, 2003), evidence suggests that these channels function independently of each other (Zhang and Verkman, 2008). Passage of water through AQP4 is bidirectional (Nagelhus and Ottersen, 2013) – genetic deletion of AQP4 has led to both increases (Yao et al., 2008) and reductions (Haj-Yasein et al., 2012) of the extracellular space volume. Differences in directionality may be due to different stimuli that trigger AQP4 activity, i.e. following neuronal activity (Haj-Yasein et al., 2012).

### *1.6.3 KCCs and the vasculature*

As previously mentioned, there are four isoforms of KCCs (KCC1-4) (Mount et al., 1999; Race et al., 1999; Song et al., 2002; Gagnon et al., 2007). All isoforms are expressed in the nervous system (Mount et al., 1999; Karadsheh et al., 2004; Benesova et al., 2012; Medina et al., 2014), whereas KCC3 is particularly important in the cardiovascular system (Mount et al., 1999; Rust et al., 2006). Interestingly, *KCC3*$^{-/-}$ mice eventually acquire a combination of neurological impairments (Boettger et al., 2003; Coull et al., 2003) and abnormally high blood pressure

(Boettger et al., 2003; Adragna et al., 2004; Rust et al., 2006). While KCC3 knockout mice have significantly higher arterial blood pressure, their heart rates were comparable to wildtype mice (Boettger et al., 2003; Adragna et al., 2004). Higher arterial blood pressure in KCC3 knockout mice are observed regardless of whether measurements are made during the day (when mice are normally inactive), or when made during the night (when mice are normally active) (Adragna et al., 2004). Of note, KCC3 knockout mice have been found to consume a 22% greater volume of water than wildtype mice over a period of 24 hours (Adragna et al., 2004). Moreover, vascular smooth muscle cells (VSMCs) of small arteries and arterioles express both KCC3 (Di Fulvio et al., 2001) and $Ca^{2+}$-activated $Cl^-$ channels (CaCCs) (Large and Wang, 1996). However, while the cerebrovasculature of *KCC3*$^{-/-}$ mice are hypertensive, vascular smooth muscle tone regulation may occur independent of KCC3 (Rust et al., 2006). This suggests that the cause of hypertension seen in *KCC3*$^{-/-}$ mice may not be intrinsic to the VSMCs per se, but instead may be due to upstream mechanism(s), which originate externally, acting on VSMCs (i.e. neurogenic hypertension). Taken together, these findings suggest that the activity of KCC3 in particular may play a crucial role for cerebrovascular health.

### 1.7 Hypothesis

Further elucidation of the mechanisms underlying the functions of astrocytes amongst neurons and vasculature is very important. Comprehensive understanding of processes during "normal" conditions in healthy tissue will allow for the accurate localization of deficits when things go awry in disease states. Evident by a relatively limited literature, there is still a great deal to be discovered about the physiological mechanisms of how astrocytes respond to modest changes in extracellular $K^+$. Elevated extracellular $K^+$ is a commonly occurring consequence of

neuronal action potentials that astrocytes help to mitigate; however, extracellular $K^+$ levels are coupled to intracellular processes of astrocytes that may regulate unknown physiological functions. Moreover, a rise in extracellular $K^+$ is a vasoactive phenomenon with consequences for brain blood flow. Despite the implications within both neuronal and vascular realms, the mechanism(s) through which elevations in extracellular $K^+$ originating from neurons translates to astrocyte functions and dilations of the parenchymal arterioles is still poorly understood.

A preliminary observation in the Gordon lab has led us to investigate the effects of elevating extracellular $K^+$ on astrocyte resting $Ca^{2+}$. While experimentally bath applying 'physiological' increases in $K^+$, which is known to dilate arterioles, we observed a large drop in resting free astrocyte $Ca^{2+}$ in the soma and endfeet, which could not be accounted for by dye dilution from an accompanying cell volume increase. This observation leads us to test the **hypothesis that modest changes to the extracellular $K^+$ concentration controls astrocyte resting free $Ca^{2+}$ and impacts arteriole tone.**

# CHAPTER TWO: MATERIALS AND METHODS

## 2.1 Acute Brain Slice Preparation

Care and use of animals for this project was carried out in accordance with approved guidelines set forth by the University of Calgary Animal Care and Use Committee. Male Sprague Dawley rats (P21-P30) were deeply anaesthetized with gaseous isofluorane (5%) and then decapitated using a rodent guillotine. The brain was rapidly and surgically removed, then submerged for ~2 minutes in ice-cold slicing solution containing (in mM): 119.9 N-methyl-D-glucamine, 2.5 KCl, 25 $NaHCO_3$, 1.0 $CaCl_2$-$2H_2O$, 6.9 $MgCl_2$-$6H_2O$, 1.4 $NaH_2PO_4$-$H_2O$, and 20 D-glucose. The brain was then Krazy Glued onto a vibratome tray (Leica Instruments, VT1200S) and then re-submerged in ice-cold slicing solution. Acute coronal slices were prepared from the somatosensory cortex (400 μm thick). The slices were incubated for 45 minutes at 33ºC in a recovery chamber filled with artificial cerebrospinal fluid (ACSF) containing (in mM): 126 NaCl, 2.5 KCl, 25 $NaHCO_3$, 1.3 $CaCl_2$-$2H_2O$, 1.2 $MgCl_2$-$6H_2O$, 1.25 $NaH_2PO_4$-$H_2O$, 10 glucose. At all steps of tissue preparation and for all experiments using bicarbonate buffered ACSF, the brain/slices were continuously bubbled with carbogen (95% oxygen, 5% carbon dioxide).

## 2.2 Contents of Various ACSF Solutions

High $K^+$ ACSF was bath applied in order to raise external [$K^+$] to 5.0 mM. In order to keep high $K^+$ ACSF solutions iso-osmotic with regular ACSF, the solutions were prepared by adding additional KCl to achieve 5.0 mM while an equimolar amount of NaCl was removed. This solution contained (in mM): 123 NaCl, 5 KCl, 25 $NaHCO_3$, 1.3 $CaCl_2$-$2H_2O$, 1.2 $MgCl_2$-$6H_2O$, 1.25 $NaH_2PO_4$-$H_2O$, 10 glucose. For all experiments using bicarbonate buffered ACSF, the brain slices were continuously bubbled with carbogen (95% oxygen, 5% carbon dioxide).

In bicarbonate-free experiments, slices will be transferred into 4-(2-hydroxyethyl)-1-piperazineethanesulfonic acid (HEPES) buffered ACSF after the 45 minute incubation (mentioned above) in bicarbonate buffered ACSF. The HEPES buffered ACSF contains (in mM): 142 NaCl, 2.5 KCl, 10 HEPES, 1.3 $CaCl_2$-$2H_2O$, 1.2 $MgCl_2$-$6H_2O$, 1.25 $NaH_2PO_4$-$H_2O$, 10 glucose. The HEPES buffered ACSF used to increase extracellular [$K^+$] to 5.0 mM contains (in mM): 139 NaCl, 5 KCl, 10 HEPES, 1.3 $CaCl_2$-$2H_2O$, 1.2 $MgCl_2$-$6H_2O$, 1.25 $NaH_2PO_4$-$H_2O$, 10 glucose. For all experiments using HEPES buffered ACSF, the brain slices were continuously bubbled with 100% oxygen and pH corrected with NaOH to 7.4.

For experiments substituting $Na^+$, NaCl was replaced with choline chloride ($C_5H_{14}ClNO$) in order to maintain $Cl^-$ levels and osmolarity. This solution contained (in mM): 126 $C_5H_{14}ClNO$, 2.5 KCl, 25 $NaHCO_3$, 1.3 $CaCl_2$-$2H_2O$, 1.2 $MgCl_2$-$6H_2O$, 1.25 $NaH_2PO_4$-$H_2O$, 10 glucose. The ACSF used to increase extracellular [$K^+$] to 5.0 mM with this substitution contained (in mM): 123 $C_5H_{14}ClNO$, 5 KCl, 25 $NaHCO_3$, 1.3 $CaCl_2$-$2H_2O$, 1.2 $MgCl_2$-$6H_2O$, 1.25 $NaH_2PO_4$-$H_2O$, 10 glucose. Brain slices were continuously bubbled with carbogen (95% oxygen, 5% carbon dioxide).

For experiments substituting $Cl^-$, NaCl was replaced with sodium gluconate ($C_6H_{11}NaO_7$) in order to maintain $Na^+$ levels and osmolarity. This solution contained (in mM): 126 $C_6H_{11}NaO_7$, 2.5 KCl, 25 $NaHCO_3$, 1.3 $CaCl_2$-$2H_2O$, 1.2 $MgCl_2$-$6H_2O$, 1.25 $NaH_2PO_4$-$H_2O$, 10 glucose. The ACSF used to increase extracellular [$K^+$] to 5.0 mM with this substitution contained (in mM): 123 $C_6H_{11}NaO_7$, 5 KCl, 25 $NaHCO_3$, 1.3 $CaCl_2$-$2H_2O$, 1.2 $MgCl_2$-$6H_2O$, 1.25 $NaH_2PO_4$-$H_2O$, 10 glucose. Brain slices were continuously bubbled with carbogen (95% oxygen, 5% carbon dioxide).

In experiments removing external $Ca^{2+}$, $Ca^{2+}$ free ACSF external solutions were made. This solution contained (in mM): 126 NaCl, 2.5 KCl, 25 $NaHCO_3$, 1.2 $MgCl_2$-$6H_2O$, 1.25 $NaH_2PO_4$-$H_2O$, 10 glucose. The $Ca^{2+}$-free solution used to increase extracellular $[K^+]$ to 5.0 mM contained (in mM): 123 NaCl, 5 KCl, 25 $NaHCO_3$, 1.2 $MgCl_2$-$6H_2O$, 1.25 $NaH_2PO_4$-$H_2O$, 10 glucose. Brain slices were continuously bubbled with carbogen (95% oxygen, 5% carbon dioxide).

**2.3 Loading Dyes in Astrocytes, Neurons, and Arterioles**

After recovery from slicing, the tissue was incubated in a 3 mL well at 33ºC for 45 minutes with the calcium indicator Rhodamine-2 acetoxymethyl ester (Rhod-2 AM) (15 μM) and the morphological dye Calcein Green AM (17 μM) (Biotium, Fremont, CA, USA); 0.2% DMSO; 0.006% Pluronic Acid; 0.0002% Cremophore EL. During incubation in the small well, slices received very fine carbogen bubbling using a flexible 34 gauge pipette tip (WPI, Sarasota, FL, USA). This dual labelling allowed us to take a ratio of the changes in the fluorescence of the calcium indicator over that of the changes in the morphological dye. Astrocytes were identified by their bright uptake of Rhod-2 AM and by their perivascular endfeet (Simard et al., 2003; Mulligan and MacVicar, 2004). Rhod-2 and Calcein trace data were independently normalized ($F = F_1/F_0$) – where F is fluorescence, $_1$ is any given time point and $_0$ is an average baseline value – followed by a ratio of the two ($F_{Rhod\text{-}2}/F_{Calcein}$).

For experiments that examined parenchymal arterioles, the animal received a tail vein injection of 15 mg Fluorescein Isothiocyanate (FITC) dextran (2000 kDa, Sigma Aldrich) dissolved in 300 μL of lactated Ringer's solution under isoflurane anesthesia (5% induction, 2% maintenance) before decapitation. Luminal FITC-dextran permitted visualization of the brain

microvasculature and the arteriole diameter was quantified as a change in lumen area. For an experiment, a given slice was transferred to a superfusion chamber on the rig and was perfused using a pressure driven (carbogen) solution delivery system at ~1.0 mL per minute, maintained at room temperature. For experiments examining arterioles, the thromboxane A2 analog U46619 (100 nM) was present continually in the bath to provide constant artificial tone, as was done previously (Institoris et al., 2015).

### 2.4 Two-Photon Fluorescence Microscopy

Slices were imaged using a custom built two-photon microscope (Rosenegger et al., 2014) fed by a Ti:Sapph laser source (Coherent Ultra II, ~4 W average output at 800 nm, ~80 MHz). Image data were acquired using MatLab (2013) running an open source scanning microscope control software called ScanImage (version 3.81, HHMI/Janelia Farms) (Pologruto et al., 2003). Imaging was performed at an excitation wavelength of 850 nm for Rhod-2/Calcein experiments. The microscope was equipped with a primary dichroic mirror at 695 nm and green and red fluorescence was split and filtered using a secondary dichroic at 560 nm and two bandpass emission filters: 525-40 nm and 605-70 nm (Chroma Technologies). Time series images were acquired at 0.98 Hz with a pixel density of 512 by 512 and a field of view size of ~150 μm. Imaging used an Olympus 40x water dipping objective lens (NA 0.8, WD 3.0 mm).

### 2.5 Fluorescence Lifetime Imaging Microscopy (FLIM)

**Time resolved fluorescent lifetime imaging:** Acute slices from Sprague Dawley rats (P21-28) were incubated in 1 μM SR101 to load astrocytes for identification for whole-cell patch clamp. The pipette recording solution consisted of (in mM): 113 K-Gluconate, 3 KCl, 8 Na-

Gluconate, 2 $MgCl_2$, 4 $K_2ATP$, 0.3 NaGTP, 10 HEPES, 1 EGTA, 0.23 $CaCl_2$, 0.2 OGB-1 Hexapotassium salt (Thermo Fischer), pH and osmolarity adjusted to 7.25 (with KOH) and 290 mOsm, respectively. SR101 positive cells were whole-cell patch clamped and were dialyzed for at least 20 min prior to imaging to permit sufficient OGB-1 dye dialysis to gap-junctionally coupled neighbours. FLIM images were acquired with a Zeiss LSM 7 imaging system retrofitted with FLIM hardware module (SPC-150) from Becker Hickl. OGB-1 was imaged at 800nm using a tunable pulsed 2-photon Ti:Sa femtosecond laser (Coherent) with a 80MHz repetition rate and a 20X water immersion objective (NA=1). Individual images were acquired at 256x256 (x,y) pixels, 32 frame scans per image, with images acquired in 30s intervals to avoid phototoxicity. Lifetime decay data from individual pixels were binned with neighbouring pixels by a factor of 2 to ensure at least 10 photon counts were present at the end of each trial and ensuring proper exponential fitting. The lifetime data were fit based on a 2-component multiexponential decay calculation using Becker & Hickl's SPCImage (version 6.5) software based on goodness of fit. Raw data are presented as 'Tau mean' ($\tau_{mean}$), encompassing the weighted contributions of each component of the full decay curve and is expressed as: $\tau_{mean} = \alpha_1\tau_1 + \alpha_2\tau_2$ , where $\alpha_1$ and $\alpha_2$ represent the fractional relative intensities (i.e. $\alpha_1+\alpha_2=1$) of the respective tau components $\tau_1$ and $\tau_2$ . Mean lifetime was used over 'intensity-weighted average lifetime' (i.e. decay components weighted by intensity integrals) as $\tau_{mean}$ calculations are more sensitive to changes at fast lifetimes and therefore low $Ca^{2+}$ concentrations (Becker, 2012). Calculated $\tau_{mean}$ data were compared to their respective $Ca^{2+}$ concentrations via *in vitro* calibration (below).

***in vitro* OGB-1 Lifetime Calibration:** OGB-1 calibration was performed in sealed recording electrodes at 33$^{o}$C similar to that described previously (Zheng et al., 2015). Electrodes were filled with an electrophysiological recording solution consistent of (in mM): 93 K-

Gluconate, 8 Na-Gluconate, 2 $MgCl_2$, 4 $K_2ATP$, 0.3 NaGTP, 10 HEPES, 10 EGTA, 0.2 OGB-1 hexapotassium salt. 1.17-20,000nM of free $Ca^{2+}$ (added as $CaCl_2$) was calculated using Webmaxc Standard (http://web.stanford.edu/~cpatton/webmaxcS.htm) and balanced accordingly with KCl and pH adjusted to pH=7.25 with KOH. Note that OGB-1 lifetimes are not affected by changes in pH, temperature, or viscosity (Zheng et al., 2015). Calibration data were fit to a four-variable logistic (sigmoid) function: Y=-4.87*10^6+(3300+4.87*10^6)/(1+10^((2.075-X)*1.573)), where Y = Tau(mean) and X= calcium concentration.

**2.6 Enriched Environment**

For the enriched animal experiments, 7 Sprague Dawley rats (P21 to P42-45) lived communally in an enriched environment, which was approximately 2 feet x 1.5 feet x 1.5 feet in size for 3 weeks. Within this environment were: a running wheel, tunnels, ladders, hammocks, shelters, and readily accessible food and water.

**2.7 Astrocyte Patch-Clamp**

To be selected for patch-clamp, astrocytes were required to be located between ~25 to 40 μm below the surface of the slice and within ~30 to 50 μm from the arteriole of interest. A Giga-Ohm seal was maintained for 5 minutes, followed by a whole-cell configuration with 15 minutes of astrocyte filling for adequate diffusion of the internal solution into the astrocyte network. AlexaFluor-488 sodium hydrazide (100-200 μM) was included in the intracellular solution in order to visualize the extent of solution diffusion throughout the astrocyte network. The intracellular solution also contained (in mM): 108 potassium gluconate, 8 KCl, 8 sodium gluconate, 2 $MgCl_2$, 10 HEPES, 1.0 potassium EGTA, 4 ATP, and 0.3 sodium GTP. Moreover,

the solution was corrected for osmolarity to ~285 mosmol and corrected for pH with KOH to 7.2. The astrocyte cell type was confirmed by the following: a low input resistance (10-20 MΩ), extensive dye transfer between coupled cells via gap junctions, and visibly loaded endfeet apposed to microvasculature.

### 2.8 Data Collection

In a given experiment, if more than one astrocyte was imaged in the field of view (typical), the normalized ratios from each were averaged together for an 'n' of 1. Thus, each experiment, conducted on an independent brain slice constituted a statistical 'n' and all data sets used at least N=3 animals. Imaging data were stored on a computer for off-line analysis using ImageJ and GraphPad Prism (Version 6). Experimental values are presented as mean ± SEM; statistical analyses were performed using two-tailed student's t-test (paired or unpaired as appropriate). Values of $p<0.05$ were accepted as statistically significant (* = $p<0.05$, ** = $p<0.01$, *** = $p<0.001$, **** = $p<0.0001$).

# CHAPTER THREE: RESULTS

## 3.1 Modest changes in external $[K^+]_o$ bidirectionally control astrocyte resting free $Ca^{2+}$ and soma volume

The level of extracellular potassium ($[K^+]_o$) fluctuates with neural activity (Somjen, 1979) and, along with the other main ionic constituents of the brain interstitial space, $K^+$ displays state-dependent and stable changes in concentration between sleep, wake or anesthesia (Ding et al., 2016). Astrocytes are key regulators and responders to changes in $[K^+]_o$ via $Ca^{2+}$ independent mechanisms within and slightly beyond the physiological $[K^+]_o$ range. We tested the hypothesis that astrocytes exhibit changes to free intracellular $Ca^{2+}$ in response to modest changes in $[K^+]_o$. If supported, this would open up new experimental avenues to explore $Ca^{2+}$ dependent effects in astrocytes initiated by $K^+$ and any subsequent impact on neurons or vasculature. Using two-photon fluorescence imaging, we bath applied isosmotic high $[K^+]_o$ solutions onto acute slices of the somatosensory cortex from Sprague Dawley rats. Slices were bulk loaded with the bright, relatively high-affinity $Ca^{2+}$ indicator Rhod-2/AM, along with the morphological dye Calcein/AM. Astrocytes are known to respond to isosmotic increases in $[K^+]_o$ with volume increases (Florence et al., 2012), which may obscure the detection of small changes in free $Ca^{2+}$; thus we took the ratio of the normalized Rhod-2 fluorescence signal over the normalized Calcein fluorescence signal to correct for apparent decreases in $Ca^{2+}$ that were the result of cell swelling (Figure 1A). Indeed, we observed decreases in both the Rhod-2 $Ca^{2+}$ signal and Calcein signal in response to a +2.5 mM $[K^+]_o$ challenge (going from 2.5 mM to 5 mM $K^+$), yet interestingly, the drop in Rhod-2 fluorescence was nearly double that of the morphological fluorescence (Figure 1B). This suggested a decrease in $[Ca^{2+}]_i$ beyond that predicted by a cell volume increase alone. Quantifying the Rhod-2/Calcein ratio revealed a highly significant decrease in response to a +2.5

mM $[K^+]_o$ challenge due to the high fidelity/repeatability of the phenomenon between different astrocytes in a given image sequence and between separate slice experiments (-16.9 ± 1.5%, $p<0.0001$, n=9, Figure 1C-E). As physiological increases in $[K^+]_o$ likely do not exceed 1 mM above baseline (Somjen, 1979), we tested if we could detect a shift in astrocyte steady-state $Ca^{2+}$ in response to a +1 mM challenge. Increasing $[K^+]_o$ from 2.5 mM to 3.5 mM similarly decreased $Ca^{2+}$ (-13.4 ± 0.7%, p=0.0003, n=4) but to a lesser degree than a +2.5 mM challenge. Moving beyond the physiological range, a +5 mM challenge (2.5 to 7.5 mM) caused a proportionally larger drop in astrocyte $Ca^{2+}$ (-28.2 ± 2.3%, p=0.0011, n=4). Due to up and down shifts in steady-state $[K^+]_o$ observed *in vivo* (Ding et al., 2016), next we pondered whether decreasing $[K^+]_o$ would produce an opposite effect. For this experiment, we maintained our slices in 3.5 mM $K^+$ and decreased $[K^+]_o$ to 2.5 mM (-1 mM $K^+$ challenge) and found a significant increase in astrocyte free $Ca^{2+}$ (+6.7 ± 2.4%, p=0.0467, n=5, Figure 1F,G) (dose response summary Figure 1H). These data suggest that external $[K^+]_o$ controls the resting steady-state free $Ca^{2+}$ concentration in astrocytes in a bidirectional manner.

Finally, we confirmed a previously described volume increase in astrocytes to a modest elevation in $[K^+]_o$. A +2.5 mM $[K^+]_o$ challenge increased soma area (+12.4 ± 1.2%, p=0.0001, n=6, Figure 1I,J,L), which also supported our observed decrease in the morphological Calcein signal. However, expanding on previous findings, we found these volume changes were bidirectional in nature and occurred in response to smaller changes in $[K^+]_o$, similar to what we observed for astrocyte $Ca^{2+}$. For example, a -1 mM $[K^+]_o$ test decreased soma area (Figure 1K). Collectively, these data suggest that $[K^+]_o$ within and slightly beyond the physiological range bidirectionally controls free $Ca^{2+}$ in astrocytes, along with cell volume.

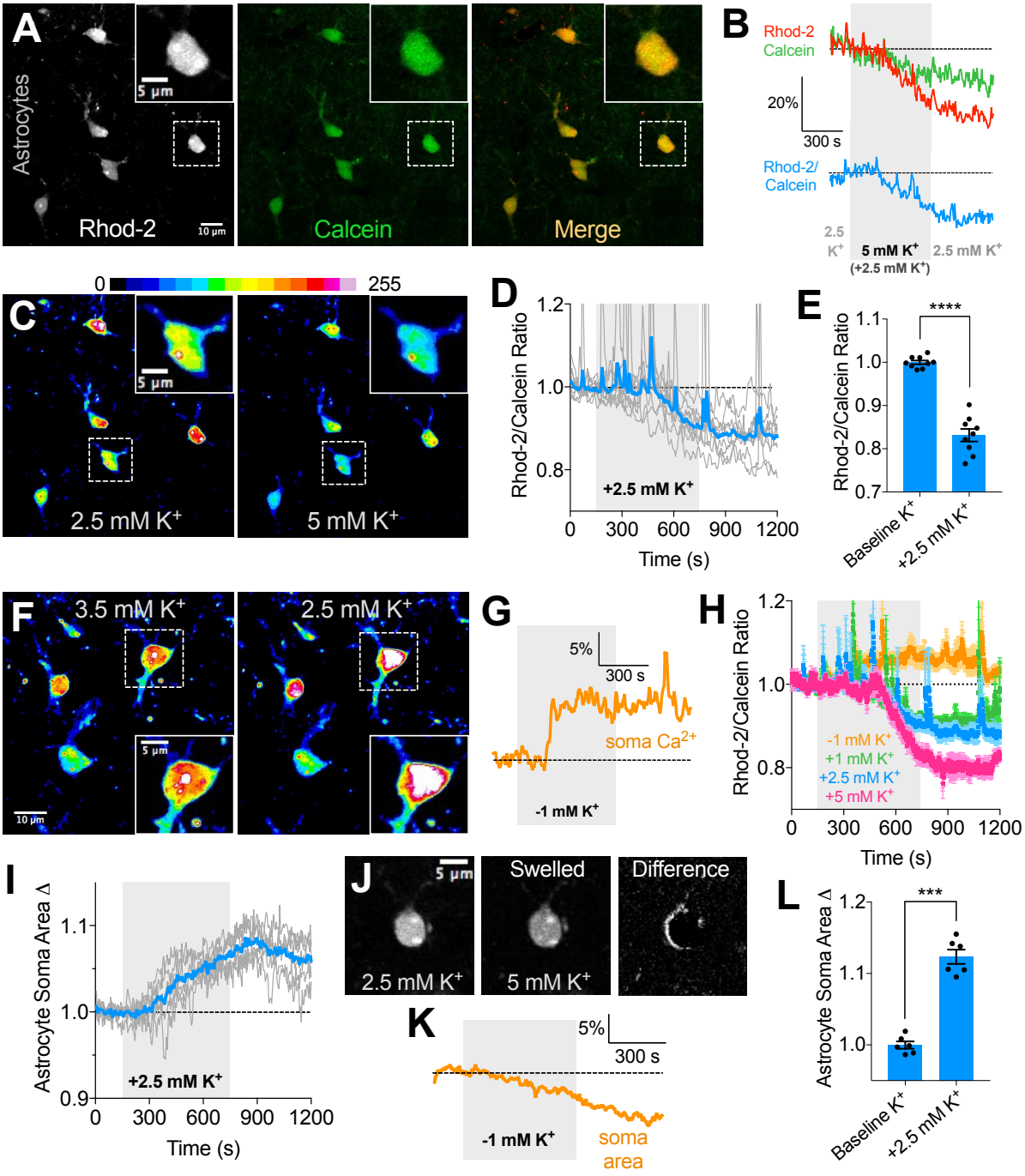
A
Astrocytes
5 µm
Rhod-2
10 µm
Calcein
Merge
B
Rhod-2
Calcein
20%
300 s
Rhod-2/
Calcein
2.5
K+
5 mM K+
2.5 mM K+
(+2.5 mM K+)
0
255
C
5 µm
2.5 mM K+
5 mM K+
D
Rhod-2/Calcein Ratio
1.2
1.0
0.8
+2.5 mM K+
0
300
600
900
1200
Time (s)
E
Rhod-2/Calcein Ratio
1.1
1.0
0.9
0.8
0.7
****
Baseline K+
+2.5 mM K+
F
3.5 mM K+
2.5 mM K+
5 µm
10 µm
G
5%
300 s
soma Ca2+
-1 mM K+
H
Rhod-2/Calcein Ratio
1.2
1.0
0.8
-1 mM K+
+1 mM K+
+2.5 mM K+
+5 mM K+
0
300
600
900
1200
Time (s)
I
Astrocyte Soma Area Δ
1.1
1.0
0.9
+2.5 mM K+
0
300
600
900
1200
Time (s)
J
5 µm
Swelled
Difference
2.5 mM K+
5 mM K+
K
5%
300 s
-1 mM K+
soma
area
L
Astrocyte Soma Area Δ
1.2
1.1
1.0
***
Baseline K+
+2.5 mM K+

**Figure 1: Modest changes in external $[K^+]$ bidirectionally control astrocyte resting free $Ca^{2+}$ and soma volume**

**A**) Astrocytes in an acute somatosensory cortical brain slice co-loaded with Rhod-2/AM (left) and Calcein/AM (middle). Inset images show a close-up of a single astrocyte soma. **B**) Normalized Rhod-2 and Calcein traces (upper) measured from an astrocyte soma and the corresponding ratio (lower) in response to a modest $[K^+]_o$ challenge (+2.5 mM): from 2.5 mM to 5 mM (grey bar) back to 2.5 mM. **C**) Pseudo coloured Rhod-2 images showing the decrease in $Ca^{2+}$ signal to a +2.5 mM $[K^+]_o$ increase. **D**) $Ca^{2+}$ trace summary showing individual experiment traces (grey) and overall average (blue). **E**) $Ca^{2+}$ summary showing the peak of effect of individual experiments (peaks at different time points for each) for the +2.5 mM $[K^+]_o$ increase. **F**) Pseudo coloured Rhod-2 images showing the increase in astrocyte $Ca^{2+}$ signal to a -1.0 mM $[K^+]_o$ decrease. **G**) $Ca^{2+}$ trace from a single experiment showing the $Ca^{2+}$ increase from a $[K^+]_o$ decrease of 1 mM. **H**) $Ca^{2+}$ summary trace data showing the dose response to $[K^+]_o$ changes. **I**) Astrocyte soma area measures showing individual experiment traces (grey) and overall average (blue) to the +2.5 mM $[K^+]_o$ challenge. **J**) Images depicting the soma volume increase. Difference image subtracts the large volume astrocyte from the small volume state. **K**) Soma area trace from one experiment showing a decrease in cell area when $[K^+]_o$ is decreased by 1 mM (3.5 to 2.5 mM). **L**) Soma area summary showing the peak of effect of individual experiments for the +2.5 mM $[K^+]_o$ increase experiments. *** $p<0.001$, **** $p<0.0001$

### 3.2 FLIM reveals a quantitative decrease in astrocyte free $Ca^{2+}$ in response to a modest elevation in external $K^+$

To test the idea that a modest increase in external $K^+$ causes a bon-a-fide decrease in the resting free $Ca^{2+}$ concentration in astrocytes, we performed two-photon Fluorescence Lifetime Imaging Microscopy (FLIM). This is a quantitative method for assessing cell $Ca^{2+}$ in which measurements are independent of dynamic changes in dye concentration, or to changes in optical properties of tissue. Though Rhod-2 exhibits excellent two-photon absorbance (So et al., 2000) and readily loads astrocytes (Mulligan and MacVicar, 2004), a higher affinity dye such as OGB-1 ($K_d$ ~170 nM vs $K_d$ ~550 nM for Rhod-2) used with FLIM would help circumvent the potential problems associated with standard two-photon fluorescence imaging using Rhod-2 and Calcein during $K^+$-induced astrocyte swelling. Our calibration of the OGB-1 FLIM decay to various levels of free $Ca^{2+}$ in solution (see methods) placed the $K_d$ at 192 nM, ideal to detect small shifts in resting astrocyte free $Ca^{2+}$. We patch loaded single astrocytes with OGB-1 salt, which readily diffused to neighboring astrocytes that were coupled via gap junctions to the patched cell. We allowed 20 min for OGB-1 diffusion through the astrocyte network. As previously reported (Zheng et al., 2015), the patched astrocyte displayed elevated resting $Ca^{2+}$ compared to the adjacent coupled astrocytes (patched: 115.6 ± 9.7 nM; coupled: 69.5 ± 5.5 nM, p=0.001, n=8, Figure 2B,D,E). Similar to our results using the Rhod-2/Calcein ratio, bath application of an isosmotic +2.5 mM $K^+$ challenge (2.5 to 5 mM $K^+$) deceased (quickened) the OGB-1 FLIM $Ca^{2+}$ signal in the soma and processes of both the patched astrocyte (soma: -38.2 ± 9.6 nM, p=0.0052, n=8; processes: -51.5 ± 7.8 nM, p=0.0006, n=7, Figure 2D,E) and the coupled cells (soma: -26.0 ± 3.9 nM, p=0.0003, n=8; processes: -40.3 ± 8.1 nM, p=0.0041, n=6, Figure 2D,E). We also noted decreased resting $Ca^{2+}$ levels in astrocytic perivascular endfeet (-24.7 ± 3.1 nM, p=0.0040,

n=4, Figure 2F,G), in response to high $[K^+]_o$, showing that this is a cell-wide phenomenon. We then examined astrocytic endfeet apposed to blood vessels using our Rhod-2/Calcein approach and observed a similar decrease in $Ca^{2+}$ caused by +2.5 mM high $[K^+]_o$ (-25.7 ± 4.2%, p=0.0256, n=3, Figure 2H,I) and clear endfoot swelling (Figure 2J). These data suggest that a modest elevation in external $K^+$ causes a genuine decrease in the free, steady-state $Ca^{2+}$ concentration in astrocytes across the cell.

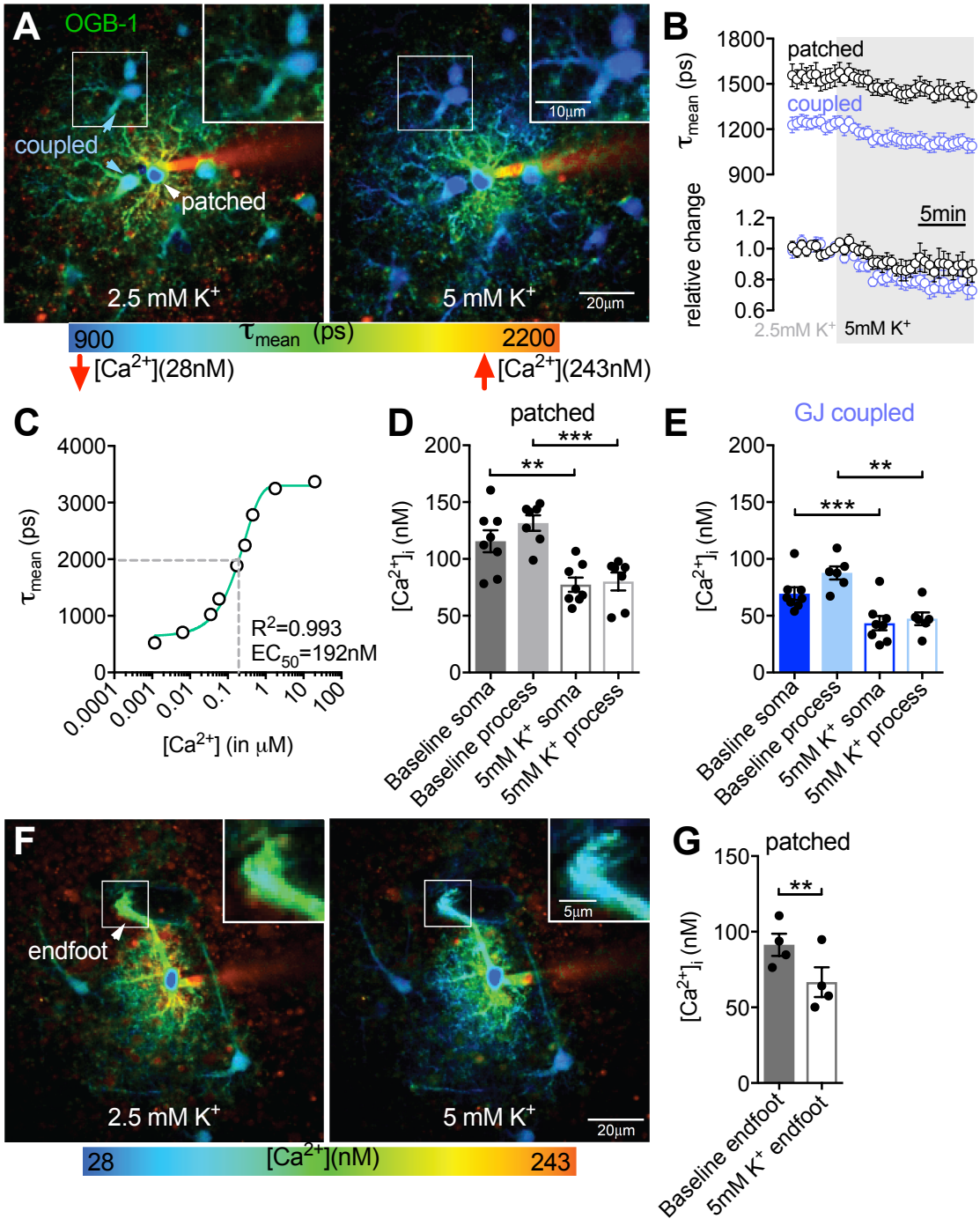
A
OGB-1
coupled
patched
2.5 mM K+
5 mM K+
10µm
20µm
900
τmean (ps)
2200
[Ca2+](28nM)
[Ca2+](243nM)
B
patched
coupled
τmean (ps)
1800
1500
1200
900
relative change
1.2
1.0
0.8
0.6
5min
2.5mM K+
5mM K+
C
τmean (ps)
4000
3000
2000
1000
0
R2=0.993
EC50=192nM
0.0001
0.001
0.01
0.1
1
10
100
[Ca2+] (in µM)
D
patched
[Ca2+]i (nM)
200
150
100
50
0
**
***
Baseline soma
Baseline process
5mM K+ soma
5mM K+ process
E
GJ coupled
[Ca2+]i (nM)
200
150
100
50
0
**
***
Basline soma
Baseline process
5mM K+ soma
5mM K+ process
F
endfoot
2.5 mM K+
5 mM K+
5µm
20µm
28
[Ca2+](nM)
243
G
patched
[Ca2+]i (nM)
150
100
50
0
**
Baseline endfoot
5mM K+ endfoot
H
2.5 mM K+
5 mM K+
Rhod-2
5 µm
0
255
I
Rhod-2/Calcein Ratio
1.1
1.0
0.9
0.8
0.7
+2.5 mM K+
Indiv Endfoot
J
2.5 mM K+
5 mM K+
5 µm
Swelled
Difference

**Figure 2: Fluorescence Lifetime Imaging Microscopy (FLIM) reveals a quantitative decrease in astrocyte free $Ca^{2+}$ in response to a modest elevation in external $K^+$**

**A**) Two-photon FLIM images showing a whole-cell patched astrocyte loaded with OGB-1 (200 μM), and coupled astrocyte also loaded, in response to a +2.5 mM $K^+$ increase. Pseudo colouring corresponds to the $\tau_{mean}$ value of the lifetime decay curves (cooler colours: faster decay = lower $Ca^{2+}$; warmer colours: slower decay = higher $Ca^{2+}$). High $K^+$ results in a shift towards faster lifetimes (cooler colours) thus decreased free $Ca^{2+}$ in both the patched and coupled astrocytes. **B**) Averaged raw OGB-1 lifetime values (top panel) and relative changes (bottom panel) comparing the time course of responses for patched and coupled astrocytes in the presence of high $K^+$. **C**) OGB-1 Lifetime-$Ca^{2+}$ concentration calibration curve. **D**) Summary comparing baseline $Ca^{2+}$ to the averaged individual peak effects of high $K^+$ in patched astrocyte somata and processes. **E**) Averaged individual peak responses to high $K^+$ in gap-junctionally (GJ) coupled somata and processes. **F**) Exemplar images of a patched astrocyte with its endfoot visible in the imaging plane. Scale bar is post-calibration intracellular $Ca^{2+}$ concentration. **G**) Summary data of the individual peak effects of high $K^+$ on steady-state endfoot $Ca^{2+}$. **H**) Pseudo coloured Rhod-2 images showing the $Ca^{2+}$ drop in perivascular astrocyte endfeet in response to a +2.5 mM $K^+$ increase. **I)** Summary data of maximal astrocyte endfeet $Ca^{2+}$ decrease as measured by the Rhod-2/Calcein ratio. **J)** Rhod-2 images depicting the endfoot volume increase. Difference image subtracts the large volume endfoot from the small volume state. ** $p<0.01$, *** $p<0.001$

### 3.3 $K^+$-mediated astrocyte $Ca^{2+}$ decrease does not depend on neuronal firing or display plastic changes

Glutamate-mediated decreases in resting astrocyte $Ca^{2+}$ that occur in response to theta-burst afferent activity appear long-lasting, achieving a new steady-state $Ca^{2+}$ level well after the cessation of theta burst (>15 min) (Mehina et al., 2017). We extended the time frame of our $K^+$ experiment and examined the washout period using Rhod-2 and Calcein. We observed a complete washout of the $Ca^{2+}$ drop to a +2.5 mM $[K^+]_o$ challenge (+1.7 ± 2.6%, p=0.534, n=9, Figure 3A), in contrast to the enduring effect of glutamate previously reported. Due to the return of cytosolic $Ca^{2+}$ to baseline after washout and because a shift in $[K^+]_o$ of this magnitude likely has negligible impact on neural excitability (Somjen, 1979), we test the hypothesis that the $K^+$-induced drop in astrocyte $Ca^{2+}$ would be insensitive to TTX. Indeed, a +2.5 mM $[K^+]_o$ increase in the presence of the voltage-gated sodium channel blocker TTX (500 nM) had no effect on the astrocyte $Ca^{2+}$ decrease (-15.7 ± 1.6%, p=0.595, n=6, Figure 3B). Theta-burst dependent decreases in astrocyte steady-state resting $Ca^{2+}$ are occluded in enriched animals, likely from wide-spread plastic changes throughout the neocortex after enrichment (Mehina et al., 2017). With washout of the $K^+$ effect and no reliance on neural action potential firing, we pondered whether the $K^+$-induced decrease in astrocyte $Ca^{2+}$ would be unaltered after enrichment. Seven Sprague Dawley rats were housed in an enrichment environment for three weeks (see methods) before acute slices were prepared and the same +2.5 mM $[K^+]_o$ experiment was conducted. We found that enrichment had no effect on the magnitude of the astrocyte $Ca^{2+}$ decrease to high $K^+$ when compared to our control data set (-17.9 ± 2.8%, p=0.727, n=6, Figure 3C-F). These data suggest that the astrocyte free $Ca^{2+}$ decrease following a modest elevation in $[K^+]_o$ neither depends on changes in neural activity nor on plastic mechanisms. When also considering the

bidirectional nature of the effect described above, these data collectively suggest that changes to steady-state $[K^+]_o$ reciprocally controls steady-state free $Ca^{2+}$ in astrocytes: when $[K^+]_o$ is elevated, astrocyte free $Ca^{2+}$ decreases and when $[K^+]_o$ is decreased, astrocyte free $Ca^{2+}$ increases.

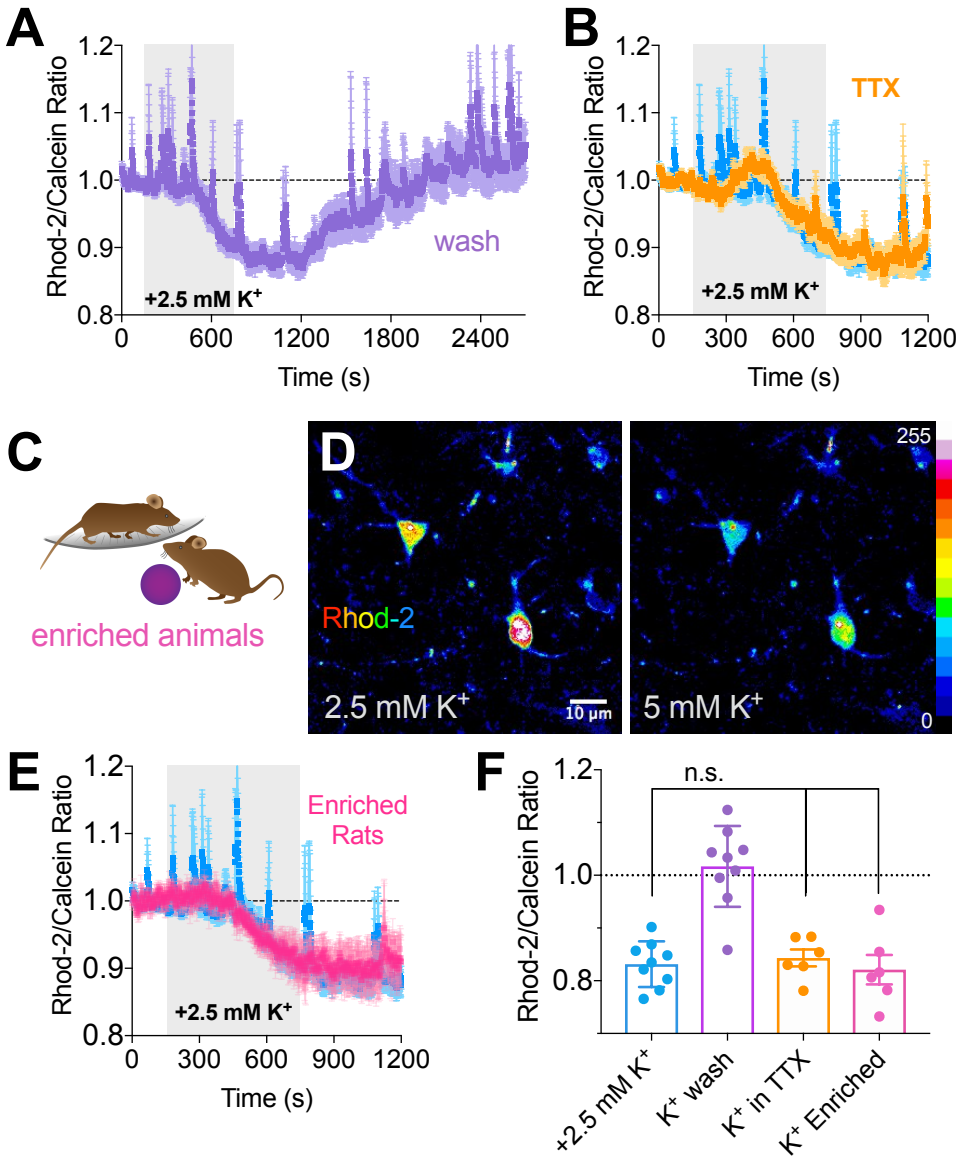
A
Rhod-2/Calcein Ratio
1.2
1.1
1.0
0.9
0.8
+2.5 mM K+
wash
0
600
1200
1800
2400
Time (s)
B
Rhod-2/Calcein Ratio
TTX
+2.5 mM K+
0
300
600
900
1200
Time (s)
C
enriched animals
D
Rhod-2
2.5 mM K+
10 µm
5 mM K+
255
0
E
Rhod-2/Calcein Ratio
Enriched Rats
+2.5 mM K+
0
300
600
900
1200
Time (s)
F
Rhod-2/Calcein Ratio
n.s.
+2.5 mM K+
K+ wash
K+ in TTX
K+ Enriched

**Figure 3: The $K^+$ mediated decrease in astrocyte $Ca^{2+}$ does not exhibit a reliance on neural firing or display plastic changes**

**A**) Average summary time series $Ca^{2+}$ data showing that the decrease in astrocyte $Ca^{2+}$ caused by a +2.5 mM $K^+$ challenge recovers completely upon return to the baseline $K^+$ level. **B**) The decrease in astrocyte $Ca^{2+}$ caused by high $K^+$ still occurs when action potential signaling is blocked by TTX. **C**) Cartoon depicting animals that received 3 weeks of enrichment. **D**) Pseudo coloured images of Rhod-2 astrocytes from enriched animals showing the decrease in $Ca^{2+}$ signals in response to a $K^+$ challenge. **E**) Average summary time series $Ca^{2+}$ data of the enriched animal high $K^+$ experiment (pink) compared to animals under standard housing (blue). **F**) Summary data of the maximal decrease in astrocyte $Ca^{2+}$ in each experiment.

### 3.4 $K^+$-mediated astrocyte $Ca^{2+}$ decrease depends on external $Ca^{2+}$ and not ER stored $Ca^{2+}$

The observations described above directed us to explore whether external $K^+$ affected the movement of $Ca^{2+}$ and other ions (and small charged molecules) across the astrocyte plasma membrane. It is well appreciated that increases in external $K^+$ depolarize the astrocyte resting membrane potential which is predominately controlled by $E_K$. Shifting membrane potential would change the driving force for $Ca^{2+}$ entry, as well as alter the activity of electrogenic transporters. To start, we tested whether the $K^+$ effect relied on an external $Ca^{2+}$ source or an internal one. We pre-incubated our brain slices with the potent SERCA pump inhibitor thapsigargin (1 μM) for 30 min to run down intracellular $Ca^{2+}$ stores. After this treatment, we were unable to evoke large glutamate-mediated $Ca^{2+}$ transients in astrocytes (Mehina et al., 2017). In this condition, a +2.5 mM $[K^+]_o$ challenge still produced the same decrease in resting $Ca^{2+}$ measured by the Rhod-2/Calcein ratio (-19.1 ± 1.0%, p=0.211, n=11, Figure 4A,B), suggesting $Ca^{2+}$ stores were not involved. In contrast, incubating our slices in a $Ca^{2+}$ free ACSF external solution, significantly attenuated both the drop in free $Ca^{2+}$ (-10.3 ± 0.8%, p=0.0015, n=8, Figure 4C,E,F) and the astrocyte swelling (+7.4 ± 0.6%, p=0.0011, n=7, Figure 4D,G,H) that normally occurred in response to high $[K^+]_o$.

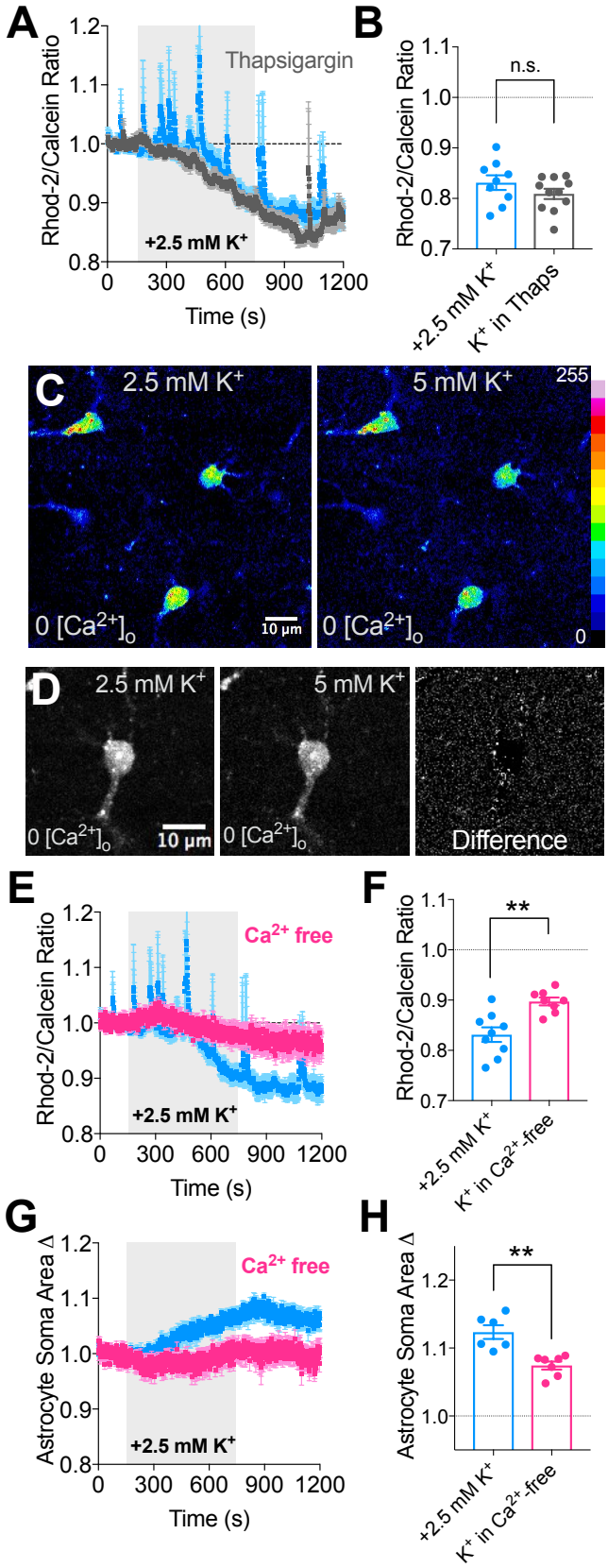
A
Rhod-2/Calcein Ratio
Thapsigargin
+2.5 mM K+
Time (s)
B
Rhod-2/Calcein Ratio
n.s.
+2.5 mM K+
K+ in Thaps
C
2.5 mM K+
5 mM K+
255
0 [Ca2+]o
10 µm
0
D
2.5 mM K+
5 mM K+
0 [Ca2+]o
10 µm
Difference
E
Rhod-2/Calcein Ratio
Ca2+ free
+2.5 mM K+
Time (s)
F
Rhod-2/Calcein Ratio
**
+2.5 mM K+
K+ in Ca2+ -free
G
Astrocyte Soma Area Δ
Ca2+ free
+2.5 mM K+
Time (s)
H
Astrocyte Soma Area Δ
**
+2.5 mM K+
K+ in Ca2+ -free

**Figure 4: The $K^+$ effect does not depend on ER stored $Ca^{2+}$ but on external $Ca^{2+}$**

**A**) Average summary time series $Ca^{2+}$ data showing no effect on the $K^+$-mediated decrease when internal $Ca^{2+}$ stores are emptied with a 30 min pretreatment with the SERCA pump inhibitor thapsigargin (1 μM). **B**) Summary of the peak decreases in $Ca^{2+}$ from individual experiments. **C**) Pseudo coloured two-photon images of astrocytes loaded with Rhod-2 in a $Ca^{2+}$ free external solution. A +2.5 mM $K^+$ challenge produces little change to resting astrocyte $Ca^{2+}$. **D**) Image of an astrocyte at baseline $K^+$ (left), elevated $K^+$ (middle) and a difference image (5 mM $K^+$ minus 2.5 mM $K^+$) showing little change to astrocyte soma area in response to high $K^+$. **E**) Average summary time series of $Ca^{2+}$ data in response to high $K^+$ in a $Ca^{2+}$ free external solution. **F**) Summary data of the maximal decrease in astrocyte $Ca^{2+}$ in each experiment. **G**) Average summary time series of soma area data in response to high $K^+$ in a $Ca^{2+}$ free external solution. **H**) Summary data of the maximal increase in astrocyte soma area in each experiment. ** $p<0.01$

### 3.5 $K^+$-mediated astrocyte $Ca^{2+}$ decrease relies on bicarbonate but not carbonic anhydrase-mediated pH changes

Bicarbonate movement into astrocytes plays a major role in volume regulation (Florence et al., 2012; Larsen and MacAulay, 2017) and pH alkalization (Zhou et al., 2010; Larsen and MacAulay, 2017) during $K^+$ challenges. We tested if removing bicarbonate from our external solution, by instead buffering the ACSF with HEPES, affected astrocyte $Ca^{2+}$. Notably, in bicarbonate-free conditions, a +2.5 mM $K^+$ challenge failed to decrease astrocyte free $Ca^{2+}$ (-3.8 ± 0.8%, $p<0.0001$, n=6, Figure 5A-C) and, as previously reported, this condition blocked cell swelling (+4.2 ± 0.5%, $p<0.0001$, n=5, Figure 5D,E). Cell swelling also depends on the pH change via the action of carbonic anhydrase (Florence et al., 2012), but a reliance on pH for $Ca^{2+}$ changes is unclear. Interestingly, blocking carbonic anhydrase activity with acetazolamide (100 µM) had no impact on the drop in astrocyte $Ca^{2+}$ observed in response to high $[K^+]_o$ (-19.5 ± 0.9%, $p=0.240$, n=5, Figure 5F,G). These data suggest that bicarbonate, but not pH per se, plays an important role in the free $Ca^{2+}$ decrease observed in response to a modest $[K^+]_o$ increase.

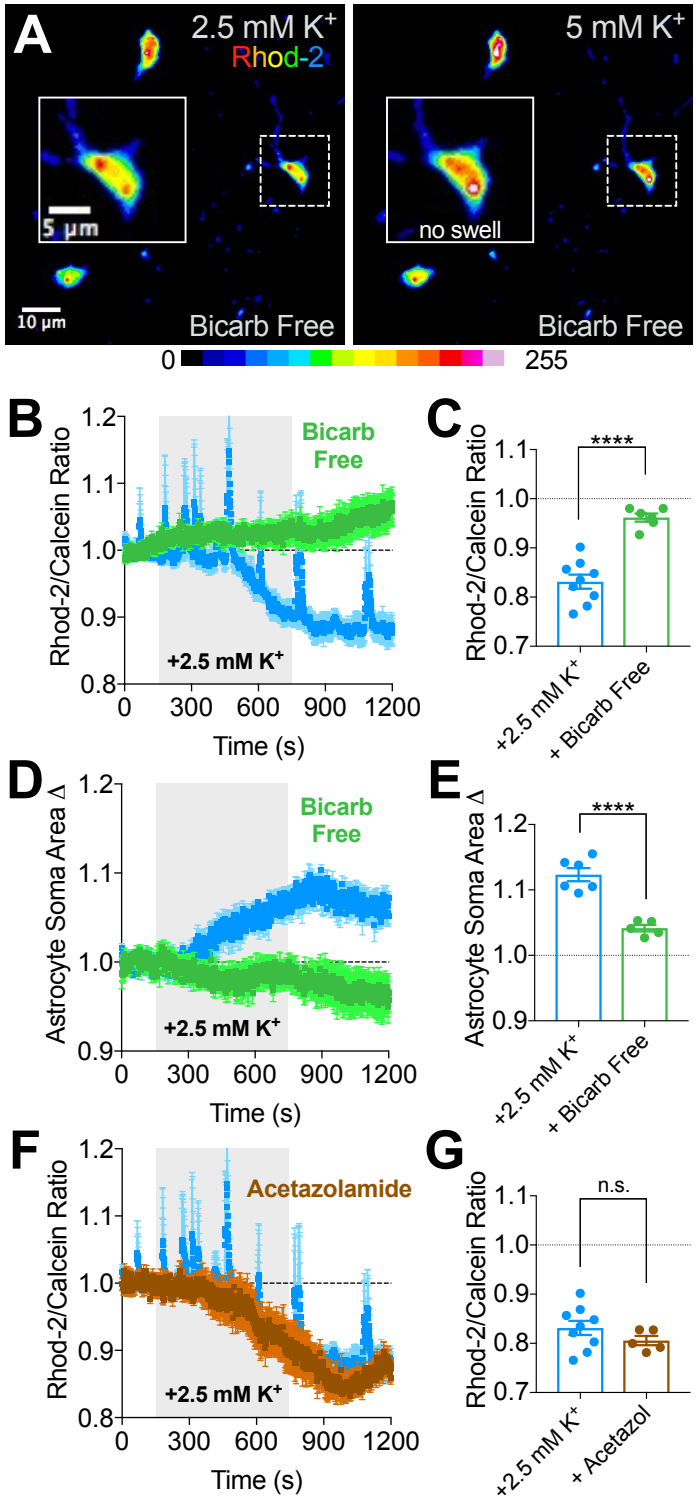
A
2.5 mM K+
Rhod-2
5 µm
10 µm
Bicarb Free
5 mM K+
no swell
Bicarb Free
0
255
B
Rhod-2/Calcein Ratio
Bicarb Free
+2.5 mM K+
Time (s)
C
Rhod-2/Calcein Ratio
****
+2.5 mM K+
+ Bicarb Free
D
Astrocyte Soma Area Δ
Bicarb Free
+2.5 mM K+
Time (s)
E
Astrocyte Soma Area Δ
****
+2.5 mM K+
+ Bicarb Free
F
Rhod-2/Calcein Ratio
Acetazolamide
+2.5 mM K+
Time (s)
G
Rhod-2/Calcein Ratio
n.s.
+2.5 mM K+
+ Acetazol

**Figure 5: The $K^+$ effect depends on bicarbonate but not carbonic anhydrase-mediated pH changes**

**A)** Pseudo coloured two-photon images of astrocytes loaded with Rhod-2, showing no decrease in free $Ca^{2+}$ to a +2.5 mM $K^+$ challenge when bicarbonate is removed from the external solution (HEPES buffered ACSF). Inset shows an astrocyte close up and the lack of cell swelling to high $[K^+]_o$ in a bicarbonate free external solution. **B**) Summary times series of $Ca^{2+}$ data for the same experiment in (*A*) compared to control. **C**) Summary data of peak decreases in $Ca^{2+}$ from each experiment. **D**) Summary time series of soma area data in response to high $[K^+]_o$ in a bicarbonate free external solution. **E**) Summary data of peak increases in soma area from each experiment. **F**) Summary time series of $Ca^{2+}$ data in response to high $[K^+]_o$ in the presence of acetazolamide (100 μM) compared to control. **G**) Summary data of peak decreases in $Ca^{2+}$ in each experiment from acetazolamide vs. control. **** $p<0.0001$

### 3.6 $K^+$-mediated astrocyte $Ca^{2+}$ decrease is independent of inward rectifiers, the SLC4A4-sAC pathway, or $Na^+$ ions

Astrocytes help buffer the extracellular space from $K^+$ increases, partly through inward rectifying potassium 4.1 channels (Chever et al., 2010). To test for the involvement of these channels in our $Ca^{2+}$ decrease, we tested high $[K^+]_o$ in the presence of $BaCl_2$ (100 μM), but this treatment failed to block the effect (-15.5 ± 1.0%, p=0.523, n=5, Figure 6A). Next we pondered whether the shift in $E_K$ and thus astrocyte membrane potential influenced electrogenic negative transporters. For example, astrocytes show high levels of the sodium bicarbonate cotransporter SLC4A4 (Cahoy et al., 2008), which enable the net negative charge transfer of $HCO_3^-$ into astrocytes along with $Na^+$ (3:1). $K^+$-mediated $HCO_3^-$ influx increases pH (Ransom et al., 2000), is involved in cell swelling (Florence et al., 2012), and activates the bicarbonate sensor soluble adenylyl cyclase, which increases intracellular cAMP (Choi et al., 2012). To explore this pathway, first we tested the +2.5 mM $K^+$ change in the presence of the SLC4A4 antagonist S0859 (100 μM), but found no attenuation in the decrease in astrocyte $Ca^{2+}$ (-21.9 ± 3.1%, p=0.1155, n=4, Figure 6B). Next we tested high $[K^+]_o$ in the presence of the soluble adenylyl cyclase inhibitor KH7 (10 μM), but again found no effect on the drop in $Ca^{2+}$ measured by the Rhod-2/Calcein ratio (-13.5 ± 2.3%, p=0.267, n=12, Figure 6C). To more broadly probe for the involvement of transporters or exchangers that rely on $Na^+$ fluxes, such as the $Na^+$-$K^+$-$Cl^-$ cotransporter or the $Na^+/Ca^{2+}$ exchanger, we tested high $[K^+]_o$ in the presence of a low $Na^+$ external ACSF solution. By replacing NaCl with choline chloride ($[Na^+]_o$ decreasing from 153.2 mM to 26.3 mM), we found no reduction in the decrease in free astrocyte $Ca^{2+}$ caused by high $K^+$ (-14.3 ± 1.1%, p=0.164, n=11, Figure 6D), potentially ruling out all channels and ion transport mechanisms that rely on the driving force of $Na^+$ entry.

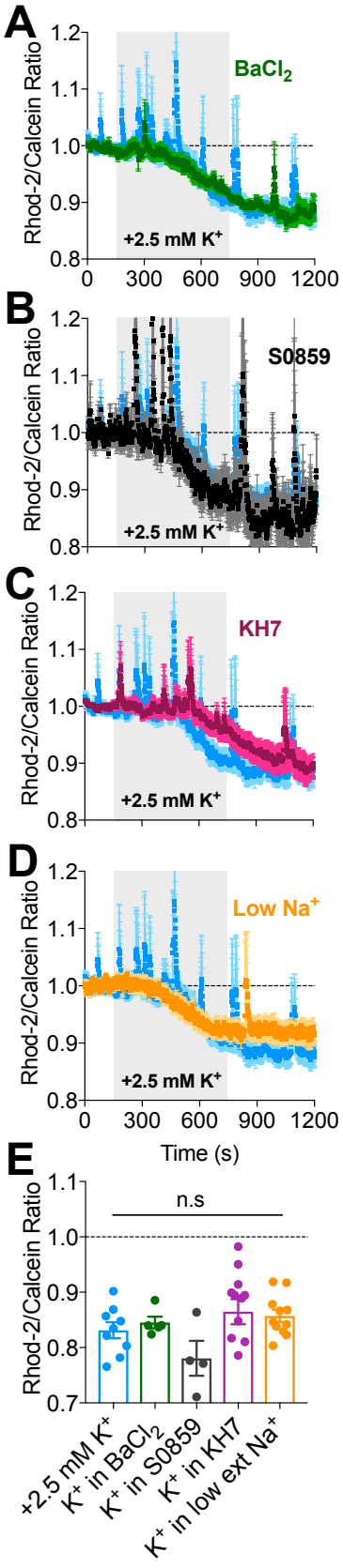
A
B
C
D
E
Rhod-2/Calcein Ratio
BaCl2
S0859
KH7
Low Na+
+2.5 mM K+
Time (s)
n.s
+2.5 mM K+
K+ in BaCl2
K+ in S0859
K+ in KH7
K+ in low ext Na+

**Figure 6: The $K^+$ mediated $Ca^{2+}$ decrease does not depend on inward rectifiers, $Na^+$ ions or the SLC4A4-sAC pathway**

**A-D**) Average summary time series $Ca^{2+}$ data showing no effect on the $K^+$-mediated decrease when antagonizing inward rectifying potassium channels with $BaCl_2$ (100 μM) (*A*), blocking SLC4A4 with S0859 (100 μM) (*B*), or antagonizing soluble adenylyl cyclase using KH7 (10 μM) (*C*), or lowering external $Na^+$ to 26.3 mM (*D*). **E**) Summary data of the maximal decrease in astrocyte $Ca^{2+}$ in each experiment.

### 3.7 Anion channels separately control $K^+$-mediated astrocyte $Ca^{2+}$ decrease and swelling

$K^+$ and $Cl^-$ are moved simultaneously across the plasma membrane by the sodium potassium chloride cotransporter (NKCC) and the potassium chloride cotransporter (KCC). Other $K^+$ transport mechanisms, such as the $Na^+/K^+$ pump, thus influence $Cl^-$ movement via these routes (Hertz et al., 2015). $Cl^-$ ion fluxes have been implicated in astrocyte volume regulation in the hippocampus (Larsen and MacAulay, 2017) and in helping control resting membrane potential in a variety of cells (Jentsch et al., 2002). Therefore, we set out to test whether external $Cl^-$ was involved in our phenomenon. Reducing external $Cl^-$ from 132.1 mM to 5.2 mM by substituting NaCl with sodium gluconate decreased the magnitude of both the decrease in $Ca^{2+}$ (-9.9 ± 1.3%, p=0.0034, n=8, Figure 7A,B) and the soma swelling caused by a +2.5 mM $K^+$ challenge. We then explored the involvement of anion channels and transporters that move $Cl^-$. Our first attempt with the broad-spectrum $Cl^-$ channel antagonist DIDS (500 μM) was untenable due to volume dysregulation (blebbing) and $Ca^{2+}$ escalation in the brain slice from applying this compound alone (data not shown). However, a different broad-spectrum anion channel antagonist NPPB (100 μM), which targets Volume Regulated Anion Channels (Inoue and Okada, 2007), $Ca^{2+}$-dependent $Cl^-$ Channels (Huang et al., 2012), and Maxi Anion channels (Dutta et al., 2008), was tenable within the time frame of the experiment. While NPPB also caused aberrant cell volume changes across the brain slice at approximately 20 min into the application (red brackets Figure 7E,F), we were able to conduct a 5 min NPPB pre-incubation with a +2.5 mM $[K^+]_o$ challenge. Interestingly, the drop in astrocyte $Ca^{2+}$ still occurred in NPPB (-17.0 ± 2.0%, p=0.964, n=8, Figure 7C,E,L), yet the cell swelling was completely blocked up to 900 seconds (+5.5 ± 0.8%, p=0.0006, n=5, Figure 7D,F,M), after which time brain slice stability was degraded by the NPPB treatment. To test $Cl^-$ transporters, we focused on proteins that

moved both $K^+$ and $Cl^-$. For example, KCC moves $K^+$ and $Cl^-$ out of the cell and is detected in astrocytes (Cahoy et al., 2008; Ringel and Plesnila, 2008) and glioma cells (Ernest et al., 2005; Gagnon et al., 2007). We employed bumetanide, a common NKCC and KCC antagonist that is far more potent for NKCC by ~250-500 fold ($K_i$ ~100 nM against NKCC; $K_i$ ~25-50 μM against KCC) (Payne et al., 2003). We found that a dose of bumetanide that antagonized both transporters (100 μM) clearly blocked the decrease in astrocyte free $Ca^{2+}$ in response to high $[K^+]_o$ (-7.5 ± 1.6%, p=0.0005, n=8, Figure 7G,I,L), whereas a lower dose that blocks only NKCC (2 μM) had no effect (-21.0 ± 1.7%, p=0.0854, n=7, Figure 7K). Interestingly, high dose bumetanide had little impact on cell swelling caused by high $[K^+]_o$ (+11.4 ± 1.0%, p=0.5082, n=8, Figure 7H,J,M). Collectively, the differential effects of NPPB and bumetanide on swelling and $Ca^{2+}$ strongly suggest these phenomena occur through distinct mechanisms: $K^+$-induced swelling depended on $Cl^-$ ion channels and the $K^+$-induced $Ca^{2+}$ change depended on KCC activity, whereas both phenomena depended on external bicarbonate and external $Cl^-$.

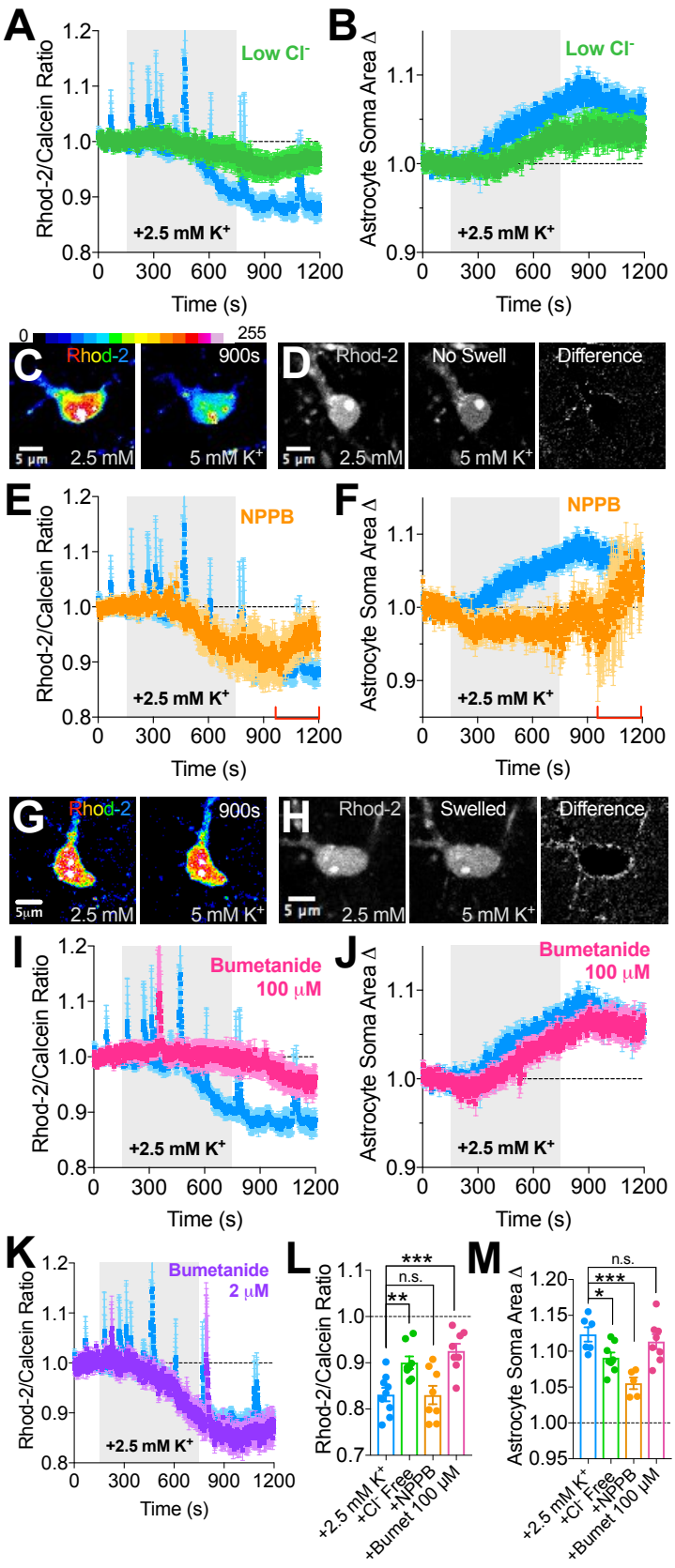
A
Rhod-2/Calcein Ratio
Low Cl-
+2.5 mM K+
Time (s)
B
Astrocyte Soma Area Δ
Low Cl-
+2.5 mM K+
Time (s)
0
255
C
Rhod-2
900s
5 µm
2.5 mM
5 mM K+
D
Rhod-2
No Swell
Difference
5 µm
2.5 mM
5 mM K+
E
Rhod-2/Calcein Ratio
NPPB
+2.5 mM K+
Time (s)
F
Astrocyte Soma Area Δ
NPPB
+2.5 mM K+
Time (s)
G
Rhod-2
900s
5µm
2.5 mM
5 mM K+
H
Rhod-2
Swelled
Difference
5 µm
2.5 mM
5 mM K+
I
Rhod-2/Calcein Ratio
Bumetanide
100 µM
+2.5 mM K+
Time (s)
J
Astrocyte Soma Area Δ
Bumetanide
100 µM
+2.5 mM K+
Time (s)
K
Rhod-2/Calcein Ratio
Bumetanide
2 µM
+2.5 mM K+
Time (s)
L
Rhod-2/Calcein Ratio
***
n.s.
**
+2.5 mM K+
+Cl- Free
+NPPB
+Bumet 100 µM
M
Astrocyte Soma Area Δ
n.s.
***
*
+2.5 mM K+
+Cl- Free
+NPPB
+Bumet 100 µM

**Figure 7: Anion channels and the potassium chloride co-transporter separately control cell swelling and the $Ca^{2+}$ decrease in response to high $[K^+]_o$**

**A)** Summary time series of $Ca^{2+}$ data in response to high $[K^+]_o$ in the presence of a low $Cl^-$ external solution (5.2 mM) compared to control. **B)** Summary time series of soma area data in response to high $[K^+]_o$ in a low $Cl^-$ external solution. Both the $Ca^{2+}$ drop and cell swelling are reduced in low $Cl^-$ ACSF. **C)** Pseudo coloured two-photon images of an astrocyte loaded with Rhod-2, showing the same decrease in free $Ca^{2+}$ to a +2.5 mM $K^+$ challenge when anion channels were blocked with NPPB (100 μM). **D)** Two-photon images of an astrocyte showing the high $K^+$-induced cell swelling is blocked in NPPB: no border or edge in difference image. **E and F)** Summary time series data of astrocyte $Ca^{2+}$ (*E*) and astrocyte soma area (*F*) in the same NPPB experiment depicted in (*C*) and (*D*). Red brackets indicate periods where severe tissue distortion occurred across the brain slice, compromising our measures. **G)** Pseudo coloured images of a Rhod-2 loaded astrocyte showing little decrease in free $Ca^{2+}$ to a +2.5 mM $K^+$ challenge in the presence of the KCC blocker bumetanide (100 μM). **H)** Images of an astrocyte showing that the high $K^+$-induced cell swelling still occurs with bumetanide. **I and J)** Summary time series data of astrocyte $Ca^{2+}$ (*I*) and astrocyte soma area (*J*) in the same bumetanide experiment depicted in (*G*) and (*H*). **K**) A lower dose of bumetanide (2 μM) targeting NKCC is ineffective at reducing the decrease in astrocyte $Ca^{2+}$ to high $[K^+]_o$. **L**) Summary data of peak decreases in astrocyte $Ca^{2+}$ in each experiment. **M**) Summary data of peak increases in astrocyte soma area in each experiment. * $p<0.05$, ** $p<0.01$, *** $p<0.001$

### 3.8 $K^+$-mediated vasodilation is sensitive to KCC blockade and astrocyte patching

We set out to explore a functional consequence to the change in $Ca^{2+}$, $Cl^-$ and $HCO_3^-$ occurring in astrocytes in response to a moderate $[K^+]_o$ challenge. We recently described a new mechanism for how astrocytes set basal arteriole tone via the astrocytic steady-state resting $Ca^{2+}$ concentration (Rosenegger et al., 2015; Mehina et al., 2017). Therefore, we tested the hypothesis that the external $K^+$ concentration affects arteriole tone through an astrocyte-dependent mechanism. $K^+$ effects on the cerebrovasculature are well described, yet most investigations use $K^+$ challenges beyond the physiological range (>5 mM). Furthermore, these studies have focused on the direct actions of $K^+$ relaxing vascular smooth muscle via increases in inward rectifying $K^+$ channel opening (Filosa et al., 2006; Girouard et al., 2010). Notably, smaller $K^+$ elevations dilate surface pial vasculature through a mechanism that is $K_{ir}$-independent (Horiuchi et al., 2002), but the effect of physiological $K^+$ challenges on parenchymal arterioles is unclear. First, we tested if a +2.5 mM $[K^+]_o$ increase was capable of actuating cerebral penetrating arterioles in brain slices. Indeed, this moderate $K^+$ challenge significantly increased arteriole diameter (+4.4 ± 1.2%, p=0.0029, n=13, Figure 8A,B,C), which returned to baseline after high $[K^+]_o$ washout. As the KCC blocker bumetanide (100 μM) blocked the drop in free $Ca^{2+}$ caused by high $[K^+]_o$ without affecting cell swelling, we tested if this treatment could alter the vessel response to $K^+$. Notably, we found that bumetanide completely blocked the high $[K^+]_o$ induced dilation, resulting in the appearance of a small vasoconstriction (-4.2 ± 1.0%, p=0.0042, n=8, Figure 8B,C). This meant a significantly reduced arteriole diameter versus the control without bumetanide (-8.4 ± 1.7%, p<0.0001, n=8, Figure 8B,C). Importantly, the bumetanide effect may not necessarily localize to astrocytes, as studies on arterioles outside the brain have described a role for KCC3 in contractile function (Garneau et al., 2016). To test the idea that the influence of $K^+$ on the arteriole was

conducted through astrocytes, we pondered whether disrupting normal ion homeostasis in the network of astrocytes surrounding a penetrating arteriole compromises $K^+$-induced vasodilation. For example, a common intracellular whole-cell patch solution involving EGTA, low $[Cl^-]_i$, and a HEPES pH buffer, perturbs the natural level and/or movements of $Ca^{2+}$ (Zheng et al., 2015), $Cl^-$ (Kyrozis and Reichling, 1995), and $HCO_3^-$ (Staley and Proctor, 1999). Such perturbations may be especially apparent in astrocytes, which have a higher internal $[Cl^-]$ than neurons. We patched peri-arteriole astrocytes and loaded them with a standard intracellular solution plus Alexa 488 sodium hydrazide (200 μM) to visualize the extent of astrocyte network loading and to ensure the solution infiltrated endfeet apposed to the vessel wall. Previously we reported that this intracellular solution had little impact on resting arteriole tone (Rosenegger et al., 2015). After allowing at least 10 min for the astrocyte patch solution to diffuse and equilibrate, we bath applied a +2.5 mM $[K^+]_o$ challenge and found that high $K^+$-induced dilation was converted into a vasoconstriction (-9.0 ± 2.4%, p=0.0336, n=4, Figure 8D-G). To control for the possibility that the patching process itself caused the switch from vasodilation to vasoconstriction, as opposed to a disruption of the intracellular milieu of astrocytes, we conduced mock patching experiments. Here, rather than achieving astrocyte whole-cell, an on-cell configuration was maintained. Under these circumstances, the $K^+$-induced vasodilation was preserved (+5.9 ± 2.0%, p=0.0193, n=9, Figure 8F,G), resulting in a significantly greater arteriole diameter versus the patched astrocytes (+10.8 ± 3.2%, p=0.0068, n=9, Figure 8F,G). These data suggest that antagonizing KCC activity or a general disruption of the internal astrocytic environment, blocks vasodilation to a modest increase in external $K^+$.

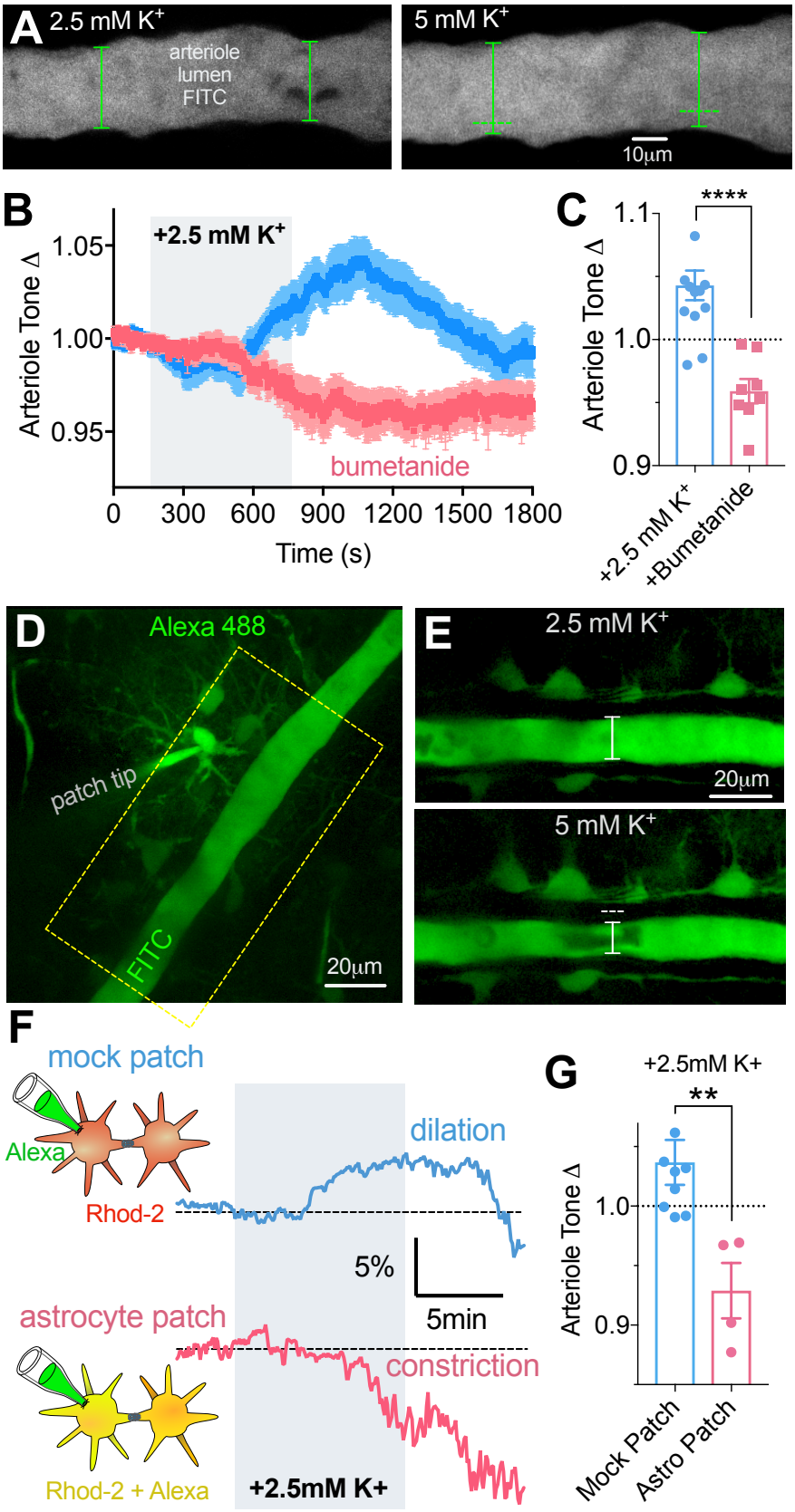
A
2.5 mM K+
arteriole
lumen
FITC
5 mM K+
10μm
B
+2.5 mM K+
Arteriole Tone Δ
1.05
1.00
0.95
bumetanide
0
300
600
900
1200
1500
1800
Time (s)
C
****
Arteriole Tone Δ
1.1
1.0
0.9
+2.5 mM K+
+Bumetanide
D
Alexa 488
patch tip
FITC
20μm
E
2.5 mM K+
20μm
5 mM K+
F
mock patch
Alexa
Rhod-2
dilation
5%
5min
astrocyte patch
constriction
Rhod-2 + Alexa
+2.5mM K+
G
+2.5mM K+
**
Arteriole Tone Δ
1.0
0.9
Mock Patch
Astro Patch

**Figure 8: $K^+$-mediated vasodilation is sensitive to KCC blockade and astrocyte patching**

**A**) Images of the arteriole lumen filled with FITC-dextran showing a vasodilation in response to a +2.5 mM increase in external $K^+$. **B**) Summary time series data of arteriole diameter in response to +2.5 mM $K^+$ in the control condition (blue), and in the presence of bumetanide (pink). Bumetanide blocks the high $K^+$ mediated vasodilation, which instead manifests as a small vasoconstriction. **C**) Summary data of peak arteriole diameter changes. **D**) Two-photon z-stack image showing Alexa 488 in the patched astrocyte, the coupled astrocytes, and perivascular endfeet apposed to a penetrating arteriole (FITC-dextran in lumen). **E**) Close up images of the arteriole and apposed endfeet loaded with Alexa 488 via the patched astrocyte (not shown, above the image plane). A +2.5 mM $K^+$ increase caused a vasoconstriction when the astrocyte was patched. **F**) Upper: trace of the vasodilation observed in response to high $K^+$ in the presence of a 'mock astrocyte patch' experiment (patching approach to the cell membrane but no whole-cell). Lower: trace of the vasoconstriction observed in response to high $K^+$ in the presence of astrocyte network filling with a standard, HEPES buffered internal solution. **G**) Summary data of peak arteriole diameter changes. ** $p<0.01$, **** $p<0.0001$

## CHAPTER FOUR: DISCUSSION

Here we show that a modest increase or decrease in external $[K^+]$ bi-directionally controls the resting free $Ca^{2+}$ concentration and cell volume in astrocytes. While demonstrated predominantly using relative $Ca^{2+}$ measurements with a ratio against a morphological dye, we also demonstrated the essential phenomenon using quantitative FLIM $Ca^{2+}$ imaging. We found that the $Ca^{2+}$ decrease and cell swelling caused by high $K^+$ was sensitive to lowering the external concentration of $Ca^{2+}$, $Cl^-$, and bicarbonate, but was not sensitive to lowering external $Na^+$; thus, ruling out $Na^+$ dependent transport. Further exploration of the $Cl^-$ dependency revealed that cell swelling, but not the decrease in $Ca^{2+}$, was sensitive to the anion channel blocker NPPB, whereas the $Ca^{2+}$ effect, but not the cell swelling, was sensitive to the KCC antagonist bumetanide, suggesting cell volume and resting $Ca^{2+}$ were regulated through separate processes. Elevated $[K^+]_o$ also caused cerebral arteriole dilation, which was sensitive to KCC blockade with bumetanide and to whole-cell patching a peri-arteriole astrocyte.

While our data delineate several novel aspects of $K^+$-astrocyte-arteriole interactions, there is still much to explore in order to understand this new phenomenon. We specifically examined the impact of $[K^+]_o$ on resting, steady-state free $Ca^{2+}$ in astrocytes. Resting $Ca^{2+}$ is a recent consideration, given observations that astrocytes appear to have a higher resting $Ca^{2+}$ concentration than neurons *in vitro* and *in vivo* (Shigetomi et al., 2012; 2013b; Zheng et al., 2015) and that there exist at least two populations of astrocytes designated by different resting $Ca^{2+}$ levels (Zheng et al., 2015). Furthermore, resting $Ca^{2+}$ is thought to contribute to: 1) constitutive D-serine release from astrocytes (Shigetomi et al., 2013b), 2) basal arteriole tone regulation via tonic prostaglandin release (Rosenegger et al., 2015; Mehina et al., 2017), and 3) basal release probability at excitatory synapses (Panatier et al., 2011). Robust spontaneous

microdomain $Ca^{2+}$ transients that occur all over the cell may significantly influence the steady-state $Ca^{2+}$ concentration in the cytosol. Thus, an important consideration is whether or not the $K^+$ induced decrease in steady-state astrocyte $Ca^{2+}$ is really through a decrease in the frequency or amplitude of these spontaneous $Ca^{2+}$ signals. Our data argue against this possibility as we found that the presence vs. absence of these microdomain signals from brain slice to brain slice is highly variable, yet we observed the same faithful decrease in astrocyte $Ca^{2+}$ from experiment to experiment. It is clear that external $Ca^{2+}$ does enter into astrocytes across the plasma membrane constantly. Some propose a $Ca^{2+}$ influx pathway through TRPA1 channels (Shigetomi et al., 2012). In this model, TRPA1 mediates transient microdomain $Ca^{2+}$ influx in which the cumulative effect contributes to the resting steady-state free $Ca^{2+}$ concentration in the cytosol (Shigetomi et al., 2012). Using a quantitative ratiometric $Ca^{2+}$ indicator, bath application of a TRPA1 antagonist decreased resting free $Ca^{2+}$ in astrocyte cultures and in astrocytes *in situ*. While others have shown that TRPA1 is not responsible for the microdomain $Ca^{2+}$ transients in astrocytes using pharmacology and the TRPA1 knockout mouse (Rungta et al., 2016), resting $Ca^{2+}$ in the soma, major processes, or endfeet were not examined in this study, leaving TRPA1 as a possible contributor to steady-state $Ca^{2+}$ levels. In fact, a follow up study by Shigetomi (Shigetomi et al., 2013b) showed that TRPA1 contributes significantly to the resting $Ca^{2+}$ concentration, as TRPA1 antagonism fails to decrease resting $Ca^{2+}$ in the TRPA1 knockout. Notably, in the Rungta et al. study, bath applying a $Ca^{2+}$ free external solution with EGTA not only decreases the frequency of spontaneous microdomain $Ca^{2+}$ transients, but also decreases the baseline $Ca^{2+}$ level in Fluo-4 patch loaded astrocytes. This suggests that a constant influx of $Ca^{2+}$ from the extracellular space helps maintain the resting $Ca^{2+}$ concentration in astrocytes under these conditions. That our high $[K^+]_o$ treatment decreased $Ca^{2+}$ influx is consistent with our block

of the $Ca^{2+}$ drop in a $Ca^{2+}$ free external solution. We expect that the resting $Ca^{2+}$ decrease already occurred in the $Ca^{2+}$ free solution, and thus could not be decreased further when $[K^+]_o$ became elevated.

It remains unclear how free cytosolic $Ca^{2+}$ decreases due to decreased influx. The bidirectional nature of the $Ca^{2+}$ change, and the well-documented influence of external $K^+$ in controlling astrocyte resting membrane potential, leads us to speculate that a change in membrane voltage is a key aspect to the phenomenon. Small increases in external $K^+$ of 1 mM will shift $E_K$ ~9 mV, which, after a subsequent depolarizing shift in membrane potential, would lessen the driving force for the inward movement of $Ca^{2+}$. From this, one might expect that we could block the drop in $Ca^{2+}$ by clamping membrane potential at a hyperpolarized value. However, astrocytes are poorly voltage clamped, given their high resting permeability to $K^+$ and very low input resistance (Steinhäuser et al., 1992). For example, our FLIM experiments employed astrocyte patching and 'holding' the astrocyte membrane potential at -85 mV, yet, we still detected the $Ca^{2+}$ drop in the soma of the patched cell. Even if membrane potential changes were important in the phenomenon, the lack of a block in voltage clamp would be expected. In future experiments, it would be interesting to test if one can block the drop in $Ca^{2+}$ to high $[K^+]_o$ using voltage clamp in the presence of quinine, which increases astrocyte input resistance significantly by blocking two pore domain $K^+$ channels (primarily TREK-1 and TWIK-1). These are key channels that govern the resting permeability of astrocytes to $K^+$ (Zhou et al., 2009) and are responsible for the large errors associated with voltage clamping astrocytes (Ma et al., 2014). Quinine should improve the clamp and one could test if a direct astrocyte depolarization via the patch pipette decreases free $Ca^{2+}$ or if a hyperpolarization increases free $Ca^{2+}$, or if simply

clamping membrane voltage at a hyperpolarized level is able to prevent the free $Ca^{2+}$ decrease to high $[K^+]_o$.

Though $K_{ir}4.1$ contributes to $K^+$ buffering, and the $K^+$ influx could increase KCC activity, we found no effect of 100 μM $BaCl_2$ on the $K^+$-induced decrease in astrocyte $Ca^{2+}$. Previous work has observed that decreasing external $K^+$ can increase $Ca^{2+}$ via a $BaCl_2$ sensitive pathway in cultured astrocytes and *in situ* (Dallwig et al., 2000). While this is analogous to the effects we observed with a 1 mM decrease in $[K^+]_o$, this work employed a larger drop than we explored: moving from 5 mM to 0.2 or 0.4 mM $[K^+]_o$. What invokes KCCs if not inward rectifiers? High $[K^+]_o$ will increase $Na^+/K^+$-ATPase activity, increasing intracellular $[K^+]$, which could subsequently increase the efflux of $K^+$ and $Cl^-$ via KCC. However, blocking this crucial ATPase to test its role in our effect is untenable in brain slices at the micron-level due to robust cell volume changes to the antagonist ouabain (Joshi and Andrew, 2001). While increasing $Na^+/K^+$-ATPase activity, high external $K^+$ would also limit KCC activity by acting against the outward movement of $K^+$ and $Cl^-$ ions. The cumulative effect on KCC activity (up or down) would depend on the relative expression and kinetics of each transport system. Undoubtedly though, changing KCC activity will affect the intracellular $K^+$ and $Cl^-$ concentrations, as well as membrane potential due to differences in the resting permeability of each ion and potentially due to secondary transport mechanisms. For instance, bumetanide itself influences membrane potential in kidney cells (Wang et al., 2013), skeletal muscle (van Mil et al., 1997), and can prevent membrane potential changes to osmotic stimuli (van Mil et al., 1997). The cumulative effect of bumetanide on membrane potential in astrocytes will likely depend on the relative expression of NKCC vs KCC. Astrocyte transcriptome evidence from the neocortex shows no detectable expression of NKCCs in astrocytes, whereas KCC1 is clearly transcribed (Cahoy et

al., 2008; Zhang et al., 2014). Importantly, bumetanide blocks KCC1 (Gillen and Forbush, 1999). We envisage that bumetanide depolarizes the astrocyte membrane potential and lessens the ability of external $K^+$ to cause depolarization, thus preventing the ability of $K^+$ to decrease $Ca^{2+}$ influx. This idea can be easily tested by recording astrocytes in current clamp in response to high $K^+$ alone, bumetanide alone, and high $K^+$ in the presence of bumetanide. Importantly, KCCs are ubiquitous proteins (though subtypes in certain cells vary) (Mount et al., 1999; Race et al., 1999; Song et al., 2002; Gagnon et al., 2007); thus the effect of bumetanide on blocking $K^+$-induced vasodilation could be due to a direct effect of this drug on the arteriole under study. Indeed, KCC3 is expressed in VSMCs (Di Fulvio et al., 2001; Rust et al., 2006). While we cannot explicitly rule out a direct effect on vasculature, our data point to two astrocyte-specific effects in the $K^+$-induced vasodilation. First, the astrocyte free $Ca^{2+}$ decrease was associated with vasodilation and bumetanide blocked both the $Ca^{2+}$ drop and the vasodilation. Second, simply patch-clamping a peri-arteriole astrocyte blocked high $[K^+]_o$ induced vasodilation. If high $[K^+]_o$ acted directly on VSMC KCC proteins, patching the astrocyte should not have blocked the dilating effect of high $[K^+]_o$.

With an important role for $Cl^-$, $HCO_3^-$, and KCC, our data could indicate the involvement of GABA and $GABA_A$ channels. $GABA_A$ receptors rely on the $Cl^-$ gradient and are permeable to $HCO_3^-$. Astrocytes express $GABA_A$ and $GABA_B$ receptors, which upon activation elevates free $Ca^{2+}$ (Nilsson et al., 1993; Fraser et al., 1994; Young et al., 2010). Furthermore, $GABA_A$ channel activation decreases cell volume (Florence et al., 2012), suggesting a potential role for GABA in $Ca^{2+}$ and volume regulation. Astrocytes may also be capable of releasing GABA. One notable hypothesis involves the tonic release of GABA through the $Ca^{2+}$ dependent, large-pore anion channel Bestrophin-1 (Best1) (Lee et al., 2010; Yoon et al., 2011). Best1 is open at resting levels

of $Ca^{2+}$ (~100 nM) and shows a steep decline in current as $Ca^{2+}$ decreases from the resting level (Lee et al., 2010), which would decrease GABA release and ultimately decrease $Ca^{2+}$ due to less $GABA_A$ activation. Furthermore, Best1 is sensitive to NPPB. However, NPPB had little impact on the drop in $Ca^{2+}$ to high $[K^+]_o$, and astrocytes were still capable of swelling even when the $Ca^{2+}$ drop was blocked with bumetanide. This suggests that the anion channel in question for the volume change is exclusively involved in that process, not the $Ca^{2+}$ decrease. Thus, a $Ca^{2+}$ independent anion channel is more likely to underlie the volume change, such as Volume Regulated Anion Channels (VRACs), Maxi-Anion Channels, or voltage gated chloride channels. NPPB does block some voltage gated chloride channels, such as CLCNKA and B (Pusch and Jentsch, 1994); however, these transcripts are not detected in neocortical astrocytes (Zhang et al., 2014). Volume Regulated Anion Channels are activated in response to cell swelling, and help restore cell volume (Mulligan and MacVicar, 2006). One line of thinking is that the involvement of these channels is unlikely because one might expect larger astrocyte swelling in response to high $[K^+]_o$ in the presence of NPPB, which we did not observe. Alternatively, if VRACs are working constantly to keep cell volume low, NPPB could produce astrocyte swelling itself, occluding the effect of high $[K^+]_o$ induced swelling. The role of VRAC could be tested pharmacologically when compared to another potential candidate: the Maxi-Anion Channel. Cultured astrocytes may functionally express the Maxi-Anion Channel (Liu et al., 2008; Zhao et al., 2017). Its contribution is determined by a sensitivity to NPPB and $Gd^{3+}$, but an insensitivity to other $Cl^-$ channel blockers such as niflumic acid, carbenoxolone, or $Zn^{2+}$ (Rungta et al., 2015). VRACs are only sensitive to NPPB (and DIDS, which was untenable for us); thus $Gd^{3+}$ sensitivity, or insensitivity, could help us differentiate between VRACs and Maxi-Anion

channels. In future work it will be important to use these other pharmacological tools to see what channel fits the pharmacological profile.

Regarding the astrocyte $Ca^{2+}$ drop caused by high $[K^+]_o$, the effect was blocked with a low external $Cl^-$ solution but not by NPPB, suggesting a $Cl^-$ pathway that does not involve VRACs, CLCNKA/B, and the Maxi-Anion Channel. While bumetanide was effective at blocking the $Ca^{2+}$ drop, there could be an additional contribution from a voltage dependent chloride channel that is insensitive to NPPB. Voltage dependent $Cl^-$ channels are important for regulating resting membrane potential in cells (Pusch and Jentsch, 1994), and thus a small shift in membrane potential from high $[K^+]_o$ could increase channel opening, allowing $Cl^-$ movements. In astrocytes, this would likely entail $Cl^-$ efflux due to the resting membrane potential being more hyperpolarized to $E_{Cl}$. This would enhance the depolarization caused by high $[K^+]_o$. If a decrease in the driving force for $Ca^{2+}$ due to depolarization was an important process in the observed $Ca^{2+}$ decrease in response to high $[K^+]_o$, the low external $Cl^-$ solution itself could enhance $Cl^-$ efflux from astrocytes, depolarize the membrane potential, and potentially occlude the drop in $Ca^{2+}$ caused by high $[K^+]_o$. CLCN2 transcripts are present in astrocytes (Zhang et al., 2014), and CLCN2 is insensitive to NPPB (Rungta et al., 2015). It would be interesting to explore the role of this channel in future experiments.

$Ca^{2+}$ influx through TRPA1 is an interesting candidate for arteriole diameter control, given that this channel is sensitive to factors that also affect blood vessels, such as epoxyeicosatrienoic acids (EETs). EETs activate TRPA1 (Koivisto et al., 2014) and have potent effects on contractile vasculature (Alkayed et al., 1996a; Liu et al., 2012). Furthermore, EETs are proposed to be an abundant product of astrocytes after the metabolism of arachidonic acid by CYP450 enzyme subtypes (Alkayed et al., 1996b; Lecrux et al., 2012). A drop in astrocyte $Ca^{2+}$

could mean a decrease in the production of a tonic vasoconstrictor, or the generation of a vasodilator, or both, where a subtle shift in the balance towards dilating over constricting factors could produce the vasodilation we observe. Given that $Ca^{2+}$ is important in the production of vasoactive metabolites such as eicosanoids, we envision that the decrease in astrocyte $Ca^{2+}$ is decreasing the production of a tonically produced vasoconstrictor, such as prostaglandin F2 alpha, more so than producing vasodilators like EETs. To our knowledge, we are not aware of a study examining the relationship between subtle changes in resting free cytosolic $Ca^{2+}$ and the relative production of various vasoactive messengers from astrocytes or other cells. The general concept is supported by literature at the high end of $[Ca^{2+}]_i$, where elevations in free $Ca^{2+}$ up to 500 nM produce vasodilation, whereas exceeding this threshold results in vasoconstriction (Girouard et al., 2010). It is important to note that a slightly higher elevation in $[K^+]_o$ (~10 mM) causes robust increases in lactate release from astrocytes due to $HCO_3^-$ influx through the sodium bicarbonate co-transporter, the activation of soluble adenylyl cyclase, and increased cAMP signaling (Choi et al., 2012). Lactate itself has been shown to be vasoactive, by enhancing the level of extracellular dilatory PGE2 (Gordon et al., 2008). Though our data argue against the sodium bicarbonate co-transporter and soluble adenylyl cyclase being involved in the $Ca^{2+}$ decrease caused by $K^+$, the arteriole was not examined. It is conceivable that this pathway is involved in the arteriole effect we described, as our data suggests $Ca^{2+}$ may not be sufficient by itself (more below).

Our previous study is the only one to examine a decrease in free astrocyte $Ca^{2+}$ using patch clamp while measuring adjacent arterioles. We previously observed a vasoconstriction when astrocyte $Ca^{2+}$ was lowered cell-wide via a BAPTA loaded patch pipette (Rosenegger et al., 2015). This is opposite to what we observed with high $[K^+]_o$, in which a free $Ca^{2+}$ decrease

produces a vasodilation. This suggests that although we observe a global decrease in $Ca^{2+}$ as evidenced by a freely diffusible $Ca^{2+}$ indicator in response to high $[K^+]_o$, it is likely that the location where $Ca^{2+}$ is decreasing in the micro-domain of the cell is what dictates the effect observed. In the $Ca^{2+}$ clamping patch experiment, BAPTA is present everywhere in the cytosol, and the observed vasoconstriction suggests this is a dominant effect over the pathways controlling arteriole dilation in response to high $[K^+]_o$. This idea was forwarded previously, where a constriction mechanism dominated over a co-existing dilation mechanism, and to observe dilation, the constriction pathway had to be blocked (Gordon et al., 2008). Finally, the effect of high $[K^+]_o$ in decreasing astrocyte $Ca^{2+}$ and causing vasodilation is also, at first, contrary to the previous described effects of glutamate we observed. We previously showed that glutamate decreases astrocyte free $Ca^{2+}$, resulting in increased vessel tone or vasoconstriction (similar to astrocyte BAPTA) (Mehina et al., 2017). However, this is clearly though a different mechanism than $K^+$, as glutamate produced a long-lasting effect, where basal free $Ca^{2+}$ and arteriole diameter obtained a new, lower, steady-state level after plasticity inducing trains of afferent neural activity, or in response to glutamate itself. In contrast, the high $K^+$-induced decrease in astrocyte $Ca^{2+}$ only lasted as long as $K^+$ was applied, and $Ca^{2+}$, as well as arteriole diameter, returned fully to baseline after $K^+$ washout. Furthermore, the glutamate effect required multiple glutamate receptors, nitric oxide, and the effect partially involved enhanced loading of intracellular $Ca^{2+}$ stores via SERCA pumps (Mehina et al., 2017). Our $K^+$-induced decrease in free $Ca^{2+}$ did not involve intracellular stores, as thapsigargin pre-incubation was ineffective. Thus, similar to explaining the discrepancy between high $[K^+]_o$ and astrocyte BAPTA, the results may be reconciled by the idea that we are examining a freely diffusible, cell-wide $Ca^{2+}$ indicator.

What matters are how and where $Ca^{2+}$ is changing in the micro-domain of the cell and what cellular cascade(s) this $Ca^{2+}$ change couples to.

It is important to consider whether the decrease in astrocyte $Ca^{2+}$ is itself sufficient to cause high $K^+$-induced vasodilation. From one perspective, our data may argue against the sufficiency of astrocyte $Ca^{2+}$ as a prerequisite step. Our data show that patching a peri-arteriole astrocyte blocks $K^+$-induced vasodilation, but $Ca^{2+}$ is likely still decreasing in astrocytes. This was clearly the case given our FLIM $Ca^{2+}$ measures, which introduced OGB-1 into astrocytes via the patch pipette. In this condition, the $Ca^{2+}$ drop could be detected in all compartments of the patched cell, including perivascular endfeet. However, recall that the resting $Ca^{2+}$ level is significantly higher in the patched cell compared to coupled cells. Thus, even though $Ca^{2+}$ still decreased while patched in response to high $[K^+]_o$, the absolute level of $Ca^{2+}$ reached was not as low as non-patched astrocytes (~75 nM compared to ~40 nM). This could affect the type or amount of vasoactive messenger being released from astrocytes, which could explain why we observed a vasoconstriction to high $K^+$, instead of a vasodilation, while the perivascular astrocyte was patched. An alternate idea is that the patching process dialyzes the cell and washes out key metabolites necessary for vasodilation, such as in decreasing the available pool of intracellular arachidonic acid or prostaglandin H2. However, we observed a vasoconstriction in response to high $[K^+]$, suggesting messengers can still be produced in whole-cell configuration. This argues in favour of the $Ca^{2+}$ hypothesis over the washout of substrates for messengers.

Previous neurovascular coupling studies examining the role of $K^+$ on vasculature propose that $K^+$ becomes high in the perivascular space (between endfeet and VSMCs), which facilitates $K_{ir}2.1$ channel opening on VSMCs, and relaxes the arteriole via hyperpolarization (Filosa et al., 2006; Girouard et al., 2010; Longden et al., 2014; 2017). In these studies, higher external $K^+$

concentrations are used (8-10 mM) compared to our work (3.5-5 mM), and $Ba^{2+}$ is an effective blocker of $K^+$ evoked vasodilation. While we did not directly test $Ba^{2+}$ on vasodilation triggered by a more modest increase in external $K^+$, $Ba^{2+}$ is an unlikely candidate for two reasons: 1) $Ba^{2+}$ failed to block the decrease in astrocyte $Ca^{2+}$, which was associated with vasodilation, and 2) for elevations in external $K^+$ reaching 8-10 mM, $K_{ir}$ channels on the vasculature are thought to contribute to vasodilation. However, with smaller physiological elevations in $[K^+]_o$ (up to 5 mM), $K_{ir}$ channels are not involved, at least for cerebral pial arterioles (Horiuchi et al., 2002).

### 4.1 Conclusion

Neurons, the electrically excitable cells of the nervous system, have historically dominated the spotlight, overshadowing non-excitable glial cells such as astrocytes. Astrocytes are one of the most abundant types of cells in the brain. Moreover, astrocytes are uniformly positioned throughout the brain, as well as possessing special appendages called endfeet that collectively envelop nearly all of the cerebrovasculature. These physical features alone make a compelling argument in favour of astrocytes possessing functions that are physiologically relevant and crucial for brain health.

Astrocytes are involved in ion homeostasis, and our work here has focused on one ion in particular, potassium. Here we suggest the possibility of an alternative means through which extracellular $K^+$ plays a role in astrocyte physiology, and has relevance for the cerebrovasculature via astrocyte endfeet. Specifically, we have shown that: 1) modest changes in extracellular $K^+$ controls the resting free $Ca^{2+}$ and soma volume of astrocyte in a bidirectional manner, 2) extracellular $K^+$-mediated changes in resting $Ca^{2+}$ and volume also occur in astrocyte endfeet, 3) extracellular $K^+$-mediated changes in astrocyte $Ca^{2+}$ and soma volume are distinct,

separate phenomena that depend on certain anion channels, and 4) modest increases in extracellular $K^+$ mediates vasodilation that relies on the $K^+$-$Cl^-$ cotransporter. Therefore, a simple change in extracellular [$K^+$] results in physiologically relevant events. These findings provide the first insights into how astrocytes utilize resting free $Ca^{2+}$ to connect two crucial functions together: extracellular $K^+$ homeostasis, and brain blood flow control.

## REFERENCES


Adragna NC, Chen Y, Delpire E, Lauf PK, Morris M (2004) Hypertension in K-Cl cotransporter-3 knockout mice. Adv Exp Med Biol 559:379–385.

Agulhon C, Fiacco TA, McCarthy KD (2010) Hippocampal Short- and Long-Term Plasticity Are Not Modulated by Astrocyte Ca2+ Signaling. Science 327:1250–1254.

Agulhon C, Petravicz J, McMullen AB, Sweger EJ, Minton SK, Taves SR, Casper KB, Fiacco TA, McCarthy KD (2008) What is the role of astrocyte calcium in neurophysiology? Neuron 59:932–946.

Alkayed NJ, Birks EK, Hudetz AG, Roman RJ, Henderson L, Harder DR (1996a) Inhibition of brain P-450 arachidonic acid epoxygenase decreases baseline cerebral blood flow. Am J Physiol 271:H1541–H1546.

Alkayed NJ, Narayanan J, Gebremedhin D, Medhora M, Roman RJ, Harder DR (1996b) Molecular characterization of an arachidonic acid epoxygenase in rat brain astrocytes. Stroke 27:971–979.

Amiry-Moghaddam M, Ottersen OP (2003) The molecular basis of water transport in the brain. Nature Reviews Neuroscience 4:991–1001.

Amruthesh SC, Boerschel MF, McKinney JS, Willoughby KA, Ellis EF (1993) Metabolism of arachidonic acid to epoxyeicosatrienoic acids, hydroxyeicosatetraenoic acids, and prostaglandins in cultured rat hippocampal astrocytes. J Neurochem 61:150–159.

Anderson CM, Bergher JP, Swanson RA (2004) ATP-induced ATP release from astrocytes. J Neurochem 88:246–256.

Araque A, Parpura V, Sanzgiri RP, Haydon PG (1999) Tripartite synapses: glia, the unacknowledged partner. Trends Neurosci 22:208–215.

Arcuino G, Lin JHC, Takano T, Liu C, Jiang L, Gao Q, Kang J, Nedergaard M (2002) Intercellular calcium signaling mediated by point-source burst release of ATP. Proc Natl Acad Sci USA 99:9840–9845.

Arroyo JP, Kahle KT, Gamba G (2013) The SLC12 family of electroneutral cation-coupled chloride cotransporters. Mol Aspects Med 34:288–298.

Attwell D, Buchan AM, Charpak S, Lauritzen M, MacVicar BA, Newman EA (2010) Glial and neuronal control of brain blood flow. Nature 468:232–243.

Ayata C, Lauritzen M (2015) Spreading Depression, Spreading Depolarizations, and the Cerebral Vasculature. Physiol Rev 95:953–993.

Azevedo FAC, Carvalho LRB, Grinberg LT, Farfel JM, Ferretti REL, Leite REP, Jacob Filho W,

Lent R, Herculano-Houzel S (2009) Equal numbers of neuronal and nonneuronal cells make the human brain an isometrically scaled-up primate brain. J Comp Neurol 513:532–541.

Basarsky TA, Feighan D, MacVicar BA (1999) Glutamate release through volume-activated channels during spreading depression. J Neurosci 19:6439–6445.

Beck A, Nieden RZ, Schneider H-P, Deitmer JW (2004) Calcium release from intracellular stores in rodent astrocytes and neurons in situ. Cell Calcium 35:47–58.

Becker W (2012) The bh TCSPC Handbook, 5 ed. Berlin, Germany: Becker & Hickl Gmbh.

Benesova J, Rusnakova V, Honsa P, Pivonkova H, Dzamba D, Kubista M, Anderova M (2012) Distinct expression/function of potassium and chloride channels contributes to the diverse volume regulation in cortical astrocytes of GFAP/EGFP mice. Hetman M, ed. PLoS ONE 7:e29725.

Bergles DE, Jahr CE (1998) Glial contribution to glutamate uptake at Schaffer collateral-commissural synapses in the hippocampus. J Neurosci 18:7709–7716.

Blinder P, Shih AY, Rafie C, Kleinfeld D (2010) Topological basis for the robust distribution of blood to rodent neocortex. Proc Natl Acad Sci USA 107:12670–12675.

Blinder P, Tsai PS, Kaufhold JP, Knutsen PM, Suhl H, Kleinfeld D (2013) The cortical angiome: an interconnected vascular network with noncolumnar patterns of blood flow. Nature Neuroscience 16:889–897.

Boettger T, Rust MB, Maier H, Seidenbecher T, Schweizer M, Keating DJ, Faulhaber J, Ehmke H, Pfeffer C, Scheel O, Lemcke B, Horst J, Leuwer R, Pape H-C, Völkl H, Hübner CA, Jentsch TJ (2003) Loss of K-Cl co-transporter KCC3 causes deafness, neurodegeneration and reduced seizure threshold. EMBO J 22:5422–5434.

Bonder DE, McCarthy KD (2014) Astrocytic Gq-GPCR-linked IP3R-dependent Ca2+ signaling does not mediate neurovascular coupling in mouse visual cortex in vivo. J Neurosci 34:13139–13150.

Boulenguez P, Liabeuf S, Bos R, Bras H, Jean-Xavier C, Brocard C, Stil A, Darbon P, Cattaert D, Delpire E, Marsala M, Vinay L (2010) Down-regulation of the potassium-chloride cotransporter KCC2 contributes to spasticity after spinal cord injury. Nat Med 16:302–307.

Brune T, Fetzer S, Backus KH, Deitmer JW (1994) Evidence for electrogenic sodium-bicarbonate cotransport in cultured rat cerebellar astrocytes. Pflugers Arch 429:64–71.

Bushong EA, Martone ME, Jones YZ, Ellisman MH (2002) Protoplasmic astrocytes in CA1 stratum radiatum occupy separate anatomical domains. J Neurosci 22:183–192.

Cahoy JD, Emery B, Kaushal A, Foo LC, Zamanian JL, Christopherson KS, Xing Y, Lubischer JL, Krieg PA, Krupenko SA, Thompson WJ, Barres BA (2008) A transcriptome database for

astrocytes, neurons, and oligodendrocytes: a new resource for understanding brain development and function. J Neurosci 28:264–278.

Campbell WB, Fleming I (2010) Epoxyeicosatrienoic acids and endothelium-dependent responses. Pflugers Arch 459:881–895.

Carter BC, Bean BP (2009) Sodium entry during action potentials of mammalian neurons: incomplete inactivation and reduced metabolic efficiency in fast-spiking neurons. Neuron 64:898–909.

Chen BR, Bouchard MB, McCaslin AFH, Burgess SA, Hillman EMC (2011) High-speed vascular dynamics of the hemodynamic response. Neuroimage 54:1021–1030.

Chen Y, Cann MJ, Litvin TN, Iourgenko V, Sinclair ML, Levin LR, Buck J (2000) Soluble adenylyl cyclase as an evolutionarily conserved bicarbonate sensor. Science 289:625–628.

Chever O, Djukic B, McCarthy KD, Amzica F (2010) Implication of Kir4.1 channel in excess potassium clearance: an in vivo study on anesthetized glial-conditional Kir4.1 knock-out mice. J Neurosci 30:15769–15777.

Choi HB, Gordon GRJ, Zhou N, Tai C, Rungta RL, Martinez J, Milner TA, Ryu JK, McLarnon JG, Tresguerres M, Levin LR, Buck J, MacVicar BA (2012) Metabolic communication between astrocytes and neurons via bicarbonate-responsive soluble adenylyl cyclase. Neuron 75:1094–1104.

Connors B, Dray A, Fox P, Hilmy M, Somjen G (1979) LSD's effect on neuron populations in visual cortex gauged by transient responses of extracellular potassium evoked by optical stimuli. Neuroscience Letters 13:147–150.

Cornell-Bell AH, Finkbeiner SM, Cooper MS, Smith SJ (1990) Glutamate induces calcium waves in cultured astrocytes: long-range glial signaling. Science 247:470–473.

Coull JAM, Boudreau D, Bachand K, Prescott SA, Nault F, Sík A, De Koninck P, De Koninck Y (2003) Trans-synaptic shift in anion gradient in spinal lamina I neurons as a mechanism of neuropathic pain. Nature 424:938–942.

Dallwig R, Vitten H, Deitmer JW (2000) A novel barium-sensitive calcium influx into rat astrocytes at low external potassium. Cell Calcium 28:247–259.

Davis RJ, Murdoch CE, Ali M, Purbrick S, Ravid R, Baxter GS, Tilford N, Sheldrick RLG, Clark KL, Coleman RA (2004) EP4 prostanoid receptor-mediated vasodilatation of human middle cerebral arteries. Br J Pharmacol 141:580–585.

de Los Heros P, Alessi DR, Gourlay R, Campbell DG, Deak M, Macartney TJ, Kahle KT, Zhang J (2014) The WNK-regulated SPAK/OSR1 kinases directly phosphorylate and inhibit the K+-Cl- co-transporters. Biochem J 458:559–573.

de Los Heros P, Kahle KT, Rinehart J, Bobadilla NA, Vázquez N, San Cristobal P, Mount DB, Lifton RP, Hebert SC, Gamba G (2006) WNK3 bypasses the tonicity requirement for K-Cl cotransporter activation via a phosphatase-dependent pathway. Proc Natl Acad Sci USA 103:1976–1981.

Di Fulvio M, Lincoln TM, Lauf PK, Adragna NC (2001) Protein kinase G regulates potassium chloride cotransporter-4 [corrected] expression in primary cultures of rat vascular smooth muscle cells. J Biol Chem 276:21046–21052.

Diaz MR, Wadleigh A, Hughes BA, Woodward JJ, Valenzuela CF (2011) Bestrophin1 Channels are Insensitive to Ethanol and Do not Mediate Tonic GABAergic Currents in Cerebellar Granule Cells. Front Neurosci 5:148.

Ding F, O'Donnell J, Xu Q, Kang N, Goldman N, Nedergaard M (2016) Changes in the composition of brain interstitial ions control the sleep-wake cycle. Science 352:550–555.

Distler C, Dreher Z, Stone J (1991) Contact spacing among astrocytes in the central nervous system: an hypothesis of their structural role. Glia 4:484–494.

Dutta AK, Korchev YE, Shevchuk AI, Hayashi S, Okada Y, Sabirov RZ (2008) Spatial distribution of maxi-anion channel on cardiomyocytes detected by smart-patch technique. Biophys J 94:1646–1655.

Ernest NJ, Weaver AK, Van Duyn LB, Sontheimer HW (2005) Relative contribution of chloride channels and transporters to regulatory volume decrease in human glioma cells. Am J Physiol, Cell Physiol 288:C1451–C1460.

Filosa JA, Bonev AD, Straub SV, Meredith AL, Wilkerson MK, Aldrich RW, Nelson MT (2006) Local potassium signaling couples neuronal activity to vasodilation in the brain. Nat Neurosci 9:1397–1403.

Filosa JA, Morrison HW, Iddings JA, Du W, Kim KJ (2016) Beyond neurovascular coupling, role of astrocytes in the regulation of vascular tone. Neuroscience 323:96–109.

Florence CM, Baillie LD, Mulligan SJ (2012) Dynamic Volume Changes in Astrocytes Are an Intrinsic Phenomenon Mediated by Bicarbonate Ion Flux. PLoS ONE 7:e51124.

Fraser DD, Mudrick-Donnon LA, MacVicar BA (1994) Astrocytic GABA receptors. Glia 11:83–93.

Gagnon KBE, Adragna NC, Fyffe REW, Lauf PK (2007) Characterization of glial cell K-Cl cotransport. Cell Physiol Biochem 20:121–130.

Gamba G (2005) Molecular physiology and pathophysiology of electroneutral cation-chloride cotransporters. Physiol Rev 85:423–493.

Garneau AP, Marcoux A-A, Noël M, Frenette-Cotton R, Drolet M-C, Couet J, Larivière R,

Isenring P (2016) Ablation of Potassium-Chloride Cotransporter Type 3 (Kcc3) in Mouse Causes Multiple Cardiovascular Defects and Isosmotic Polyuria. Fotiadis D, ed. PLoS ONE 11:e0154398.

Gillen CM, Forbush B (1999) Functional interaction of the K-Cl cotransporter (KCC1) with the Na-K-Cl cotransporter in HEK-293 cells. Am J Physiol 276:C328–C336.

Girouard H, Bonev AD, Hannah RM, Meredith A, Aldrich RW, Nelson MT (2010) Astrocytic endfoot Ca2+ and BK channels determine both arteriolar dilation and constriction. Proc Natl Acad Sci USA 107:3811–3816.

Girouard H, Iadecola C (2006) Neurovascular coupling in the normal brain and in hypertension, stroke, and Alzheimer disease. J Appl Physiol 100:328–335.

Gordon GRJ, Baimoukhametova DV, Hewitt SA, Rajapaksha WR, Fisher TE, Bains JS (2005) Norepinephrine triggers release of glial ATP to increase postsynaptic efficacy. Nat Neurosci 8:1078–1086.

Gordon GRJ, Choi HB, Rungta RL, Ellis-Davies GCR, MacVicar BA (2008) Brain metabolism dictates the polarity of astrocyte control over arterioles. Nature 456:745–749.

Gordon GRJ, Iremonger KJ, Kantevari S, Ellis-Davies GCR, MacVicar BA, Bains JS (2009) Astrocyte-mediated distributed plasticity at hypothalamic glutamate synapses. Neuron 64:391–403.

Grosche J, Matyash V, Möller T, Verkhratsky A, Reichenbach A, Kettenmann H (1999) Microdomains for neuron-glia interaction: parallel fiber signaling to Bergmann glial cells. Nat Neurosci 2:139–143.

Haj-Yasein NN, Jensen V, Østby I, Omholt SW, Voipio J, Kaila K, Ottersen OP, Hvalby Ø, Nagelhus EA (2012) Aquaporin-4 regulates extracellular space volume dynamics during high-frequency synaptic stimulation: a gene deletion study in mouse hippocampus. Glia 60:867–874.

Halassa MM, Fellin T, Takano H, Dong J-H, Haydon PG (2007) Synaptic islands defined by the territory of a single astrocyte. J Neurosci 27:6473–6477.

Hansen AJ, Zeuthen T (1981) Extracellular ion concentrations during spreading depression and ischemia in the rat brain cortex. Acta Physiol Scand 113:437–445.

Harder DR, Roman RJ, Gebremedhin D, Birks EK, Lange AR (1998) A common pathway for regulation of nutritive blood flow to the brain: arterial muscle membrane potential and cytochrome P450 metabolites. Acta Physiol Scand 164:527–532.

Hartzell HC, Qu Z, Yu K, Xiao Q, Chien L-T (2008) Molecular physiology of bestrophins: multifunctional membrane proteins linked to best disease and other retinopathies. Physiol Rev 88:639–672.

Hassinger TD, Guthrie PB, Atkinson PB, Bennett MV, Kater SB (1996) An extracellular signaling component in propagation of astrocytic calcium waves. Proc Natl Acad Sci USA 93:13268–13273.

Haustein MD, Kracun S, Lu X-H, Shih T, Jackson-Weaver O, Tong X, Xu J, Yang XW, O'Dell TJ, Marvin JS, Ellisman MH, Bushong EA, Looger LL, Khakh BS (2014) Conditions and constraints for astrocyte calcium signaling in the hippocampal mossy fiber pathway. Neuron 82:413–429.

Heinemann U, Lux HD (1977) Ceiling of stimulus induced rises in extracellular potassium concentration in the cerebral cortex of cat. Brain Res 120:231–249.

Henneberger C, Papouin T, Oliet SHR, Rusakov DA (2010) Long-term potentiation depends on release of D-serine from astrocytes. Nature 463:232–236.

Hertz L, Song D, Xu J, Peng L, Gibbs ME (2015) Role of the Astrocytic Na(+), K(+)-ATPase in K(+) Homeostasis in Brain: K(+) Uptake, Signaling Pathways and Substrate Utilization. Neurochem Res 40:2505–2516.

Horiuchi T, Dietrich HH, Hongo K, Dacey RG (2002) Mechanism of extracellular K+-induced local and conducted responses in cerebral penetrating arterioles. Stroke 33:2692–2699.

Huang WC, Xiao S, Huang F, Harfe BD, Jan YN, Jan LY (2012) Calcium-activated chloride channels (CaCCs) regulate action potential and synaptic response in hippocampal neurons. Neuron 74:179–192.

Hubbard JA, Hsu MS, Seldin MM, Binder DK (2015) Expression of the Astrocyte Water Channel Aquaporin-4 in the Mouse Brain. ASN Neuro 7:175909141560548.

Hübner CA, Stein V, Hermans-Borgmeyer I, Meyer T, Ballanyi K, Jentsch TJ (2001) Disruption of KCC2 reveals an essential role of K-Cl cotransport already in early synaptic inhibition. Neuron 30:515–524.

Iadecola C (2004) Neurovascular regulation in the normal brain and in Alzheimer's disease. Nat Rev Neurosci 5:347–360.

Inoue H, Okada Y (2007) Roles of volume-sensitive chloride channel in excitotoxic neuronal injury. J Neurosci 27:1445–1455.

Institoris Á, Rosenegger DG, Gordon GR (2015) Arteriole dilation to synaptic activation that is sub-threshold to astrocyte endfoot Ca2+ transients. J Cereb Blood Flow Metab 35:1411–1415.

Jennings ML, Schulz RK (1991) Okadaic acid inhibition of KCl cotransport. Evidence that protein dephosphorylation is necessary for activation of transport by either cell swelling or N-ethylmaleimide. J Gen Physiol 97:799–817.

Jentsch TJ, Stein V, Weinreich F, Zdebik AA (2002) Molecular structure and physiological function of chloride channels. Physiol Rev 82:503–568.

Joshi I, Andrew RD (2001) Imaging anoxic depolarization during ischemia-like conditions in the mouse hemi-brain slice. Journal of Neurophysiology 85:414–424.

Jourdain P, Bergersen LH, Bhaukaurally K, Bezzi P, Santello M, Domercq M, Matute C, Tonello F, Gundersen V, Volterra A (2007) Glutamate exocytosis from astrocytes controls synaptic strength. Nat Neurosci 10:331–339.

Kahle KT, Simard JM, Staley KJ, Nahed BV, Jones PS, Sun D (2009) Molecular mechanisms of ischemic cerebral edema: role of electroneutral ion transport. Physiology (Bethesda) 24:257–265.

Kanemaru K, Sekiya H, Xu M, Satoh K, Kitajima N, Yoshida K, Okubo Y, Sasaki T, Moritoh S, Hasuwa H, Mimura M, Horikawa K, Matsui K, Nagai T, Iino M, Tanaka KF (2014) In vivo visualization of subtle, transient, and local activity of astrocytes using an ultrasensitive Ca(2+) indicator. Cell Rep 8:311–318.

Karadsheh MF, Byun N, Mount DB, Delpire E (2004) Localization of the KCC4 potassium-chloride cotransporter in the nervous system. Neuroscience 123:381–391.

Katzman R (1976) Maintenance of a constant brain extracellular potassium. Fed Proc 35:1244–1247.

Kettenmann H, Ransom BR (2004) The concept of neuroglia: a historical perspective. In: Neuroglia, 2nd ed. Oxford University Press.

Kimelberg HK (2010) Functions of Mature Mammalian Astrocytes: A Current View. The Neuroscientist 16:79–106.

Kimelberg HK, MacVicar BA, Sontheimer H (2006) Anion channels in astrocytes: biophysics, pharmacology, and function. Glia 54:747–757.

Knot HJ, Zimmermann PA, Nelson MT (1996) Extracellular K(+)-induced hyperpolarizations and dilatations of rat coronary and cerebral arteries involve inward rectifier K(+) channels. J Physiol 492:419–430.

Kofuji P, Newman EA (2004) Potassium buffering in the central nervous system. Neuroscience 129:1045–1056.

Koivisto A, Chapman H, Jalava N, Korjamo T, Saarnilehto M, Lindstedt K, Pertovaara A (2014) TRPA1: a transducer and amplifier of pain and inflammation. Basic Clin Pharmacol Toxicol 114:50–55.

Kronschläger MT, Drdla-Schutting R, Gassner M, Honsek SD, Teuchmann HL, Sandkühler J (2016) Gliogenic LTP spreads widely in nociceptive pathways. Science 354:1144–1148.

Kuffler SW (1967) Neuroglial cells: physiological properties and a potassium mediated effect of neuronal activity on the glial membrane potential. Proc R Soc Lond, B, Biol Sci 168:1–21.

Kunz A, Park L, Abe T, Gallo EF, Anrather J, Zhou P, Iadecola C (2007) Neurovascular protection by ischemic tolerance: role of nitric oxide and reactive oxygen species. J Neurosci 27:7083–7093.

Kyrozis A, Reichling DB (1995) Perforated-patch recording with gramicidin avoids artifactual changes in intracellular chloride concentration. J Neurosci Methods 57:27–35.

Lackowicz JR (2006) Principles of fluorescence spectroscopy, 3rd ed. Spinger.

Large WA, Wang Q (1996) Characteristics and physiological role of the Ca(2+)-activated Cl- conductance in smooth muscle. Am J Physiol 271:C435–C454.

Larsen BR, Assentoft M, Cotrina ML, Hua SZ, Nedergaard M, Kaila K, Voipio J, MacAulay N (2014) Contributions of the Na+/K+-ATPase, NKCC1, and Kir4.1 to hippocampal K+ clearance and volume responses. Glia 62:608–622.

Larsen BR, MacAulay N (2017) Activity-dependent astrocyte swelling is mediated by pH-regulating mechanisms. Glia 65:1668–1681.

Lascola CD, Kraig RP (1996) Whole-cell chloride currents in rat astrocytes accompany changes in cell morphology. J Neurosci 16:2532–2545.

Lascola CD, Nelson DJ, Kraig RP (1998) Cytoskeletal actin gates a Cl- channel in neocortical astrocytes. J Neurosci 18:1679–1692.

Lauf PK, Adragna NC (2000) K-Cl cotransport: properties and molecular mechanism. Cell Physiol Biochem 10:341–354.

Lecrux C, Kocharyan A, Sandoe CH, Tong X-K, Hamel E (2012) Pyramidal cells and cytochrome P450 epoxygenase products in the neurovascular coupling response to basal forebrain cholinergic input. J Cereb Blood Flow Metab 32:896–906.

Lee S, Yoon B-E, Berglund K, Oh S-J, Park H, Shin H-S, Augustine GJ, Lee CJ (2010) Channel-mediated tonic GABA release from glia. Science 330:790–796.

Liu H-T, Toychiev AH, Takahashi N, Sabirov RZ, Okada Y (2008) Maxi-anion channel as a candidate pathway for osmosensitive ATP release from mouse astrocytes in primary culture. Cell Res 18:558–565.

Liu Q-S, Xu Q, Arcuino G, Kang J, Nedergaard M (2004) Astrocyte-mediated activation of neuronal kainate receptors. Proc Natl Acad Sci USA 101:3172–3177.

Liu X, Li C, Falck JR, Harder DR, Koehler RC (2012) Relative contribution of cyclooxygenases, epoxyeicosatrienoic acids, and pH to the cerebral blood flow response to vibrissal

stimulation. Am J Physiol Heart Circ Physiol 302:H1075–H1085.

Longden TA, Dabertrand F, Hill-Eubanks DC, Hammack SE, Nelson MT (2014) Stress-induced glucocorticoid signaling remodels neurovascular coupling through impairment of cerebrovascular inwardly rectifying K+ channel function. Proc Natl Acad Sci USA 111:7462–7467.

Longden TA, Dabertrand F, Koide M, Gonzales AL, Tykocki NR, Brayden JE, Hill-Eubanks D, Nelson MT (2017) Capillary K+-sensing initiates retrograde hyperpolarization to increase local cerebral blood flow. Nature Neuroscience 20:717–726.

Lothman E, LaManna J, Cordingley G, Rosenthal M, Somjen G (1975) Responses of electrical potential, potassium levels, and oxidative metabolic activity of the cerebral neocortex of cats. Brain Res 88:15–36.

Ma B, Xu G, Wang W, Enyeart JJ, Zhou M (2014) Dual patch voltage clamp study of low membrane resistance astrocytes in situ. Mol Brain 7:18.

Marcaggi P, Attwell D (2004) Role of glial amino acid transporters in synaptic transmission and brain energetics. Glia 47:217–225.

Mathiisen TM, Lehre KP, Danbolt NC, Ottersen OP (2010) The perivascular astroglial sheath provides a complete covering of the brain microvessels: an electron microscopic 3D reconstruction. Glia 58:1094–1103.

Matsuura T, Bures J (1971) The minimum volume of depolarized neural tissue required for triggering cortical spreading depression in rat. Exp Brain Res 12:238–249.

Medina I, Friedel P, Rivera C, Kahle KT, Kourdougli N, Uvarov P, Pellegrino C (2014) Current view on the functional regulation of the neuronal K(+)-Cl(-) cotransporter KCC2. Front Cell Neurosci 8:27.

Mehina EMF, Murphy-Royal C, Gordon GR (2017) Steady-State Free Ca2+ in Astrocytes Is Decreased by Experience and Impacts Arteriole Tone. J Neurosci 37:8150–8165.

Mellergård P, Ouyang YB, Siesjö BK (1993) Intracellular pH regulation in cultured rat astrocytes in CO2/HCO3(-)-containing media. Exp Brain Res 95:371–380.

Metea MR, Kofuji P, Newman EA (2007) Neurovascular coupling is not mediated by potassium siphoning from glial cells. J Neurosci 27:2468–2471.

Metea MR, Newman EA (2006) Glial cells dilate and constrict blood vessels: a mechanism of neurovascular coupling. J Neurosci 26:2862–2870.

Minieri L, Pivonkova H, Harantova L, Anderova M, Ferroni S (2015) Intracellular Na(+) inhibits volume-regulated anion channel in rat cortical astrocytes. Journal of Neurochemistry 132:286–300.

Mishima T, Hirase H (2010) In vivo intracellular recording suggests that gray matter astrocytes in mature cerebral cortex and hippocampus are electrophysiologically homogeneous. J Neurosci 30:3093–3100.

Mishra A, Reynolds JP, Chen Y, Gourine AV, Rusakov DA, Attwell D (2016) Astrocytes mediate neurovascular signaling to capillary pericytes but not to arterioles. Nature Neuroscience 19:1619–1627.

Mothet JP, Parent AT, Wolosker H, Brady RO, Linden DJ, Ferris CD, Rogawski MA, Snyder SH (2000) D-serine is an endogenous ligand for the glycine site of the N-methyl-D-aspartate receptor. Proc Natl Acad Sci USA 97:4926–4931.

Mount DB, Mercado A, Song L, Xu J, George AL, Delpire E, Gamba G (1999) Cloning and characterization of KCC3 and KCC4, new members of the cation-chloride cotransporter gene family. J Biol Chem 274:16355–16362.

Mulligan SJ, MacVicar BA (2004) Calcium transients in astrocyte endfeet cause cerebrovascular constrictions. Nature 431:195–199.

Mulligan SJ, MacVicar BA (2006) VRACs CARVe a path for novel mechanisms of communication in the CNS. Sci STKE 2006:pe42–pe42.

Murphy K, Gerzanich V, Zhou H, Ivanova S, Dong Y, Hoffman G, West GA, Winn HR, Simard JM (2003) Adenosine-A2a receptor down-regulates cerebral smooth muscle L-type Ca2+ channel activity via protein tyrosine phosphatase, not cAMP-dependent protein kinase. Mol Pharmacol 64:640–649.

Nagelhus EA, Ottersen OP (2013) Physiological roles of aquaporin-4 in brain. Physiol Rev 93:1543–1562.

Navarrete M, Araque A (2010) Endocannabinoids Potentiate Synaptic Transmission through Stimulation of Astrocytes. Neuron 68:113–126.

Nedergaard M, Ransom B, Goldman SA (2003) New roles for astrocytes: redefining the functional architecture of the brain. Trends Neurosci 26:523–530.

Nett WJ, Oloff SH, McCarthy KD (2002) Hippocampal astrocytes in situ exhibit calcium oscillations that occur independent of neuronal activity. J Neurophysiol 87:528–537.

Nguyen J, Nishimura N, Fetcho RN, Iadecola C, Schaffer CB (2011) Occlusion of cortical ascending venules causes blood flow decreases, reversals in flow direction, and vessel dilation in upstream capillaries. J Cereb Blood Flow Metab 31:2243–2254.

Nilsson M, Eriksson PS, Rönnbäck L, Hansson E (1993) GABA induces Ca2+ transients in astrocytes. Neuroscience 54:605–614.

Nishimura N, Schaffer CB, Friedman B, Lyden PD, Kleinfeld D (2007) Penetrating arterioles are

a bottleneck in the perfusion of neocortex. Proc Natl Acad Sci USA 104:365–370.

Oberheim NA, Takano T, Han X, He W, Lin JHC, Wang F, Xu Q, Wyatt JD, Pilcher W, Ojemann JG, Ransom BR, Goldman SA, Nedergaard M (2009) Uniquely hominid features of adult human astrocytes. J Neurosci 29:3276–3287.

Oberheim NA, Tian G-F, Han X, Peng W, Takano T, Ransom B, Nedergaard M (2008) Loss of astrocytic domain organization in the epileptic brain. J Neurosci 28:3264–3276.

Oberheim NA, Wang X, Goldman S, Nedergaard M (2006) Astrocytic complexity distinguishes the human brain. Trends Neurosci 29:547–553.

Ochoa-de la Paz LD, Lezama R, Toscano B, Pasantes-Morales H (2005) Mechanisms of chloride influx during KCl-induced swelling in the chicken retina. Pflugers Arch 449:526–536.

Palma E, Amici M, Sobrero F, Spinelli G, Di Angelantonio S, Ragozzino D, Mascia A, Scoppetta C, Esposito V, Miledi R, Eusebi F (2006) Anomalous levels of Cl- transporters in the hippocampal subiculum from temporal lobe epilepsy patients make GABA excitatory. Proc Natl Acad Sci USA 103:8465–8468.

Panatier A, Theodosis DT, Mothet J-P, Touquet B, Pollegioni L, Poulain DA, Oliet SHR (2006) Glia-derived D-serine controls NMDA receptor activity and synaptic memory. Cell 125:775–784.

Panatier A, Vallée J, Haber M, Murai KK, Lacaille J-C, Robitaille R (2011) Astrocytes are endogenous regulators of basal transmission at central synapses. Cell 146:785–798.

Park H, Han K-S, Oh S-J, Jo S, Woo J, Yoon B-E, Lee CJ (2013) High glutamate permeability and distal localization of Best1 channel in CA1 hippocampal astrocyte. Mol Brain 6:54.

Park H, Oh S-J, Han K-S, Woo DH, Park H, Mannaioni G, Traynelis SF, Lee CJ (2009) Bestrophin-1 encodes for the Ca2+-activated anion channel in hippocampal astrocytes. J Neurosci 29:13063–13073.

Parpura V, Haydon PG (2000) Physiological astrocytic calcium levels stimulate glutamate release to modulate adjacent neurons. Proc Natl Acad Sci USA 97:8629–8634.

Pascual O, Casper KB, Kubera C, Zhang J, Revilla-Sanchez R, Sul J-Y, Takano H, Moss SJ, McCarthy K, Haydon PG (2005) Astrocytic purinergic signaling coordinates synaptic networks. Science 310:113–116.

Paulson OB, Newman EA (1987) Does the release of potassium from astrocyte endfeet regulate cerebral blood flow? Science 237:896–898.

Payne JA, Rivera C, Voipio J, Kaila K (2003) Cation-chloride co-transporters in neuronal communication, development and trauma. Trends Neurosci 26:199–206.

Pedersen SF, Kapus A, Hoffmann EK (2011) Osmosensory mechanisms in cellular and systemic volume regulation. J Am Soc Nephrol 22:1587–1597.

Peng X, Zhang C, Alkayed NJ, Harder DR, Koehler RC (2004) Dependency of cortical functional hyperemia to forepaw stimulation on epoxygenase and nitric oxide synthase activities in rats. J Cereb Blood Flow Metab 24:509–517.

Petravicz J, Fiacco TA, McCarthy KD (2008) Loss of IP3 receptor-dependent Ca2+ increases in hippocampal astrocytes does not affect baseline CA1 pyramidal neuron synaptic activity. J Neurosci 28:4967–4973.

Pettus BJ, Bielawska A, Subramanian P, Wijesinghe DS, Maceyka M, Leslie CC, Evans JH, Freiberg J, Roddy P, Hannun YA, Chalfant CE (2004) Ceramide 1-phosphate is a direct activator of cytosolic phospholipase A2. J Biol Chem 279:11320–11326.

Piechotta K, Lu J, Delpire E (2002) Cation chloride cotransporters interact with the stress-related kinases Ste20-related proline-alanine-rich kinase (SPAK) and oxidative stress response 1 (OSR1). J Biol Chem 277:50812–50819.

Piet R, Vargová L, Syková E, Poulain DA, Oliet SHR (2004) Physiological contribution of the astrocytic environment of neurons to intersynaptic crosstalk. Proc Natl Acad Sci USA 101:2151–2155.

Pologruto TA, Sabatini BL, Svoboda K (2003) ScanImage: flexible software for operating laser scanning microscopes. Biomed Eng Online 2:13.

Porter JT, McCarthy KD (1996) Hippocampal astrocytes in situ respond to glutamate released from synaptic terminals. J Neurosci 16:5073–5081.

Prince DA, Lux HD, Neher E (1973) Measurement of extracellular potassium activity in cat cortex. Brain Res 50:489–495.

Pusch M, Jentsch TJ (1994) Molecular physiology of voltage-gated chloride channels. Physiol Rev 74:813–827.

Race JE, Makhlouf FN, Logue PJ, Wilson FH, Dunham PB, Holtzman EJ (1999) Molecular cloning and functional characterization of KCC3, a new K-Cl cotransporter. Am J Physiol 277:C1210–C1219.

Rangroo Thrane V, Thrane AS, Wang F, Cotrina ML, Smith NA, Chen M, Xu Q, Kang N, Fujita T, Nagelhus EA, Nedergaard M (2013) Ammonia triggers neuronal disinhibition and seizures by impairing astrocyte potassium buffering. Nat Med 19:1643–1648.

Ransom BR (1992) Glial modulation of neural excitability mediated by extracellular pH: a hypothesis. In: Neuronal-Astrocytic Interactions - Implications for Normal and Pathological CNS Function, pp 37–46 Progress in Brain Research. Elsevier.

Ransom BR (2000) Glial modulation of neural excitability mediated by extracellular pH: a hypothesis revisited. In: Volume Transmission Revisited, pp 217–228 Progress in Brain Research. Elsevier.

Ransom CB, Ransom BR, Sontheimer H (2000) Activity-dependent extracellular K+ accumulation in rat optic nerve: the role of glial and axonal Na+ pumps. Journal of Physiology 522 Pt 3:427–442.

Rinehart J, Maksimova YD, Tanis JE, Stone KL, Hodson CA, Zhang J, Risinger M, Pan W, Wu D, Colangelo CM, Forbush B, Joiner CH, Gulcicek EE, Gallagher PG, Lifton RP (2009) Sites of regulated phosphorylation that control K-Cl cotransporter activity. Cell 138:525–536.

Ringel F, Plesnila N (2008) Expression and functional role of potassium-chloride cotransporters (KCC) in astrocytes and C6 glioma cells. Neuroscience Letters 442:219–223.

Rivera C, Voipio J, Payne JA, Ruusuvuori E, Lahtinen H, Lamsa K, Pirvola U, Saarma M, Kaila K (1999) The K+/Cl- co-transporter KCC2 renders GABA hyperpolarizing during neuronal maturation. Nature 397:251–255.

Roman RJ (2002) P-450 metabolites of arachidonic acid in the control of cardiovascular function. Physiol Rev 82:131–185.

Rosenegger DG, Gordon GR (2015) A slow or modulatory role of astrocytes in neurovascular coupling. Microcirculation 22:197–203.

Rosenegger DG, Tran CHT, LeDue J, Zhou N, Gordon GR (2014) A high performance, cost-effective, open-source microscope for scanning two-photon microscopy that is modular and readily adaptable. PLoS ONE 9:e110475.

Rosenegger DG, Tran CHT, Wamsteeker Cusulin JI, Gordon GR (2015) Tonic Local Brain Blood Flow Control by Astrocytes Independent of Phasic Neurovascular Coupling. J Neurosci 35:13463–13474.

Rouach N, Glowinski J, Giaume C (2000) Activity-dependent neuronal control of gap-junctional communication in astrocytes. J Cell Biol 149:1513–1526.

Rouach N, Koulakoff A, Abudara V, Willecke K, Giaume C (2008) Astroglial metabolic networks sustain hippocampal synaptic transmission. Science 322:1551–1555.

Ruffin VA, Salameh AI, Boron WF, Parker MD (2014) Intracellular pH regulation by acid-base transporters in mammalian neurons. Front Physiol 5:43.

Rungta RL, Bernier L-P, Dissing-Olesen L, Groten CJ, LeDue JM, Ko R, Drissler S, MacVicar BA (2016) Ca(2+) transients in astrocyte fine processes occur via Ca(2+) influx in the adult mouse hippocampus. Glia 64:2093–2103.

Rungta RL, Choi HB, Tyson JR, Malik A, Dissing-Olesen L, Lin PJC, Cain SM, Cullis PR, Snutch TP, MacVicar BA (2015) The cellular mechanisms of neuronal swelling underlying cytotoxic edema. Cell 161:610–621.

Rusakov DA (2015) Disentangling calcium-driven astrocyte physiology. Nat Rev Neurosci 16:226–233.

Rusan ZM, Kingsford OA, Tanouye MA (2014) Modeling glial contributions to seizures and epileptogenesis: cation-chloride cotransporters in Drosophila melanogaster. McCabe BD, ed. PLoS ONE 9:e101117.

Rust MB, Alper SL, Rudhard Y, Shmukler BE, Vicente R, Brugnara C, Trudel M, Jentsch TJ, Hübner CA (2007) Disruption of erythroid K-Cl cotransporters alters erythrocyte volume and partially rescues erythrocyte dehydration in SAD mice. J Clin Invest 117:1708–1717.

Rust MB, Faulhaber J, Budack MK, Pfeffer C, Maritzen T, Didié M, Beck F-X, Boettger T, Schubert R, Ehmke H, Jentsch TJ, Hübner CA (2006) Neurogenic mechanisms contribute to hypertension in mice with disruption of the K-Cl cotransporter KCC3. Circ Res 98:549–556.

Sachse G, Faulhaber J, Seniuk A, Ehmke H, Pongs O (2014) Smooth muscle BK channel activity influences blood pressure independent of vascular tone in mice. J Physiol 592:2563–2574.

Salameh AI, Hübner CA, Boron WF (2017) Role of Cl--HCO3-exchanger AE3 in intracellular pH homeostasis in cultured murine hippocampal neurons, and in crosstalk to adjacent astrocytes. J Physiol 595:93–124.

Schell MJ, Brady RO Jr, Molliver ME, Snyder SH (1997) D-Serine as a Neuromodulator: Regional and Developmental Localizations in Rat Brain Glia Resemble NMDA Receptors. J Neurosci 17:1604–1615.

Schell MJ, Molliver ME, Snyder SH (1995) D-serine, an endogenous synaptic modulator: localization to astrocytes and glutamate-stimulated release. Proc Natl Acad Sci USA 92:3948–3952.

Schmitt BM, Berger UV, Douglas RM, Bevensee MO, Hediger MA, Haddad GG, Boron WF (2000) Na/HCO3 cotransporters in rat brain: expression in glia, neurons, and choroid plexus. J Neurosci 20:6839–6848.

Serrano A, Haddjeri N, Lacaille J-C, Robitaille R (2006) GABAergic network activation of glial cells underlies hippocampal heterosynaptic depression. J Neurosci 26:5370–5382.

Sherwood MW, Arizono M, Hisatsune C, Bannai H, Ebisui E, Sherwood JL, Panatier A, Oliet SHR, Mikoshiba K (2017) Astrocytic IP3 Rs: Contribution to Ca(2+) signalling and hippocampal LTP. Glia 65:502–513.

Shigetomi E, Bushong EA, Haustein MD, Tong X, Jackson-Weaver O, Kracun S, Xu J, Sofroniew MV, Ellisman MH, Khakh BS (2013a) Imaging calcium microdomains within

entire astrocyte territories and endfeet with GCaMPs expressed using adeno-associated viruses. J Gen Physiol 141:633–647.

Shigetomi E, Jackson-Weaver O, Huckstepp RT, O'Dell TJ, Khakh BS (2013b) TRPA1 channels are regulators of astrocyte basal calcium levels and long-term potentiation via constitutive D-serine release. J Neurosci 33:10143–10153.

Shigetomi E, Kracun S, Sofroniew MV, Khakh BS (2010) A genetically targeted optical sensor to monitor calcium signals in astrocyte processes. Nat Neurosci 13:759–766.

Shigetomi E, Tong X, Kwan KY, Corey DP, Khakh BS (2012) TRPA1 channels regulate astrocyte resting calcium and inhibitory synapse efficacy through GAT-3. Nat Neurosci 15:70–80.

Shih AY, Rühlmann C, Blinder P, Devor A, Drew PJ, Friedman B, Knutsen PM, Lyden PD, Mateo C, Mellander L, Nishimura N, Schaffer CB, Tsai PS, Kleinfeld D (2015) Robust and fragile aspects of cortical blood flow in relation to the underlying angioarchitecture. Microcirculation 22:204–218.

Shrode LD, Putnam RW (1994) Intracellular pH regulation in primary rat astrocytes and C6 glioma cells. Glia 12:196–210.

Simard M, Arcuino G, Takano T, Liu Q-S, Nedergaard M (2003) Signaling at the gliovascular interface. J Neurosci 23:9254–9262.

Simpson PB, Russell JT (1997) Role of sarcoplasmic/endoplasmic-reticulum Ca2+-ATPases in mediating Ca2+ waves and local Ca2+-release microdomains in cultured glia. Biochem J 325:239–247.

Singer W, Lux HD (1975) Extracellular potassium gradients and visual receptive fields in the cat striate cortex. Brain Res 96:378–383.

So PT, Dong CY, Masters BR, Berland KM (2000) Two-photon excitation fluorescence microscopy. Annu Rev Biomed Eng 2:399–429.

Somjen GG (1979) Extracellular potassium in the mammalian central nervous system. Annu Rev Physiol 41:159–177.

Somjen GG (2002) Ion regulation in the brain: implications for pathophysiology. Neuroscientist 8:254–267.

Song L, Mercado A, Vázquez N, Xie Q, Desai R, George AL, Gamba G, Mount DB (2002) Molecular, functional, and genomic characterization of human KCC2, the neuronal K-Cl cotransporter. Brain Res Mol Brain Res 103:91–105.

Sorg O, Magistretti PJ (1992) Vasoactive intestinal peptide and noradrenaline exert long-term control on glycogen levels in astrocytes: blockade by protein synthesis inhibition. J Neurosci

12:4923–4931.

Srinivasan R, Huang BS, Venugopal S, Johnston AD, Chai H, Zeng H, Golshani P, Khakh BS (2015) Ca2+ signaling in astrocytes from Ip3r2-/- mice in brain slices and during startle responses in vivo. Nat Neurosci 18:708–717.

Staley KJ, Proctor WR (1999) Modulation of mammalian dendritic GABA(A) receptor function by the kinetics of Cl- and HCO3- transport. Journal of Physiology 519 Pt 3:693–712.

Steinhäuser C, Berger T, Frotscher M, Kettenmann H (1992) Heterogeneity in the Membrane Current Pattern of Identified Glial Cells in the Hippocampal Slice. Eur J Neurosci 4:472–484.

Straub SV, Bonev AD, Wilkerson MK, Nelson MT (2006) Dynamic inositol trisphosphate-mediated calcium signals within astrocytic endfeet underlie vasodilation of cerebral arterioles. J Gen Physiol 128:659–669.

Sun W, McConnell E, Pare J-F, Xu Q, Chen M, Peng W, Lovatt D, Han X, Smith Y, Nedergaard M (2013) Glutamate-dependent neuroglial calcium signaling differs between young and adult brain. Science 339:197–200.

Syková E, Rothenberg S, Krekule I (1974) Changes of extracellular potassium concentration during spontaneous activity in the mesencephalic reticular formation of the rat. Brain Res 79:333–337.

Takano T, Kang J, Jaiswal JK, Simon SM, Lin JHC, Yu Y, Li Y, Yang J, Dienel G, Zielke HR, Nedergaard M (2005) Receptor-mediated glutamate release from volume sensitive channels in astrocytes. Proc Natl Acad Sci USA 102:16466–16471.

Takano T, Tian G-F, Peng W, Lou N, Libionka W, Han X, Nedergaard M (2006) Astrocyte-mediated control of cerebral blood flow. Nat Neurosci 9:260–267.

Tang YT, Mendez JM, Theriot JJ, Sawant PM, López-Valdés HE, Ju YS, Brennan KC (2014) Minimum conditions for the induction of cortical spreading depression in brain slices. J Neurophysiol 112:2572–2579.

Tsai PS, Kaufhold JP, Blinder P, Friedman B, Drew PJ, Karten HJ, Lyden PD, Kleinfeld D (2009) Correlations of neuronal and microvascular densities in murine cortex revealed by direct counting and colocalization of nuclei and vessels. J Neurosci 29:14553–14570.

van Mil HG, Geukes Foppen RJ, Siegenbeek van Heukelom J (1997) The influence of bumetanide on the membrane potential of mouse skeletal muscle cells in isotonic and hypertonic media. British Journal of Pharmacology 120:39–44.

Verboomen H, Wuytack F, De Smedt H, Himpens B, Casteels R (1992) Functional difference between SERCA2a and SERCA2b Ca2+ pumps and their modulation by phospholamban. Biochem J 286:591–595.

Verkhratsky A, Nedergaard M (2018) Physiology of Astroglia. Physiol Rev 98:239–389.

Vyskocil F, Kritz N, Bures J (1972) Potassium-selective microelectrodes used for measuring the extracellular brain potassium during spreading depression and anoxic depolarization in rats. Brain Res 39:255–259.

Waites CL, Craig AM, Garner CC (2005) Mechanisms of vertebrate synaptogenesis. Annu Rev Neurosci 28:251–274.

Wallraff A, Köhling R, Heinemann U, Theis M, Willecke K, Steinhäuser C (2006) The impact of astrocytic gap junctional coupling on potassium buffering in the hippocampus. J Neurosci 26:5438–5447.

Walz W (2000) Role of astrocytes in the clearance of excess extracellular potassium. Neurochem Int 36:291–300.

Wang F, Smith NA, Xu Q, Fujita T, Baba A, Matsuda T, Takano T, Bekar L, Nedergaard M (2012) Astrocytes Modulate Neural Network Activity by Ca2+-Dependent Uptake of Extracellular K. Science Signaling 5:ra26–ra26.

Wang T, Yang Y-Q, Karasawa T, Wang Q, Phillips A, Guan B-C, Ma K-T, Jiang M, Xie D-H, Steyger PS, Jiang Z-G (2013) Bumetanide hyperpolarizes madin-darby canine kidney cells and enhances cellular gentamicin uptake by elevating cytosolic Ca(2+) thus facilitating intermediate conductance Ca(2+)--activated potassium channels. Cell Biochem Biophys 65:381–398.

Wilms CD, Eilers J (2007) Photo-physical properties of Ca2+-indicator dyes suitable for two-photon fluorescence-lifetime recordings. Journal of Microscopy 225:209–213.

Wilms CD, Schmidt H, Eilers J (2006) Quantitative two-photon Ca2+ imaging via fluorescence lifetime analysis. Cell Calcium 40:73–79.

Yang Y, Ge W, Chen Y, Zhang Z, Shen W, Wu C, Poo M, Duan S (2003) Contribution of astrocytes to hippocampal long-term potentiation through release of D-serine. Proc Natl Acad Sci USA 100:15194–15199.

Yao X, Hrabetová S, Nicholson C, Manley GT (2008) Aquaporin-4-deficient mice have increased extracellular space without tortuosity change. J Neurosci 28:5460–5464.

Yoon B-E, Jo S, Woo J, Lee J-H, Kim T, Kim D, Lee CJ (2011) The amount of astrocytic GABA positively correlates with the degree of tonic inhibition in hippocampal CA1 and cerebellum. Mol Brain 4:42.

Young SZ, Platel J-C, Nielsen JV, Jensen NA, Bordey A (2010) GABA(A) Increases Calcium in Subventricular Zone Astrocyte-Like Cells Through L- and T-Type Voltage-Gated Calcium Channels. Front Cell Neurosci 4:8.

Zhang H, Verkman AS (2008) Aquaporin-4 independent Kir4.1 K+ channel function in brain glial cells. Mol Cell Neurosci 37:1–10.

Zhang J-M, Wang H-K, Ye C-Q, Ge W, Chen Y, Jiang Z-L, Wu C-P, Poo M-M, Duan S (2003) ATP released by astrocytes mediates glutamatergic activity-dependent heterosynaptic suppression. Neuron 40:971–982.

Zhang Y, Chen K, Sloan SA, Bennett ML, Scholze AR, O'Keeffe S, Phatnani HP, Guarnieri P, Caneda C, Ruderisch N, Deng S, Liddelow SA, Zhang C, Daneman R, Maniatis T, Barres BA, Wu JQ (2014) An RNA-sequencing transcriptome and splicing database of glia, neurons, and vascular cells of the cerebral cortex. J Neurosci 34:11929–11947.

Zhao B, Gu L, Liu K, Zhang M, Liu H (2017) Maxi-anion channels play a key role in glutamate-induced ATP release from mouse astrocytes in primary culture. Neuroreport 28:380–385.

Zheng K, Bard L, Reynolds JP, King C, Jensen TP, Gourine AV, Rusakov DA (2015) Time-Resolved Imaging Reveals Heterogeneous Landscapes of Nanomolar Ca(2+) in Neurons and Astroglia. Neuron 88:277–288.

Zhou M, Xu G, Xie M, Zhang X, Schools GP, Ma L, Kimelberg HK, Chen H (2009) TWIK-1 and TREK-1 are potassium channels contributing significantly to astrocyte passive conductance in rat hippocampal slices. J Neurosci 29:8551–8564.

Zhou N, Gordon GRJ, Feighan D, MacVicar BA (2010) Transient swelling, acidification, and mitochondrial depolarization occurs in neurons but not astrocytes during spreading depression. Cereb Cortex 20:2614–2624.

Zhuang Z, Yang B, Theus MH, Sick JT, Bethea JR, Sick TJ, Liebl DJ (2010) EphrinBs regulate D-serine synthesis and release in astrocytes. J Neurosci 30:16015–16024.

Zippin JH, Levin LR, Buck J (2001) CO2/HCO3−-responsive soluble adenylyl cyclase as a putative metabolic sensor. Trends in Endocrinology & Metabolism 12:366–370.

Zonta M, Angulo MC, Gobbo S, Rosengarten B, Hossmann K-A, Pozzan T, Carmignoto G (2003) Neuron-to-astrocyte signaling is central to the dynamic control of brain microcirculation. Nat Neurosci 6:43–50.